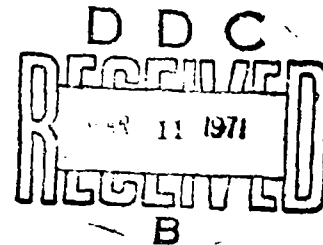
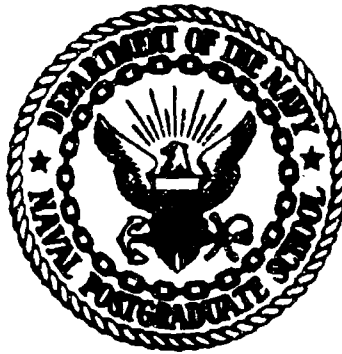


AD719895

# United States Naval Postgraduate School



DYNAMICAL MECHANISMS PRODUCING LARGE-SCALE  
TRANSPORT OF ATMOSPHERIC TRACE SUBSTANCES

by

J. D. Mahlman

October 1970

This document has been approved for public release and sale; its  
distribution is unlimited.

Reproduced by  
**NATIONAL TECHNICAL  
INFORMATION SERVICE**  
Springfield, Va. 22151

NAVAL POSTGRADUATE SCHOOL  
Monterey, California

Rear Admiral R. W. McNitt, USN  
Superintendent


M. U. Clauser  
Academic Dean

DYNAMICAL MECHANISMS PRODUCING LARGE-SCALE  
TRANSPORT OF ATMOSPHERIC TRACE SUBSTANCES

ABSTRACT:

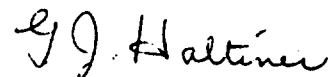
This is a compilation of research results performed under AEC Research Contract AT(49-7)-3206. All of the various efforts have been directed toward gaining a better understanding of the atmospheric processes which lead to systematic large-scale trace substance transport. A variety of approaches have been employed in this and in earlier work on this contract. The last article in this report provides an overview and critique of the applicability of these various methods.

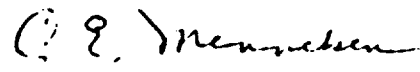
This task was supported by Atomic Energy Commission, Washington, D. C. Contract AT(49-7)-3206.

  
J. D. Mahlman  
Associate Professor of Meteorology

Approved by:

Released by:

  
G. J. Haltiner, Chairman  
Department of Meteorology

  
C. E. Menneken  
Dean of Research Administration

## TABLE OF CONTENTS

I.	On the maintenance of the polar front jet stream by J. D. Mahlman -----	I-1
II.	A numerical simulation of the advective and diffusive transfer of trace substances in the stratosphere; by H. E. Willoughby -----	II-1
III.	Numerical calculations of stratospheric ozone transport; by R. H. Stender -----	III-1
IV.	An overview of various research efforts and techniques employed for investigation of trace substance transport in the atmosphere by J. D. Mahlman -----	IV-1

ON THE MAINTENANCE OF THE POLAR FRONT JET STREAM

by

J. D. Mahlman

### Abstract

A calculation of the mean transverse circulation about the polar front jet stream is performed by using a diagnostic balance,  $\omega$ -equation model. The results show a thermally-direct mean transverse circulation about this jet stream system.

An examination of the kinetic energy balance of this jet stream reveals that the direct transverse circulation is strong enough to maintain the jet against frictional dissipation but not enough to provide lateral export of energy. However, significant amounts of energy are transferred upward into the lower stratosphere.

Further considerations are employed to show that the mean transverse circulation obtained here is compatible with the observed distributions of temperature and potential vorticity about the jet core.

## 1. Introduction

Since its quantitative documentation over twenty-five years ago, the polar front or mid-latitude jet stream has been the subject of numerous intensive investigations. Much of the early interest in this jet stream system was due to its obvious connection with the mid-latitude cyclone waves and their associated weather processes. Because these seemed to form an interacting system, many investigators became interested in the dynamical processes responsible for producing and maintaining this jet stream.

According to Rossby (1947) and Staff Members (1947), the westerly jet stream in mid-latitudes is formed by lateral mixing processes with constant absolute angular momentum to the south of the jet core and constant absolute vorticity to the north. This assumption yields a lateral velocity profile which is qualitatively reasonable. It was pointed out, however, that such a mechanism implies a thermally indirect transverse circulation about the jet core itself. Although such a mechanism is attractive because the systematic ascent of cold air and descent of warm air helps to maintain the strong lateral temperature contrast across the jet core, it leads to the possibly more difficult question, as to how the kinetic energy of the jet stream is maintained.

Making use of this scheme, Palmen (1951) included this assumed indirect transverse circulation about the polar front jet stream in his model of the mean meridional circulation. In a study by Endlich (1953), fields of adiabatic vertical velocities were computed in the vicinity of a polar

front jet stream. Although fields of rising and sinking motion were found on both sides of the jet core, the statistics indicated a slight preference for the indirect transverse circulation. However, no systematic averaging was performed relative to the jet core itself. In a separate study, Riehl and Teweles (1953) indicated results which were not incompatible with the original concept of such an indirect transverse circulation. Also, Newton and Carson (1953) and Newton (1958) indicated that, in the vicinity of a developing jet stream and an associated frontal zone, the vertical motion branch of the transverse circulation about the jet core must be in an indirect sense. However, they contended that the total transverse circulation should remain thermally direct.

An alternative hypothesis was advanced by Namias and Clapp (1949) who proposed that the jet stream forms as a result of a "confluence" of a preexisting temperature field. In this case, the compensating vertical transverse circulation is thermally direct. A similar concept was also proposed by Nyberg (1949, 1950, 1953).

The thermally-direct transverse circulation also resulted from theoretical studies by Van Miegham (1950) and Kuo (1954). This is suggested as well in theoretical studies of atmospheric frontal structure by Sawyer (1956) and by Eliassen (1959, 1962). Similar results were indicated in a numerical simulation of frontogenesis by Williams (1967).

The only previous quantitative attempt to establish the transverse circulation about the polar front jet stream was that of Clapp and Winston (1951). They found tentative evidence in favor of a direct circulation by

using adiabatic vertical velocities, averaged from the surface to 10,000 feet. Similar contentions were also presented as a result of qualitative studies by Hubert (1953), Raethjen (1953), Vuorela (1953, 1957), Reiter (1961, 1963a), Briggs and Roach (1963), and by Endlich and McLean (1965).

A number of authors have investigated the vertical motions in the vicinity of specific portions of jet streams. Murray and Daniels (1953), for example, showed that the transverse circulation is direct in the entrance zone and indirect in the exit zone of a high speed center along the jet core. In a study of upper-tropospheric frontogenesis, Reed and Sanders (1953) showed intense sinking motions in the "jet stream front" on the cyclonic side of the jet core. This was corroborated in subsequent studies by Reed (1955), Reed and Danielsen (1959), and Danielsen (1959a). These authors argued further that this frontal zone may contain subsiding stratospheric air rather than being a zone of mixing between two tropospheric air masses. This contention was corroborated in case studies by Danielsen (1959b, 1964a, b, 1966), Danielsen, Bergman, and Paulson (1962), Staley (1960, 1962), Reiter (1963a, b, 1964), Reiter and Mahlman (1964, 1965a, b), Reiter, Glasser and Mahlman (1969) and by Mahlman (1964, 1965). However, this intense sinking of stratospheric air north of the jet core was shown by Danielsen (1964a) and by Mahlman (1964, 1965) to be strongly associated with cyclogenesis in the upper troposphere. Furthermore, the relationship of this exchange mechanism to the cyclogenetic process was verified statistically by Mahlman (1966, 1969).

Even though the above mechanism is of undeniable importance in the exchange of mass between the stratosphere and troposphere and in the



dynamics of cyclone development, it occurs only during certain periods along limited sections of the jet core. As a result, such studies may not give any real insight into the nature of the net transverse circulation about the polar front jet stream.

Probably the most valuable contribution to the problem of the maintenance of jet stream systems was that presented by Riehl and Fultz (1957, 1958). From an analysis of a steady three-wave case in a rotating-"dishpan" experiment, the authors were able to demonstrate that the mean transverse circulation about the "dishpan" jet stream is thermally direct. This was the case even though the mean meridional circulation in the same latitudes was determined to operate in a thermally indirect sense. Thus, the analysis showed that the mechanisms responsible for the maintenance of the jet stream may be fundamentally different from those acting to maintain the zonal-mean wind at the same latitudes. Riehl and Fultz's results on the energetics of the "dishpan" jet stream will be compared later against the conclusions of the analysis to be performed here.

A study by Elsberry (1968) of a dishpan five-wave vacillation case also indicated the existence of a thermally-direct transverse circulation around the "dishpan" jet stream. In this case the direct circulation was a significant residual between thermally direct and indirect transverse circulations operating at the poleward and equatorward branches of the jet stream maximum, respectively. However, in the cases studied by Riehl and Fultz (1957, 1958) and by Elsberry (1968), the lateral wind shears in the jet stream regions were significantly less relative to the Coriolis parameter

than those observed in the atmosphere. Thus, it is not clear whether or not such results can be immediately applied to a system such as the polar front jet stream.

The success of Riehl and Fultz (1957, 1958) encouraged efforts to obtain analogous measurements for atmospheric jet streams. Krishnamurti (1961a, b) in a detailed study of the subtropical jet stream, showed the existence of a thermally direct transverse circulation about the jet core. Thus, the transverse circulation about the subtropical jet stream operates in the same sense as the mean meridional (Hadley) circulation in the same region.

In a study of the stratospheric polar night vortex, Mahlman (1966, 1969) found a direct transverse circulation operating below the polar night jet stream just before a major breakdown period. This was the case even though the mean meridional circulation in the same region was shown to operate in the indirect sense.

The above studies have been useful in developing our understanding of the maintenance of jet stream systems. The polar front jet stream, however, has not yet been studied in any quantitative detail as to its actual transverse circulation and corresponding energetics. This is to a great extent due to the difficulty in defining an adequate curvilinear coordinate system for such a strongly time-dependent phenomenon. Investigators have been hampered by the lack of diagnostic techniques capable of resolving the vertical motion field with sufficient accuracy to provide reasonably consistent answers. The intent of this study is to obtain a systematic calculation of the net transverse circulation about the polar front jet stream. Further, it is desired to investigate the implications of such a circulation on the

energetics of this jet and its surroundings. This will be accomplished through use of a diagnostic balance,  $\omega$ -equation model developed originally by Krishnamurti (1966, 1968).

## 2. Experimental Approach

When attempting to provide a meaningful calculation of the net transverse circulation occurring in the vicinity of a polar-front jet stream, it is highly desirable that the case selected for computation be one in which the time variations of the system are not particularly large. This is not only advantageous from the point of view of establishing a realistic coordinate system, but also because the result is likely to be more representative of the actual processes usually acting to maintain such a system.

Because of the above considerations, the case selected for analysis was an area centered over the contiguous United States for the time period 15 November 1200 GMT to 17 November 1200 GMT, 1966. This period was dominated by a polar front jet stream of moderate intensity. The flow at jet-stream level was somewhat anticyclonic over the continent bounded by relatively weak cyclones off each coast (Fig. 1). Although the Pacific Coast cyclone did move slowly eastward, bringing some precipitation to the California region, no significant cyclongenesis or large-scale system movements were observed during the five upper-air observation times contained in this selected time period. Thus, this particular case appears satisfactory for attempting to determine the basic dynamical processes acting to maintain the polar front jet stream.

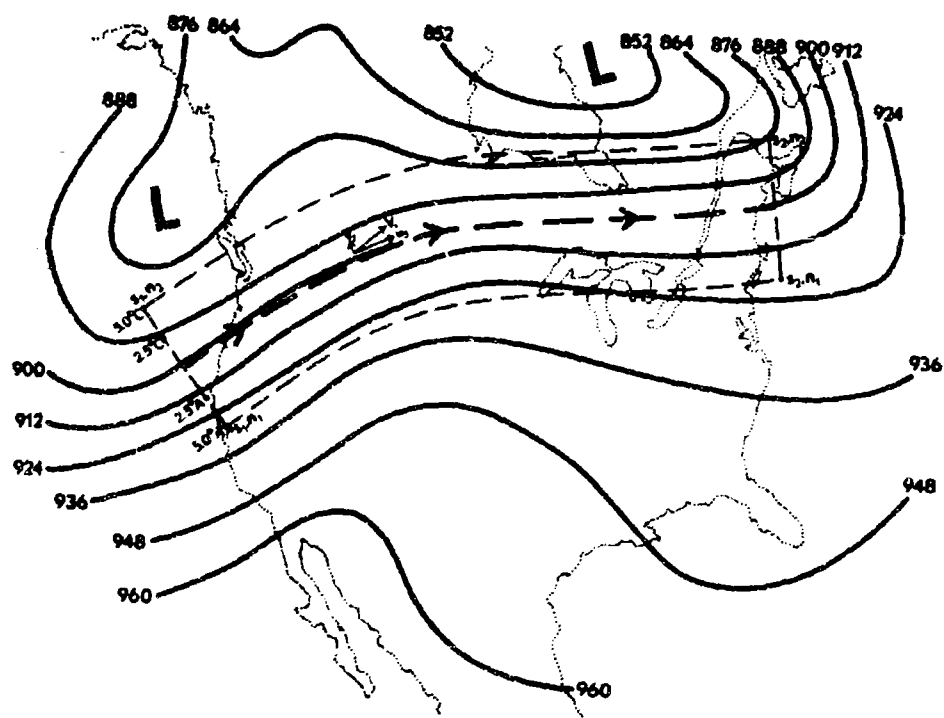


Fig. 1. Geopotential height (m) at 300 mb on 16 November 1966, 0000 GMT. Heavy dashed arrow shows position of the polar front jet stream and dashed box shows lateral boundary of computational grid. °C and °A represent normal distance in degrees latitude on the cyclonic and anti-cyclonic sides of the jet axis, respectively.

As mentioned in the Introduction, the approach used here is to employ the diagnostic balance,  $\omega$ -equation model developed originally by Krishnamurti (1966, 1968) in which the equations are scaled for motions of characteristic Rossby number less than unity ( $R_o < 1$ ). The initial data input is obtained from the National Meteorological Center objectively analyzed geopotential fields at 1000, 850, 700, 500, 300, and 200 mb. The stream function ( $\psi$ ) is assumed to be related to the geopotential field through the non-linear balance equation,<sup>1</sup>

$$\nabla \cdot f \nabla \psi + 2J \left( \frac{\partial \psi}{\partial x}, \frac{\partial \psi}{\partial y} \right) = \nabla^2 \Phi \quad (1)$$

In this study  $\psi$  is specified at the lateral boundaries by simple  $\psi = \frac{\Phi}{f_o}$ . In the event that the ellipticity condition for Eq. (1),

$$\nabla^2 \Phi + \frac{1}{2} f^2 - \nabla f \cdot \nabla \psi > 0, \quad (2)$$

is not satisfied, Eq. (1) is replaced by

$$\nabla \cdot f \nabla \psi = \nabla^2 \Phi - 2J(u_g, v_g). \quad (3)$$

Such an adjustment is frequently required on the anticyclonic side of the jet stream. Use of Eq. (2) in such cases in place of Eq. (1) permits retention of strong anticyclonic vorticities from the diagnosed height fields.

By using the balance equation (1) combined with the continuity, vorticity, and thermodynamic equations, one obtains the "complete" ( $R_o < 1$ )  $\omega$ -equation system,

---

<sup>1</sup> See the Appendix for the list of symbols.

$$\begin{aligned}
\nabla^2 \sigma \omega + f^2 \frac{\partial^2 \omega}{\partial p^2} &= f \frac{\partial}{\partial p} J(\psi, \zeta_a) + \frac{\alpha}{\theta} \nabla^2 J(\psi, \theta) \\
&- 2 \frac{\partial}{\partial t} \frac{\partial}{\partial p} J\left(\frac{\partial \psi}{\partial x}, \frac{\partial \psi}{\partial y}\right) - f \frac{\partial}{\partial p} (\zeta \nabla^2 \chi) \\
&+ f \frac{\partial}{\partial p} \left( \omega \frac{\partial}{\partial p} \nabla^2 \psi \right) + fg \frac{\partial^2}{\partial p^2} \left( \frac{\partial \tau_y}{\partial x} - \frac{\partial \tau_x}{\partial y} \right) \\
&- \frac{\chi}{p} \nabla^2 H_L - f \frac{\partial}{\partial p} (\nabla \chi \cdot \nabla \zeta_a) + f \frac{\partial}{\partial p} \left( \nabla \omega \cdot \nabla \frac{\partial \psi}{\partial p} \right) \\
&- \frac{\alpha}{\theta} \nabla^2 (\nabla \chi \cdot \nabla \theta) - \beta \frac{\partial}{\partial p} \frac{\partial}{\partial y} \frac{\partial \psi}{\partial t}, \tag{4}
\end{aligned}$$

$$\nabla^2 \chi = \frac{\partial \omega}{\partial p} \tag{5}$$

$$\begin{aligned}
\nabla^2 \frac{\partial \psi}{\partial t} &= -J(\psi, \zeta_a) + \nabla \chi \cdot \nabla \zeta_a + \zeta_a \nabla^2 \chi \\
&- \nabla \omega \cdot \nabla \frac{\partial \psi}{\partial p} - \omega \frac{\partial}{\partial p} \nabla^2 \psi - g \frac{\partial}{\partial p} \left( \frac{\partial \tau_y}{\partial x} - \frac{\partial \tau_x}{\partial y} \right) \tag{6}
\end{aligned}$$

Given suitable boundary conditions for  $\omega$ ,  $\chi$ , and  $\partial \psi / \partial t$ , this set of equations is solved for  $\omega$  by the method of sequential relaxation with the initial solution including only the first two terms on the right hand side of eq. (4). Note that this initial step is similar in form to the quasi-geostrophic  $\omega$ -equation except  $f$  and  $\sigma$  vary in the horizontal and  $\psi$  is the complete balanced stream function rather than the simple geostrophic form. Once the initial approximation for  $\omega$  is determined, Eq. (5) is solved for  $\chi$ , the velocity potential. These initial fields of  $\omega$  and  $\chi$ , along with Eq. (6), are then used to evaluate the remaining terms on the right hand side of Eq. (4). Then Eq. (4) is solved by the method of sequential relaxation as before, only with all forcing functions included. This procedure is

repeated until the difference between successive approximations of the  $\omega$  field become acceptably small. In this study, five passes were found to be sufficient. For further details in the computational procedure, see Krishnamurti (1968).

The computations are made from a five-level grid in the vertical. Fields of  $\psi$ ,  $\chi$ ,  $\Phi$ ,  $\partial\psi/\partial t$  appear at the 1000, 800, 600, 400, and 200 mb surfaces while  $\omega$ ,  $T$ ,  $\theta$ ,  $q$ , and  $q_s$  are given at the 900, 700, 500, and 300 mb levels. The horizontal grid points are spaced 2.5 degrees latitude and longitude apart. The grid extends from 55W to 135W longitude and from 25N to 60N latitude. There are 15 grid points in the meridional direction and 33 grid points in the zonal direction. The last six grid points do not contain initial data, but are used to provide cyclic continuity so that grid points 1 and 33 have the same value for any given dependent variable. Grid point values for points 28 through 32 are provided by interpolation from values at grid points 1, 2, 26, and 27.

Once the calculations for each observation time are completed, a coordinate line is defined along the polar front jet stream axis at 300 mb (as defined from a careful isotach analysis). Then parallel coordinate lines are defined at distances 2.5 and 5.0 degrees latitude perpendicular to the jet axis in the cyclonic and anticyclonic directions, respectively (see Fig. 2). It is then a comparatively straightforward procedure to calculate "mean" distributions of variables relative to the jet core. For an example of the mean wind and temperature structure relative to this jet, see Fig. 2. In this system, an "eddy" quantity is defined as the value of

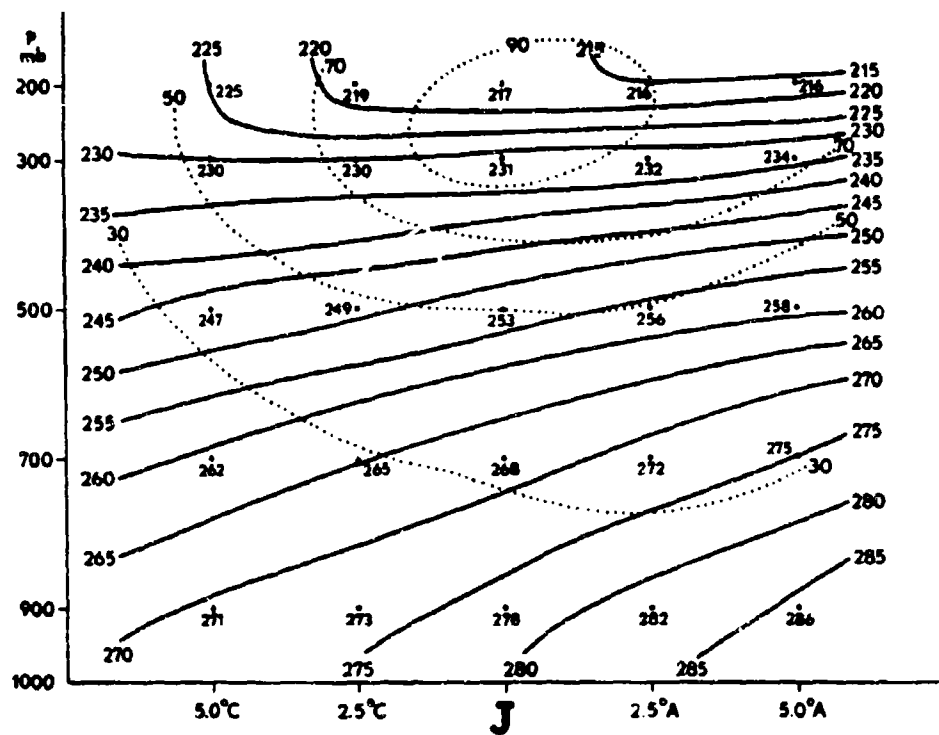


Fig. 2. Mean wind (knots) and temperature (deg K) along the polar front jet stream averaged from 15 November, 1200 GMT to 17 November 1200 GMT, 1966.



a variable at a given point minus its "mean" along the same line parallel the jet axis. At times it will be useful to discuss "mean" and "eddy" processes relative to the jet core. These are to be carefully distinguished from the mean and eddy concepts arising from the zonal averaging often employed in general circulation studies.

### 3. Mean Transverse Circulation About the Jet Core

The calculations of  $\omega$ , averaged along one complete wavelength of the polar front jet stream were prepared for all levels at the specified normal distances to the 300 mb jet core. These were prepared individually for each observation time from 15 November 1200 GMT to 17 November 1200 GMT, 1966.

The individual calculations, derived from the five observation times, all showed for the troposphere a distinct thermally direct pattern of mean vertical motion about the jet core (i.e., systematic ascent of the warm air on the anticyclonic side of the jet core relative to the colder air on the cyclonic side). Although each independent calculation revealed this, in the interest of increasing the reliability of subsequent inferences, the individual calculations were combined to form a time averaged mean  $\omega$  relative to the jet core.

The quantitative results of this are given in Fig. 3 along with the 95 percent confidence interval, determined from the time variability of the individual measurements. This figure shows a systematic mean ascent on the anticyclonic side of the jet core with maximum values at 300 mb. This



characteristic agrees well with observations of cirrus cloud shields on the anticyclonic side of the jet core (McLean, 1957; Conover, 1960; Kadlec, 1963; Oliver, Anderson, and Ferguson, 1964; Bittner, 1966; Anderson, et al., 1969). On the other hand, Fig. 3 shows ascending motion through the jet core. This result may disagree with satellite studies which contend that the cirrus shield cuts-off at the jet core or just to the anticyclonic side (Oliver, Anderson, and Ferguson, 1964; Bittner, 1966; Anderson, et al., 1969). Nevertheless, this calculated ascent in the jet core is not inconsistent with the result of Starratt (1949), which shows that precipitation tends to be a maximum directly underneath the jet core. It is also compatible with the distributions of ozone and water vapor mixing ratio in the vicinity of the jet core, given by Briggs and Roach (1963). This result is further supported by the observation that the tropopause "gap" (apparently dynamically produced) is generally located just to the cyclonic side of the jet core.

In a study such as this, where a number of types of averaging procedures must necessarily appear, it is convenient to employ the averaging notation proposed by Reiter (1969a, b). In this system the mean of an arbitrary quantity, say  $Q$ , is given by  $[Q]_{()}$ , where the quantity enclosed by small parentheses indicates the coordinate (or coordinates) over which the averaging was performed. The deviation of  $Q$  from that average is given by  $(Q)_{()}$ . Thus, for example, one might write  $Q = [Q]_{(s)} + (Q)_{(s)}$  for averaging processes along the jet axis.

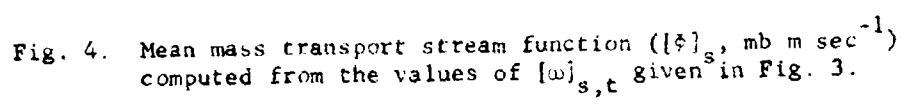
A useful way to view the mean motion relative to the jet core is through use of a mass transport stream function. Because of the large ratio of the length to the width of the jet stream in this study, one may write the averaged mass continuity equation as

$$\frac{\partial [v_J]_s}{\partial n} + \frac{\partial [\omega]_s}{\partial p} = 0 . \quad (7)$$

One can write a solution to this equation in the form of a stream function such that

$$[v_J]_s = - \frac{\partial [\Psi]_s}{\partial p} , \quad [\omega]_s = + \frac{\partial [\Psi]_s}{\partial n} . \quad (8)$$

The diagnostic balance,  $\omega$ -equation model is solved with a boundary condition of  $\omega = 0$  at 100 mb. Because of this,  $[\Psi]_s$  is arbitrarily set equal to zero on that boundary. The implied net inflow into the region is obtained by integrating Eq. (7) from 5 degrees latitude on the anticyclonic side to 5 degrees latitude to the cyclonic side of the jet core. It is then assumed that the net computed inflow or outflow can be partitioned equally on the anticyclonic and the cyclonic boundaries. Once the lateral boundary values for  $[v_J]_s$  are set, then the entire field of  $[\Psi]_s$  is determined by numerical integration of Eq. (8). The results of this determination along with the mean wind structure of the region are given in Fig. 4. This figure shows a number of interesting features. Rather strong confluence of warm and cold air appears to be taking place at about the 700 mb level under the jet core. This is in good agreement with the concept presented by Namias and Clapp (1949). Note the well-defined flow across the jet axis at 200 mb and the horizontal



splitting of streamlines on the anticyclonic side of the jet axis. This implies rather strong energy generation through  $- [v_J]_{(s)} \frac{\partial}{\partial n} [\Phi]_{(s)}$  at the jet core. Also, there is an implied horizontal divergence on the anticyclonic side of the jet core. This is compatible with the observed lateral spreading of cloud elements in the cirrus shield on the anticyclonic side of the subtropical jet stream as seen in ATS-I satellite time-lapse movies. Further, a study by Fujita, et al. (1968) of these ATS-I time lapse movies shows significant lateral convergence of plumes from the tops of lower- to mid-tropospheric convective cells to the south of the cirrus shield. This is also in agreement with the results given in Fig. 4.

It is of interest to note that the structure given in Fig. 4 is also quite similar in overall character to the qualitative model of transverse circulation about the polar front jet core given by Danielsen (1968) for cases of strong import of stratospheric air into the "jet stream front" in association with cyclogenesis. This appears to be of fundamental interest, since the case selected for analysis here had no occurrences of large-scale cyclogenesis during the period. Therefore, even though the sinking of stratospheric air on the cyclonic side of the jet core in such cases is about an order of magnitude more intense than the mean values given here (see numerous references on this phenomenon cited in the Introduction), the qualitative forms of the transverse circulations are very similar. Because of this correspondence, it is then reasonable to hypothesize that the fundamental dynamical mechanisms responsible for maintenance of the polar front jet stream and for producing rapid upper tropospheric cyclogenesis (with

associated import of stratospheric air into the troposphere), may be essentially the same. This may be the case even though the former exhibits a quasi-steady-state character while the latter is essentially discrete in nature. This hypothesis, of course, needs much more thorough examination before its validity can be strongly claimed. Such comparisons and examinations are difficult, not only because these are energetically open systems, but also because they interact very strongly with each other.

#### 4. Jet Stream "Mean" Kinetic Energy Maintenance

Given the mean transverse circulations about the polar front jet stream from the previous section, it is possible to provide quantitative estimates of the various contributions which this circulation produces toward maintaining the "mean" kinetic energy of this jet stream. The conventional approach to evaluate the energetics of open systems for volumes which do not encircle the globe, is to derive expressions for the time rate of change of the total kinetic energy of the given volume. Since the major interest here is in the maintenance of the "mean" structure of the polar front jet stream, only the balance equation for the mean kinetic energy (averaged along the jet axis) will be evaluated in any detail.

The derivation of the mean kinetic energy balance in an arbitrary curvilinear  $(s, n, p)$  coordinate system is obtained by first considering the quasi-static equations of motion in this system,

$$\frac{\partial u}{\partial t} + u_J \frac{\partial u}{\partial s} + v_J \frac{\partial u}{\partial n} + \omega \frac{\partial u}{\partial p} - f v_J + \frac{\partial \Phi}{\partial s} + F_s = 0, \quad (9)$$

$$\frac{\partial v_J}{\partial t} + u_J \frac{\partial v_J}{\partial s} + v_J \frac{\partial v_s}{\partial n} + \omega \frac{\partial v_J}{\partial p} + f u_J + \frac{\partial \Phi}{\partial n} + F_n = 0. \quad (10)$$

It should be pointed out here that the  $s$  axis is along the jet axis and not necessarily along the instantaneous streamlines. Also,  $u_J$  is the wind component along this jet axis and  $v_J$  is the wind component along the normal  $n$  axis.

Now, by multiplying Eq. (9) by  $[u_J]_{(s)}$  and Eq. (10) by  $[v_J]_{(s)}$ , adding, averaging along  $s$  and then along  $n$ , manipulating, and integrating over the mass contained between two pressure surfaces, one obtains the equation for the time rate of change of "mean" kinetic energy of the jet stream.

$$\begin{aligned} & \frac{\partial}{\partial t} \int_{p_u}^{p_l} \left\{ \frac{[u_J]_{(s)}^2 + [v_J]_{(s)}^2}{2} \right\} (n) \frac{dp}{g} = \frac{\partial K_M}{\partial t} = \\ & + \int_{p_u}^{p_l} \frac{1}{A} \frac{1}{B} c_n \left\{ \frac{[u_J]_{(s)}^2 + [v_J]_{(s)}^2}{2} (n) + [u_J]_{(s)} (u_J)_{(s)} + [v_J]_{(s)} (v_J)_{(s)} \right\} dL \frac{dp}{g} \\ & - \left[ \frac{\omega}{g} \left\{ \frac{[u_J]_{(s)}^2 + [v_J]_{(s)}^2}{2} + [u_J]_{(s)} (u_J)_{(s)} + [v_J]_{(s)} (v_J)_{(s)} \right\} \right]_{(s,n)} \Big|_{p_l} \\ & + \left[ \frac{\omega}{g} \left\{ \frac{[u_J]_{(s)}^2 + [v_J]_{(s)}^2}{2} + [u_J]_{(s)} (u_J)_{(s)} + [v_J]_{(s)} (v_J)_{(s)} \right\} \right]_{(s,n)} \Big|_{p_u} \end{aligned}$$



(d)

$$+ \int_{p_u}^{p_1} \left\{ \left[ (u_J)_{(s)} (v_J)_{(s)} \frac{\partial}{\partial n} [u_J]_{(s)} \right]_{(s,n)} + \left[ (u_J)_{(s)} (\omega)_{(s)} \frac{\partial}{\partial p} [u_J]_{(s)} \right]_{(s,n)} \right. \\ \left. + \left[ (v_J)_{(s)}^2 \frac{\partial}{\partial n} [v_J]_{(s)} \right]_{(s,n)} + \left[ (v_J)_{(s)} (\omega)_{(s)} \frac{\partial}{\partial p} [v_J]_{(s)} \right]_{(s,n)} \right\} \frac{dp}{g}$$

(e)

$$+ \int_{p_u}^{p_1} \left\{ \left[ [u_J]_{(s)} (f)_{(s)} (v_J)_{(s)} \right]_{(s,n)} - \left[ [v_J]_{(s)} (f)_{(s)} (u_J)_{(s)} \right]_{(s,n)} \right\} \frac{dp}{g}$$

(f)

$$+ \int_{p_u}^{p_1} \frac{\{ [\Phi]_{(B)} - [\Phi]_{(s,n)} \}}{A} \oint_B c_n dt \frac{dp}{g}$$

(g)

$$- \frac{1}{g} \left[ ([\omega]_{(s)})_{(n)} ([\Phi]_{(s)})_{(n)} \right]_{(n)} \Big|_{p_1}$$

(h)

$$+ \frac{1}{g} \left[ ([\omega]_{(s)})_{(n)} ([\Phi]_{(s)})_{(n)} \right]_{(n)} \Big|_{p_u}$$

(i)

$$- \int_{p_u}^{p_1} \left[ ([\omega]_{(s)})_{(n)} ([\alpha]_{(s)})_{(n)} \right]_{(n)} \frac{dp}{g}$$

(j)

$$- \int_{p_u}^{p_1} \left[ [u_J]_{(s)} [F_s]_{(s)} + [v_J]_{(s)} [F_n]_{(s)} \right]_{(n)} \frac{dp}{g} \quad (11)$$

In the above expression the separate terms, labeled (a) through (j) have the following interpretation:

- (a) flux of "mean" kinetic energy through the side boundaries;
- (b), (c) flux of "mean" kinetic energy through the lower and upper boundaries, respectively;
- (d) conversion of "eddy" kinetic energy to "mean" kinetic energy;
- (e) an additional term in the conversion from "eddy" to "mean" kinetic energy which arises because the Coriolis parameter  
..... (f) varies along the axis over which the initial average is performed. It is interpreted as a conversion term because it appears with opposite algebraic sign in the "eddy" kinetic energy equation;
- (f) mean pressure interaction term at the side boundaries arising from energy conversion in an open system;
- (g), (h) mean pressure interaction terms at the lower and upper boundaries, respectively;
- (i) conversion of potential energy into "mean" kinetic energy due to mean transverse circulation about the jet core;
- (j) dissipation of "mean" kinetic energy due to friction and sub-grid-scale mixing.

Because the coordinate system tends to be aligned nearly parallel to the flow, not only are the terms involving "eddy" products difficult to calculate, but many times they may prove to be negligibly small. Since the intent of this work is to assess the effect of the "mean" transverse circulation about the jet stream, only quantities  $a_1$ ,  $b_1$ ,  $c_1$ ,  $f$ ,  $g$ ,  $h$ , and  $i$  are computed here. A program to provide explicit calculation of "eddy" effects is being presently developed. As will be pointed out later, there may be some aspects of jet stream dynamics which are strongly dependent upon "eddy" processes relative to the jet stream. For the present analysis,

however, the "mean" kinetic energy balance is put in the simplified symbolism implied in Eq. (11),

$$\frac{\partial K_M}{\partial t} = a_1 + b_1 + c_1 + f + g + h + i - \text{"dissipation."} \quad (12)$$

Here, "dissipation" is actually a combination of terms  $a_2$ ,  $b_2$ ,  $c_2$ , and  $j$ . As a result, its algebraic sign, as well as its magnitude, is presently uncertain. The approach here is to assess the values for the remaining terms as well as for  $\partial K_M / \partial t$  so that some knowledge can be gained about the combined "eddy" and dissipation effects. The calculations are performed from 900 to 100 mb over an area  $\pm$  five degrees latitude perpendicular to the jet core. In order to gain further clarification of the processes involved, separate calculations are performed for the volumes 100 - 300 mb and 300 - 900 mb. This roughly approximates the regions above and below the jet core.

The results of these calculations are given in Table 1. First, noting the results for the entire 100 - 900 mb volume, it may be seen that terms  $a_1$ ,  $b_1$ , and  $c_1$  in Eqs. (11) and (12) produce a small net loss of energy ( $-0.8 \text{ erg cm}^{-2} \text{ mb}^{-1} \text{ sec}^{-1}$ ) to the volume due essentially to mean lateral outflow (see Fig. 5) occurring at larger mean kinetic energies than the mean inflow. The mean pressure interaction terms ( $f$ ,  $g$ , and  $h$  in Eqs. (11) and (12) also show a net loss for the 100 - 900 mb volume during this time period ( $-1.8 \text{ erg cm}^{-2} \text{ mb}^{-1} \text{ sec}^{-1}$ ). The conversion from potential to mean kinetic energy of the jet (term  $i$  in Eqs. (11) and (12)) shows a net gain of +1.9 units for the entire volume. This conversion is especially significant

Table 1

Contribution of Various Terms in Eq. (11)  
All units expressed in  $\text{erg cm}^{-2} \text{mb}^{-1} \text{sec}^{-1}$

	900-100 mb layer	below jet 900-300 mb layer	above jet 300-100 mb layer
$\frac{\partial K_H}{\partial t} =$	-5.1	-10.6	+11.2
$\int_{p_u}^{p_L} \frac{1}{A} \left[ c_n \right]_B \left\{ \frac{[u_J]_{(s)}^2 + [v_J]_{(s)}^2}{2} \right\} dt \frac{dp}{g} = (a_1) =$	-0.8	+0.3	-3.9
$- \left[ [\omega]_{(s)} \left\{ \frac{[u_J]_{(s)}^2 + [v_J]_{(s)}^2}{2} \right\} \right]_{(n)} \Big _{p_L} = (b_1) =$	+0.0	+0.0	+9.6
$+ \left[ [\omega]_{(s)} \left\{ \frac{[u_J]_{(s)}^2 + [v_J]_{(s)}^2}{2} \right\} \right]_{(n)} \Big _{p_u} = (c_1) =$	+0.0 ( $\omega=0$ at 100 mb)	-3.2	0.0 ( $\omega=0$ at 100 mb)
$+ \int_{p_u}^{p_L} \left\{ \frac{[\Phi]_B - [\Phi]_{(s,n)}}{A} \right\} \left[ c_n \right] dt \frac{dp}{g} = (f) =$	-1.8	+0.2	-8.0
$- \frac{1}{g} \left[ ([\omega]_{(s)})_{(n)} ([\Phi]_{(s)})_{(n)} \right]_{(n)} \Big _{p_L} = (g) =$	+0.2	+0.2	+14.3
$+ \frac{1}{g} \left[ ([\omega]_{(s)})_{(n)} ([\Phi]_{(s)})_{(n)} \right]_{(n)} \Big _{p_u} = (h) =$	+0.0 ( $\omega=0$ at 100 mb)	-4.8	0.0 ( $\omega=0$ at 100 mb)
$- \int_{p_u}^{p_L} \left[ ([\omega]_{(s)})_{(n)} ([\omega]_{(s)})_{(n)} \right]_{(n)} \frac{dp}{g} = (i) =$	+1.9	+3.0	-1.3
Total of right hand side terms ( $a_1, b_1, c_1, f, g, h, \text{ and } i$ )	-0.5	-4.3	+10.7
- Implied "Dissipation"	+4.6	+6.3	-0.5

since the local change term ( $\partial K_M / \partial t$ ) represents a net loss of 5.1 units for the period. The net transverse circulation about the polar front jet is thus shown to be thermally direct even when the jet is rapidly becoming less intense. As a result, the mean transverse circulation calculated here may be less intense than in cases where the jet may be in approximate steady-state or accelerating. The implied "dissipation" required for balance in this case is  $4.6 \text{ erg cm}^{-2} \text{ mb}^{-1} \text{ sec}^{-1}$ .

A number of studies have been undertaken recently by Kung (1966a, b; 1967; 1968; 1969) on the generation and dissipation of kinetic energy in the atmosphere. It is interesting to note that his most recent estimate of the annual average energy dissipation over North America is  $4.7 \text{ erg cm}^{-2} \text{ mb}^{-1} \text{ sec}^{-1}$  for the 100 - 900 mb layer. Although this value is virtually identical with the implied "dissipation" obtained here, there are a number of important differences. The transfer of kinetic energy, due to the unevaluated eddy terms in Eq. (11), is potentially important and could be of either algebraic sign. Also, Kung's dissipation values are for the total kinetic energy and not for the mean jet stream component, as calculated here. It is usually assumed that the energy dissipation of the largest scales of motion is appreciably smaller than for smaller-scale motions (e.g., see Oort (1964)). An alternative hypothesis has been advanced by Panofsky, (1970) who speculated that since the vertical scale of mesoscale and larger-scale systems is not appreciably different (particularly so in the jet stream region), large-scale kinetic energy might be transferred directly into sub-grid-scale motions without going through any significant scale cascading processes. Some

evidence for this is given by Clarke (1966) who estimated a mean dissipation rate of  $4.5 \text{ erg cm}^{-2} \text{ mb}^{-1} \text{ sec}^{-1}$  for the 100 - 500 mb layer in the vicinity of the subtropical jet stream. If this is a valid statement, it suggests that a great deal of the estimated "dissipation" in this study may be true dissipation. This suggests that only a comparatively small amount of the kinetic energy produced is exported out of the jet stream region. Presently, this can be only speculation at best, because of combined effects of computational uncertainty, unevaluated "eddy" terms, and the observed deceleration of this jet. It is, however, in agreement with the results of Riehl and Fultz (1958), who stated for the three-wave steady "dishpan" jet: "One cannot view the jet stream as a current that is the locus of generation of kinetic energy, which is then dispersed laterally to maintain the kinetic energy elsewhere, nor as a current that is 'driven by outside circulations, ...'"

If one partitions the calculations into balances for the regions below (300 - 900 mb) and above (100 - 300 mb) the jet, considerable additional information is gained. For the region below the jet, Table 1 shows a very pronounced decrease of mean kinetic energy with time  $\partial K_M / \partial t = -10.6 \text{ erg cm}^{-2} \text{ mb}^{-1} \text{ sec}^{-1}$ . It is especially interesting that the conversion to mean kinetic energy (i) is +3.0 units. There are significant losses through the boundary terms ( $c_1$  and h) across the 300-mb surface. For this volume the implied "dissipation" is 6.3 units. As before, it is not presently possible to separate out the eddy terms from the true energy dissipation. Given reasonable estimates of the dissipation (Kung's (1969) value for the 900 - 300 mb

layer is  $5.8 \text{ erg cm}^{-2} \text{ mb}^{-1} \text{ sec}^{-1}$ ) and the validity of Panofsky's (1970) hypothesis, the unevaluated eddy terms in Eq. (11) may not be particularly important for this volume. This, however, remains to be tested quantitatively.

The region above the jet appears to possess entirely different characteristics. Table 1 shows that this layer is increasing its kinetic energy ( $\partial K_M / \partial t = +11.2 \text{ erg cm}^{-2} \text{ mb}^{-1} \text{ sec}^{-1}$ ). A large portion of this increase is due to flux of mean kinetic energy (term b) into the region across the 300 mb surface (+9.6 units). Also, a very large flux of energy into the region is produced by the mean pressure interaction term at 300 mb (+14.3 units). Some of this energy is lost through the side boundaries (term  $a_1 = -3.9$  units and term f = -8.0 units). It is especially interesting to note that the conversion term (i) is a -1.3 units and thus acting to build up potential energy at the expense of mean kinetic energy. This arises because of the reversal of the mean lateral temperature contrast above the jet core. This is also compatible with the contention of Riehl (1962) that this temperature reversal above the jet core is produced dynamically by ascent on the anticyclonic side and descent on the cyclonic side of the jet core. The implied "dissipation" for this layer is -0.5 units. This value is too small to be considered reliable, even with respect to algebraic sign.

A truly steady-state condition would have been more favorable for interpretative purposes. It is quite encouraging, however, that the summation of various kinetic energy balance terms are quite compatible with the observed tendencies. This suggests that the diagnostic balance,  $\omega$ -equation model is useful for such studies. It does seem clear that the mean polar front jet

stream is maintained by a thermally direct transverse circulation below the core, and that appreciable energy is transported upward into the lower stratosphere indirectly as a result of this process.

These results carry some interesting implications. First, it is clear that the mechanisms for maintaining the jet stream at these latitudes are completely different from the processes acting to maintain the zonal mean westerlies, as viewed in the traditional approach to general circulation problems. Therefore, it appears to be inconsistent to equate these two phenomena in any way when discussing the mechanisms involved in their maintenance. The second implication is that the polar front jet stream provides a very efficient mechanism for producing upward flux of energy into the stratosphere due to the pressure interaction effect. In fact, the flux across the 300 mb surface due to term (g) in Eq. (11) and Table 1 is  $2860 \text{ erg cm}^{-2} \text{ sec}^{-1}$ . In the usual general circulation formulation of the energy equations, this would show up as a very strong eddy effect at about wave numbers 4 or 5. The above value is quite compatible with the vertical eddy pressure interaction term for the same general region obtained by Manabe and Hunt (1968) in an 18-level general circulation model. It is especially interesting to note that this large energy flux into the stratosphere occurs at the approximate location of the winter mid-latitude warm belt in the lower stratosphere. This region is known to be a strong sink of zonal and eddy available potential energy. Thus, the above process may be of fundamental importance in maintaining the kinetic energy of this somewhat unusual region of the stratosphere. It would be of interest to check this hypothesis directly through



a high-resolution numerical model of the general circulation.

## 5. Some Additional Considerations

In the previous section considerable attention was given to the balance of "mean" kinetic energy along the polar front jet stream. One can also write a companion expression to Eq. 11 for the "eddy" kinetic energy balance along the jet axis.

In the present experimental setup, it has been impossible to calculate all terms in such an "eddy" kinetic energy balance because of the difficulty in obtaining "eddy" products. However, as a means of obtaining a preliminary estimate of the energetic contribution of "eddies" relative to the polar front jet stream, a calculation of the

$$- \int_{p_u}^{p_l} \left[ (\omega)_{(s)} (\alpha)_{(s)} \right]_{(s,n)} \frac{dp}{g}$$

term in the "eddy" kinetic energy balance was performed. Physically, this represents a conversion from potential energy into "eddy" kinetic energy measured relative to the jet axis. This particular term is quite important because it helps to determine whether the "eddies," relative to the jet axis, have an internal energy source or have been produced by either boundary fluxes or conversions from "mean" kinetic energy. Figure 5 shows the average of the above expression over the five observation times at each grid point (in terms of energy units). The volume average of this conversion is  $+5.1 \text{ erg cm}^{-2} \text{ mb}^{-1} \text{ sec}^{-1}$ . This represents a rather strong energy source in the jet region and is probably large enough to balance the sub-grid scale



energy dissipation of "eddy" kinetic energy without necessitating a large input from the various other possible mechanisms.

Figure 5 shows that this energy conversion has an interesting distribution relative to the jet axis. A very strong source of "eddy" kinetic energy ( $\sim 20 \text{ erg cm}^{-2} \text{ mb}^{-1} \text{ sec}^{-1}$ ) exists in the middle troposphere on the cyclonic side of the jet axis. This source is apparently due to the asymmetric distribution of the cyclone-scale waves relative to the jet axis. On the anticyclonic side of the jet axis in the lower troposphere, a significant (but weak) sink of energy appears. This strong variation across the jet axis is somewhat surprising. Its dynamical significance is not presently obvious, although it seemingly must play an important role in the redistribution of kinetic energy in the jet stream region. The effect appears to be statistically significant because it appears in each of the five calculations at the individual observation times. As in any case study, however, companion calculations for other cases would yield valuable insight into the generality of these preliminary results.

As pointed out by Riehl (1962) and others, one of the principle difficulties with a thermally direct, transverse circulation about the jet axis is that such a circulation acts to rotate the isentropic surfaces into horizontal planes. Thus, the solenoidal field necessary to support a geostrophic jet stream is weakened by the transverse circulation. Yet, in the first approximation, geostrophic balance holds for the jet stream. This implies a restriction on the intensity of the transverse circulation depending upon the intensity of the processes capable of counteracting the adiabatic cooling on the anticyclonic side and the adiabatic heating on the cyclonic side implied

in Fig. 3. Some insight can be gained into the possible processes responsible by considering the formulation for the mean heat balance along the jet axis. By averaging the first law of thermodynamics along the jet axis and separating "mean" and "eddy" processes one obtains

$$\begin{aligned}
 \frac{\partial [T]_s}{\partial t} = & \quad (a) \quad \quad (b) \\
 & - [v_J]_s \frac{\partial [T]_s}{\partial n} - \frac{\partial}{\partial n} [(v_J)_s (T)_s]_s \\
 & - \frac{1}{s_2 - s_1} \left\{ u_J (T)_s \Big|_{s_2} - u_J (T)_s \Big|_{s_1} \right\} + \frac{[H]}{c_p(s)} \\
 & + \left\{ \frac{x}{p} - \frac{\partial}{\partial p} \right\} [(\omega)_s (T)_s]_s + [\omega]_s \left\{ \frac{[\omega]_s}{c_p} - \frac{\partial [T]_s}{\partial p} \right\} . \quad (13)
 \end{aligned}$$

A preliminary investigation has been made of the possible processes represented in Eq. (12) which may counteract the anticyclonic side cooling and cyclonic side heating resulting from term (f) in the same equation. This analysis indicates that the only term which can accomplish this is (b), which represents the convergence of "eddy" heat flux relative to the jet axis. In order for this to be valid, an "eddy" heat flux divergence is required on the cyclonic side and an "eddy" convergence on the anticyclonic side. This conclusion was also reached by Riehl and Fultz (1958) in their analysis of a three-wave "dishpan" jet. As indicated previously, a program is now underway to provide for explicit calculation of such "eddy" terms.

Another very important feature of the structure of an atmospheric jet stream is that the potential vorticity ( $P = -\frac{\partial \theta}{\partial p} (f + \xi_\theta)$ ) is almost discontinuous across the jet axis. As pointed out by Riehl (1962) such a potential vorticity distribution in the vicinity of the jet axis places a strong restriction on the type of dynamical process that can be responsible for maintenance of the jet stream. Realizing this, it may be instructive to consider whether or not the transverse circulation, alleged here to be responsible for maintenance of the polar front jet stream, is compatible with the observed strong gradients of potential vorticity across the jet axis. In this case a potential vorticity equation considering non-conservative effects is appropriate, since the time required for a parcel to make a complete circuit about the jet axis (as obtained from Fig. 4) is the order of 40-50 days. As shown by Staley (1960), potential vorticity can only be modified by a curl of the frictional force and gradients of diabatic heating. (It should be pointed out, however, that such a parcel would not in general make such a complete circuit about the axis because of rather large "eddy" and sub-grid scale turbulence effects.)

A preliminary analysis was performed to estimate possible magnitudes of the various terms in the "mean" potential vorticity balance equation. The transverse circulation of Fig. 4 and reasonable estimates on the friction and diabatic heating were employed to provide these estimates. The analysis showed that these non-conservative terms are important on the longer time scales but are not directly responsible for producing the observed potential vorticity gradient across the jet axis. The results show that the probable cause for this is that the jet core occurs at the tropopause level, and the net

transverse circulation, as seen in Figs. 3 and 4, leads naturally to such a potential vorticity distribution. On the cyclonic side of the jet axis, stable stratospheric air is being slowly brought downward while tropospheric air is being slowly lifted on the anticyclonic side. Because of the relatively small net cross-axis velocity component required to maintain the jet energetically, the mean advection normal to the jet core tends to be considerably smaller. This is particularly true at the jet core itself. In more quantitative terms, the  $-[\omega]_{(s)} \frac{\partial[P]_{(s)}}{\partial p}$  term in a potential vorticity balance relative to the jet axis clearly dominates the  $-[v_J]_{(s)} \frac{\partial[P]_{(s)}}{\partial n}$  term. Although the horizontal convergence of "eddy" potential vorticity flux cannot yet be evaluated directly, it is probable that this effect is not strong across the jet core itself, because streamlines at this level tend to be quite parallel to the axis of maximum wind.

Furthermore, from the case studies of discrete intrusions of stratospheric air into the troposphere mentioned in the Introduction, considerable vertical "eddy" flux of potential vorticity is to be expected in the vicinity of the polar front jet stream. In this case the resultant vertical convergence of "eddy" potential vorticity flux will also act to reinforce the observed near discontinuity across the jet axis. The essential similarity of this process (which occurs only at particular regions and times along the jet axis) to the net transverse circulation has already been pointed out in section 3. As a result, the conclusion, that these are reinforcing effects, is not surprising.

Thus, one may conclude that the deduced net transverse circulation about the jet core is not contradicted by either heat balance requirements or potential vorticity considerations.

## 6. Summary and Conclusions

Calculations have been made of the mean transverse circulation about the polar front jet stream, using a diagnostic balance,  $\omega$ -equation model. The results show that such a circulation is thermally direct in the troposphere, with ascent on the anticyclonic side and through the jet core and descent on the cyclonic side.

A calculation of the "mean" kinetic energy of the jet stream shows that the polar front jet is probably maintained by this direct circulation, and that no appreciable amounts of energy are either imported into or exported out of the jet stream region. The results do show, however, the existence of a comparatively large upward flux of energy into the stratosphere, resulting from the thermally-direct transverse circulation.

Preliminary analyses of the heat and the potential vorticity budgets indicate that the mean transverse circulation obtained here is compatible with the observed temperature and potential vorticity distributions in the vicinity of the polar front jet stream.

## APPENDIX

### Table of Symbols

$A$	area enclosed by lateral boundaries
$B$	index denoting averaging or integration to be performed along lateral boundaries
$c_n$	velocity component normal to the lateral boundary (+ inward)
$C_p$	specific heat of air at constant pressure
$f$	coriolis parameter
$f_0$	average $f$ over region
$F_s, F_n$	frictional force in the $s$ and $n$ directions, respectively
$g$	acceleration of gravity
$H$	diabatic heating rate
$H_L$	diabatic heating rate due to release of latent heat
$J$	Jacobian operator
$K_M$	mean kinetic energy measured with respect to the jet stream axis
$l$	length along the boundary $B$
$n$	coordinate direction oriented perpendicular to the jet stream axis
$p_l, p_u$	pressure at lower and upper boundaries of integration volume, respectively
$q, q_s$	specific humidity and saturation specific humidity, respectively
$R$	gas constant for dry air
$R_0$	Rossby number
$s$	coordinate direction oriented along the jet stream axis
$T$	temperature
$u_g, v_g$	zonal and meridional components of geostrophic wind, respectively



$u_J, v_J$	wind components along and normal to the jet stream axis, respectively
$V_s$	wind speed
$\alpha$	specific volume
$\beta$	Rossby parameter
$\zeta, \zeta_\theta$	relative vorticity on $p$ and $\theta$ surfaces, respectively
$\zeta_a$	$f + r$
$\kappa$	$R/c_p$
$\sigma$	$-\alpha/\theta \frac{\partial \theta}{\partial p}$ , a static stability parameter
$\tau_x, \tau_y$	frictional stress on the $x$ and $y$ directions, respectively
$\Phi$	geopotential
$\chi$	velocity potential
$\psi$	stream function for horizontal wind
$\Psi$	stream function for mean transverse circulation about jet stream axis
$\omega$	$dp/dt$

### ACKNOWLEDGEMENT

The author is indebted to Dr. T. N. Krishnamurti for his generous lending of the original version of the diagnostic balance,  $\omega$ -equation model. Also, thanks are due to Dr. E. R. Reiter and Dr. H. Riehl for helping to stimulate the original interest in this problem.

Special appreciation is extended to S. K. Rinard, who assisted in many phases of the computations, and to the computer facility of the Naval Post-graduate School for their provision of large amounts of free machine time. This research was sponsored by the U. S. Atomic Energy Commission under contract number AT(49-7)-3206.

## REFERENCES

- Anderson, R. K., et al., 1969: Application of meteorological satellite data in analysis and forecasting. Tech. Rept. No. 212, Air Weather Service.
- Bittner, F., 1966: Guide for interpretation of satellite photography and nephanalysis. Res. Rept. (4-67), Project FAMOS, Washington, D. C.
- Briggs, J., and W. T. Roach, 1963: Aircraft observations near jet streams. Quart. J. Roy. Meteor. Soc., 89, 225-247.
- Clapp, P. F., and J. S. Winston, 1951: A case study of confluence as related to the jet stream. J. Meteor., 8, 231-243.
- Clarke, R. H., 1966: Turbulence and the detailed structure of a subtropical jet stream. J. Atmos. Sci., 23, 516-530.
- Conover, J. H., 1960: Cirrus patterns and related air motions near the jet stream as derived by photography. J. Meteor., 17, 532-546.
- Danielsen, E. F., 1959a: A determination of the mass transported from stratosphere to troposphere over North America during a thirty-six hour interval (abstract). Mitteilungen des Deutschen Wetterdienstes, 20, 10-11.
- \_\_\_\_\_, 1959b: The laminar structure of the atmosphere and its relation to the concept of a tropopause. Arch. Meteor. Geophys. Bioklim., All, 293-332.
- \_\_\_\_\_, 1964a: Radioactivity transport from stratosphere to troposphere. Mineral Industries, 33, 1-7.
- \_\_\_\_\_, 1964b: Project Springfield Report. Washington, D. C., Defense Atomic Support Agency Rept., DASA 1517, 97, pp. (DDC).
- \_\_\_\_\_, 1968: Stratospheric-tropospheric exchange based on radioactivity, ozone and potential vorticity. J. Atmos. Sci., 25, 502-518.
- \_\_\_\_\_, K. H. Bergman and C. A. Paulson, 1962: Radioisotopes, potential temperature and potential vorticity. Rept., Dept. of Atmospheric Sciences, University of Washington, 54 pp.
- Eliassen, A., 1959: On the formation of fronts in the atmosphere. The Atmosphere and Sea in Motion, New York, Rockefeller and Oxford University Presses, 227-287.

- \_\_\_\_\_, 1962: On the vertical circulation in frontal zones. Geofys. Publikasjoner, 24, No. 4, 147-160.
- Elsberry, R. L., 1968: A high-rotation general circulation experiment with cyclic time changes. Atmospheric Science Paper No. 134, Colorado State University, 115 pp.
- Endlich, R. M., 1953: A study of vertical velocities in the vicinity of jet streams. J. Meteor., 10, 407-415.
- \_\_\_\_\_, and G. S. McLean, 1965: Jet stream structure over the Central United States determined from aircraft observations. J. Appl. Meteor., 5, 377-387.
- Fujita, T., D. L. Bradbury, C. Murino, and L. Hull, 1968: A study of meso-scale cloud motions computed from ATS-I and terrestrial photographs. Satellite and Mesometeorology Research Project. Res. Paper 71, Department of Geophysical Sciences, University of Chicago, 25 pp.
- Hubert, W. E., 1953: A case study of variations in structure and circulation about westerly jet streams over Europe. Tellus, 5, 359-372.
- Kadlec, P. W., 1963: An inflight study of the relation between jet streams, cirrus and wind shear turbulence. Final Report, Contract WB 10356, Eastern Airlines Meteorology Department.
- Krishnamurti, T. N., 1961a: The subtropical jet stream of winter. J. Meteor., 18, 172-191.
- \_\_\_\_\_, 1961b: On the role of the subtropical jet stream of winter in the atmospheric general circulation. J. Meteor., 18, 657-670.
- \_\_\_\_\_, 1966: Diagnostic studies of weather systems of low and high latitudes. Final Report, Project AF19(628)-4777. Dept. of Meteor., UCLA.
- \_\_\_\_\_, 1968: A diagnostic balance model for studies of weather systems of low and high latitudes, Rossby number less than 1. Mon. Wea. Rev. 96, 197-207.
- Kung, E. E., 1966a: Kinetic energy generation and dissipation in the large-scale atmospheric circulation. Mon. Wea. Rev., 94, 67-82.
- \_\_\_\_\_, 1966b: Large-scale balance of kinetic energy in the atmosphere. Mon. Wea. Rev., 94, 627-640.
- \_\_\_\_\_, 1967: Diurnal and long-term variations of the kinetic energy generation and dissipation for a five-year period. Mon. Wea. Rev., 95, 593-606.

- \_\_\_\_\_, 1968: On the kinetic energy dissipation in the atmosphere. Paper presented at WMO/IUGG Symposium on Numerical Weather Prediction, Tokyo.
- \_\_\_\_\_, 1969: Further study on the kinetic energy balance. Mon. Wea. Rev., 97, 573-581.
- Kuo, H. L., 1954: Symmetrical disturbances in a thin layer of fluid subject to a horizontal temperature gradient and rotation. J. Meteor., 11, 399-411.
- Mehlman, J. D., 1964: Relation of stratospheric-tropospheric mass exchange mechanisms to surface radioactivity peaks. Atmos. Sci. Tech. Paper No. 58, Colorado State University, 1-19.
- \_\_\_\_\_, 1965: Relation of stratospheric-tropospheric mass exchange mechanisms to surface radioactivity peaks. Arch. Meteor. Geophys. Bioklim., A15, 1-25.
- \_\_\_\_\_, 1966: Atmospheric general circulation and transport of radioactive debris. Atmos. Sci. Paper No. 103, Colorado State University, 184 pp.
- \_\_\_\_\_, 1969: Energetics of a "minor breakdown" of the stratospheric polar night vortex. J. Atmos. Sci., 26, 1306-1317.
- Manabe, S., and E. G. Hunt, 1968: Experiments with a stratospheric general circulation model. I. Radiative and dynamic effects. Mon. Wea. Rev., 96, 477-539.
- McLean, G. S., 1957: Cloud distributions in the vicinity of jet streams. Bull. Amer. Meteor. Soc., 38, 579-583.
- Murray, R., and S. M. Daniels, 1953: Transverse flow at entrance and exits to jet streams. Quart. J. Roy. Meteor. Soc., 79, 236-241.
- Namias, J., and P. H. Clapp, 1949: Confluence theory of the high tropospheric jet stream. J. Meteor., 6, 330-336.
- Newton, C. W., 1958: Variations in frontal structure of upper-level troughs. Geophysica, 6, 357-375.
- \_\_\_\_\_, and J. E. Carson, 1953: Structure of wind field and variations of vorticity in a summer situation. Tellus, 5, 321-339.
- Nyberg, A., 1949: An aerological study of large-scale atmospheric disturbances. Tellus, 1, 44-53.

- \_\_\_\_\_, 1950: A study of vertical motion and formation of fronts and jet streams. Roy. Met. Soc., Centenary Proceedings, London, pp. 81-89.
- \_\_\_\_\_, 1953: A further study on the relation between the jet stream and cyclone formation. Tellus, 5, 316-317.
- Oliver, V. T., R. K. Anderson and E. W. Ferguson, 1964: Some examples of the detection of jet streams from TIROS photographs. Mon. Wea. Rev., 92, 441-448.
- Oort, A. H., 1964: On estimates of the atmospheric energy cycle. Mon. Wea. Rev., 92, 483-493.
- Palmen, E., 1951: The role of atmospheric disturbances in the general circulation. Quart. J. Roy. Meteor. Soc., 77, 337-354.
- Panofsky, H. A., 1970: Microscale motions. Bull. Amer. Meteor. Soc., 51, pg 75 (paper presented at conference on Motion and Dynamic of the Atmosphere, Houston, Texas).
- Raethjen, P., 1953: Dynamik der Zyklonen. Probleme der kosmischen Physik, 384 pp.
- Reed, R. J., 1955: A study of characteristic types of upper-level frontogenesis. J. Meteor., 12, 226-237.
- \_\_\_\_\_, and E. F. Danielsen, 1959: Fronts in the vicinity of the tropopause. Arch. Meteor. Geophys. Bioklim., All, 1-17.
- \_\_\_\_\_, and F. Sanders, 1953: An investigation of the development of a mid-tropospheric frontal zone and its associated vorticity field. J. Meteor., 10, 338-349.
- Reiter, E. R., 1961: Meteorologie der Strahlströme (Jet Streams), Vienna Springer, 473 pp.
- \_\_\_\_\_, 1963a: Jet Stream Meteorology. Chicago, University of Chicago Press, 515 pp.
- \_\_\_\_\_, 1963b: A case study of radioactive fallout. J. Appl. Meteor., 2, 691-705.
- \_\_\_\_\_, 1964: Comments on paper by S. Penn and E. A. Martell, "An analysis of the radioactive fallout over North America in late September 1961." J. Geophys. Res., 69, 786-788.

- \_\_\_\_\_, 1969a: Mean and eddy motions in the atmosphere. Mon. Wea. Rev., 97, 200-204.
- \_\_\_\_\_, 1969b: Atmospheric Transport Processes, Part 1: Energy Transfers and Transformations. AEC Critical Review Series, Division of Technical Information, U. S. Atomic Energy Commission, 283 pp.
- \_\_\_\_\_, M. E. Glasser, and J. D. Mahlman, 1969: The role of the tropopause in stratospheric-tropospheric exchange processes. Pure Appl. Geophys., 75, 185-218.
- \_\_\_\_\_, and J. D. Mahlman, 1964: Atmospheric transport processes leading to radioactive fallout over the United States in November 1962. Radioactive Fallout from Nuclear Tests. U. S. Atomic Energy Commission, Division of Technical Information, 450-463.
- \_\_\_\_\_, and \_\_\_\_\_, 1965a: A case study of mass transport from stratosphere to troposphere, not associated with surface fallout. Atmos. Sci. Paper No. 70, Colorado State University, 54-83.
- \_\_\_\_\_, and \_\_\_\_\_, 1965b: Heavy radioactive fallout over the southern United States, November 1962. J. Geophys. Res., 70, 4501-4520.
- Riehl, H., 1962: Jet streams of the atmosphere. Technical Report No. 32, Department of Atmospheric Science, Colorado State University, 117 pp.
- \_\_\_\_\_, and D. Fultz, 1957: Jet stream and long waves in a steady rotating-dishpan experiment: Structure of the circulation. Quart. J. Roy. Meteor. Soc., 83, 215-231.
- \_\_\_\_\_, and \_\_\_\_\_, 1958: The general circulation in a steady rotating-dishpan experiment. Quart. J. Roy. Meteor. Soc., 84, 389-417.
- \_\_\_\_\_, and S. Teweles, 1953: A further study on the relation between the jet stream and cyclone formation. Tellus, 5, 66-79.
- Rossby, C. G., 1947: On the distribution of angular velocity in gaseous envelopes under the influence of large-scale horizontal mixing processes. Bull. Amer. Meteor. Soc., 28, 53-68.
- \_\_\_\_\_, and Staff Members, 1947: On the general circulation of the atmosphere in the middle latitudes. Bull. Amer. Meteor. Soc., 28, 255-280.
- Sawyer, J. S., 1956: The vertical circulation at meteorological fronts and its relation to cyclogenesis. Proc. Roy. Soc. (London), A234, 246-262.
- Starrett, L. G., 1949: The relation of precipitation patterns in North America to certain types of jet streams at the 300-millibar level. J. Meteor., 6, 347-352.

- Staley, D. O., 1960: Evaluation of potential vorticity changes near the tropopause and the related vertical motions, vertical advection of vorticity, and transport of radioactive debris from stratosphere to troposphere. J. Meteor., 17, 591-620.
- \_\_\_\_\_, 1962: On the mechanism of mass and radioactivity transport from stratosphere to troposphere. J. Atmos. Sci., 19, 450-457.
- Van Mieghem, J., 1950: Sur la circulation transversale associee a un coulant atmospherique. Tellus, 2, 52-55.
- Vuorela, L. A., 1953: On the air flow connected with the invasion of upper tropical air over northwestern Europe. Geophysica, 4, 105-130.
- \_\_\_\_\_, 1957: A study of vertical velocity distribution in some jet stream cases over western Europe. Geophysica, 6, 68-90.
- Williams, R. T., 1967: Atmospheric frontogenesis: A numerical experiment. J. Atmos. Sci., 24, 667-641.



A NUMERICAL SIMULATION OF THE ADVECTIVE AND DIFFUSIVE  
TRANSFER OF TRACE SUBSTANCES IN THE STRATOSPHERE

by

Hugh Edward Willoughby  
Lieutenant (junior grade), United States Navy

This portion of the report is based upon a thesis  
by Hugh Edward Willoughby which has been edited,  
updated and expanded for incorporation in the  
report.

## ABSTRACT

A numerical model which employs observed stratospheric winds to advect simulated tracers was developed. This model successfully reproduces many qualitative features of the observed fields of both ozone and radioactive debris. As the tracers evolve, the horizontal eddies constitute the principal process modifying the tracer zonal mean. Although the vertical eddies and the zonal mean cell are both an order of magnitude weaker than this process, the latter of these tends to always act in the same sense so that its effect becomes more important over long periods of time.

## TABLE OF CONTENTS

I.	BACKGROUND - - - - -	II-8
A.	OBSERVATIONS - - - - -	II-8
B.	PARAMETERIZED MODELS - - - - -	II-10
C.	GENERAL CIRCULATION MODELS - - - - -	II-12
II.	MODEL - - - - -	II-15
A.	BASIC EQUATION - - - - -	II-15
B.	TIME INTEGRATION - - - - -	II-22
C.	WIND DATA - - - - -	II-23
III.	EXPERIMENTS - - - - -	II-27
A.	OZONE SIMULATION - - - - -	II-27
1.	Boundary and Initial Conditions - - - - -	II-27
2.	Results - - - - -	II-28
B.	RADIOACTIVE DEBRIS SIMULATION - - - - -	II-41
1.	Boundary and Initial Conditions - - - - -	II-41
2.	Results - - - - -	II-42
IV.	CONCLUSIONS - - - - -	II-47
	BIBLIOGRAPHY - - - - -	II-48

# LIST OF FIGURES

Figure		Page
1	Ozone Mixing-Ratio at 50 and 100 mb on 20 November-	II-29
2	Ozone Mixing-Ratio at 50 and 100 mb on 25 November -	II-30
3	Ozone Mixing-Ratio at 100 mb on 30 November and 5 December - - - - -	II-31
4	Ozone Mixing-Ratio at 100 mb on 10 and 15 December -	II-32
5	Ozone Mixing- Ratio at 100 mb on 20 and 25 December-	II-33
6	Ozone Mixing-Ratio at 100 mb on 20 December for Reverse and Zero mean cells - - - - -	II-34
7	Zonal Mean Cross-Sections for Various Mean Cells on 5 December - - - - -	II-37
8	Processes Modifying the Zonal Mean Ozone Mixing- Ratio Field - - - - -	II-38
9	Radioactive Tracer Distributions at 100 mb on 18 and 20 November - - - - -	II-43
10	Radioactive Tracer Distributions at 100 mb on 22 and 24 November - - - - -	II-44
11	Zonal Mean Radioactive Tracer Distribution Cross- Sections- - - - -	II-45

# LIST OF SYMBOLS

$b_1-b_6$	Ratio of the time-step to the corresponding characteristic time
$b_7$	Ratio of the advection time to the diffusion time
$f(m^l, \omega^l, u^l, v^l)$	A function representing the derivative of mixing ratio due to the combined effects of diffusion and advection
$i$	Lattice index corresponding to pressure
$j$	Lattice index corresponding to latitude
$k$	Lattice index corresponding to longitude
$K_1$	Vertical eddy diffusivity
$K_2$	Horizontal eddy diffusivity
$l, n$	Lattice indices corresponding to time
$m$	Tracer mixing-ratio
$\bar{m}$	Local mean $m$
$m^*$	Departure of $m$ from $\bar{m}$
$m_{i,j,k}^n$	Value of $m$ at a lattice point $(i, j, k, n)$
$p$	Pressure
$R$	Earth's radius
$t$	Time
$u$	Zonal wind velocity
$v$	Meridional wind velocity
$x^n$	Dummy variable in time integration
$\delta t$	Time step
$\delta p$	Pressure increment

$\delta\phi$	Latitude increment
$\delta\lambda$	Longitude increment
$\phi$	Latitude
$\lambda$	Longitude
$\tau_1$	Vertical advection time
$\tau_2$	Meridional advection time
$\tau_3$	Zonal advection time
$\tau_4$	Vertical diffusion time
$\tau_5$	Meridional diffusion time
$\tau_6$	Zonal diffusion time
$\omega$	Vertical motion in pressure coordinates = $\frac{dp}{dt}$
$\omega_0, u_0, v_0$	Non-dimensionalizing constants for the wind velocities
$\bar{\omega}, \bar{u}, \bar{v}$	Local mean wind velocities
$\omega^*, u^*, v^*$	Departures of the wind velocities from the local mean
$\tilde{\omega}, \tilde{u}, \tilde{v}$	Zonal mean wind velocities
$\omega', u', v'$	Non-dimensionalized wind velocities
$\omega'', u'', v''$	Wind field with natural zonal mean replaced by an arbitrary zonal mean
$\omega_{i,j,k}^n, u_{i,j,k}^n$	Non-dimensionalized wind field tabulated at a lattice point (i, j, k, n)
$v_{i,j,k}^n$	
$\Omega, v$	Arbitrary zonal mean v and $\omega$

### ACKNOWLEDGMENT

The author wishes to express his gratitude to Professor Jerry D. Mahlman for making his wind data available, as well as for his help, advice and constructive criticism during the formulation and execution of this research; and to Professor R. T. Williams for his suggestions concerning the manuscript. Thanks are also extended to Mr. James Cerullo and Mr. Michael McDermet for drafting the figures, and to the Computer Facility at the Naval Postgraduate School for its assistance with the numerical computations.

## I. BACKGROUND

### A. OBSERVATIONS

The study of trace substance transport in the stratosphere can provide many useful insights into the dynamics of that region. The history of an evolving inert tracer depends upon its initial state and upon several statistical properties of the wind field. In the stratosphere, unprocessed observations of the wind field are not always adequate to reveal these rather subtle characteristics of the general circulation. In addition to observations of the wind, there exist some observations of the distributions of such natural tracers as ozone and radioactive debris. These observations may be used to extend the available data base, and theories of the general circulation may be tested by requiring them to simulate the advection of natural tracers.

The influence of stratospheric transport processes was first noticed when the early spectrophotometer observations of Dobson and his co-workers (Dobson et al. 1928) revealed that the distribution of total atmospheric ozone has the following characteristics:

1. The total amount of ozone per unit area increases from the equator toward the poles.
2. In high latitudes this quantity varies with season, exhibiting a pronounced maximum in late winter or early spring.
3. No apparent correlation exists between total ozone and solar activity.



4. Total ozone is correlated with the passage of upper-level synoptic systems, attaining positive departures from its long-term mean in the lows and negative departures in the highs.

Dobson's observations are consistent with those obtained by the 81 station network in the Soviet Union and reported by Bozkov (1968). These observations indicate that:

1. Minimum total ozone occurs at 10 N.
2. Maximum total ozone occurs at 60 to 70 N, with values decreasing toward both the equator and the pole.
3. The maximum zonal mean gradient of total ozone occurs between 30 and 60 N.
4. The total ozone tends to have a wavelike distribution in the horizontal with low values occurring over the western portions of continents and high values over the eastern portions.

The photochemical theory of ozone formation (See Craig, 1965) predicts that, at photochemical equilibrium, the distribution of total ozone should attain a maximum in low latitudes at the subpolar point and increase toward the poles. Brewer (1949) and Dobson (1956) attempt to reconcile this theory with observation by postulating a mean cell with ascending motion in low latitudes, northward advection in the high mid-latitude stratosphere, descent near the pole, and a return circulation at low levels in mid-latitudes. This circulation supposedly carries the ozone, which is generated by solar ultraviolet radiation in low latitudes,

northward and downward into the lower polar stratosphere where it accumulates since there it is protected from photodissociation.

The Brewer-Dobson theory is seriously challenged by airborne filter observation of the distribution of Tungsten-185 from the Hardtack nuclear tests (Feely and Spar, 1960). The center of concentration of this debris remained at 50 mb and nearly at the latitude of injection. The cloud did not migrate northward and downward, but rather spread in the meridional plane in such a manner that the isopleths of concentration sloped downward from the equator toward the pole.

#### B. PARAMETERIZED MODELS

Reed (1950) and Normand (1953) note that stratospheric troughs are regions of both high temperature and high total ozone. This leads them to postulate that, since both potential temperature and ozone mixing ratio increase upward, the lows must be regions of descending motion and the highs regions of ascent. Furthermore, the troughs and ridges move more slowly than the wind so that horizontal advection shifts the centers of greatest mixing-ratio departure downwind from the associated pressure system. Because the wind almost always has a westerly component in the winter season, the ozone maxima lie in the southerly winds east of the troughs and the minima are east of the ridges in northerly winds. Thus, the departures of both temperature and mixing-ratio are explained in terms of the systematic interaction between horizontal and vertical advection. High mixing-ratio and temperature are accompanied

by descent and poleward motion while low values of these two quantities occur with rising and equatorward motion.

Citing earlier work by Dobson (1960), Newell (1961) carries this line of reasoning one step further. He explains the poleward slope of the isopleths by invoking eddy mixing in which northward motion is correlated with descent and southward motion with ascent. In the same paper he computes the flux of ozone by correlating total ozone with the winds at 12-18 km in the maximum ozone layer. He finds that 90 percent of his computed flux is due to large-scale eddies and that the total flux is more than adequate to explain observed changes in the distribution.

Prabhakara (1961) generates zonal mean ozone distributions which depend upon the interaction of photochemistry, a mean cell that descends near the pole, and large-scale eddies parameterized as anisotropic diffusion. His results, which are in good qualitative agreement with observation, show that such transport processes can explain many departures from photochemical equilibrium.

In contrast to Prabhakara's work, in which the principal axis of eddy diffusion is horizontal, there have been a number of models simulating the transport of radioactive debris with anisotropic diffusion schemes in which the principal axis is inclined to the horizontal (Reed and German, 1965; Davidson, et al., 1965; Seitz, et al., 1968; and Fairhall and Reed, 1968). In such models it is assumed that the northward-downward velocity correlation in the large-scale eddies can be parameterized in terms of

a diffusion tensor whose principal axis slopes downward toward the pole. This means that the tracer is presented with a path of least resistance parallel to the observed slope of the isopleths of mixing ratio in the real atmosphere. In order to keep the tracer on these sloping paths and to prevent excessive vertical spreading, it is necessary to make the vertical component of the diffusion tensor much smaller than that along the principal axis. Davidson et al., (1966) used a principal diffusivity of  $4 \times 10^9 \text{ cm}^2 \text{ sec}^{-1}$  and a vertical diffusivity of about  $10^4 \text{ cm}^2 \text{ sec}^{-1}$ . However, since characteristic horizontal distances are on the order of  $10^3 \text{ km}$  while vertical distances are about  $1 \text{ km}$  and the speed of diffusion depends upon the square of these distances, a ratio of  $10^6$  between the two diffusivities is not physically unreasonable.

### C. GENERAL CIRCULATION MODELS

Hunt and Manabe (1968) and Hunt (1969) report the most extensive and realistic simulation of stratospheric tracers to date. In their experiments various simulated substances are introduced into the wind fields generated by a general circulation model, and the history of the numerically evolved mixing ratio fields is examined.

In the 1968 experiments inert tracers are permitted to evolve from zonally symmetric initial states. The first such tracer roughly corresponds to radioactive debris from an equatorial injection and is initially distributed in a band extending from the equator to ten degrees north with the maximum concentration at 50 mb pressure height.

The second experiment's initial state represents the distribution of ozone at photochemical equilibrium throughout the region of integration. Both tracers are treated as inert substances inasmuch that, except for removal of any tracer that finds its way into the troposphere, no sources or sinks are included in these experiments.

The simulated histories of both tracers are reassuringly similar to observations of real tracers in the atmosphere. Both the radioactive debris and the ozone begin at once to migrate northward and, to some extent, downward. Thus, the concentration at the equator decreases and, at the poles increases, so that the initial gradient becomes smaller and eventually reverses.

The actual transfer by the quasi-horizontal eddies is well illustrated by the evolution of the mixing ratio field at various horizontal levels in the model. The zonally symmetric character of the initial field quickly disappears, becoming sinusoidal with wave number four predominating as it does in the circulation used by the model. With the passage of time the waves become increasingly exaggerated, forming the mixing-ratio contours into long northward protrusions. Eventually the protrusions separate, leaving isolated islands of high concentration in northern latitudes.

Hunt (1969) reports two additional experiments with the same model and involving ozone transport with photochemical sources and sinks added. The mechanism of transfer in these studies and in those previously

discussed are very similar. In both, the mean cell, which produces a convergence of tracer into the subtropics, is opposed by an eddy divergence out of that region, with the eddies being particularly effective in transferring tracer northward in the region poleward of 30N. The principal difference, introduced by photochemistry, is the strong source in low latitudes which prevents reduction or reversal of the initial poleward gradient by replacing the ozone as fast as transport processes can remove it.

The weak link in any experiment, involving either parameterization or a general circulation model, lies in the possibly unrealistic specification of the transport processes, and its, at best, indirect relation to the actual motions in the stratosphere. In view of these difficulties, it seems instructive to compare advection of simulated tracers by actual observed winds with both observation and previous attempts to model both ozone and radioactive debris. The present study, therefore, employs actual observed stratospheric winds to advect simulated tracers in the presence of sub-grid-scale diffusion, and numerically integrates the equation of continuity for the tracer in time to obtain the evolution of an inert tracer from an arbitrary initial state.

This approach is largely independent of any preconceived ideas about the stratospheric general circulation, and so provides a third source of information intermediate between the parameterized models or the general circulation models and observations of real tracers.

## II. MODEL

### A. BASIC EQUATION

The present study follows the lead of Hunt and Manabe (1968) by numerically exploring the detailed advection of trace substances without resort to arbitrarily defined diffusion tensors. Furthermore, the winds used to accomplish this advection are based on actual observations of the real atmosphere and are not the result of a mathematical model that may or may not reproduce the properties of the actual general circulation.

The basic equation, on which this study depends, is the equation of continuity for an inert tracer without sources or sinks, expressed in flux form and spherical pressure coordinates.

$$-\frac{\partial m}{\partial t} = \frac{\partial}{\partial p} (m\omega) + \frac{1}{R \cos \phi} \frac{\partial}{\partial \phi} m v \cos \phi + \frac{1}{R \cos \phi} \frac{\partial}{\partial \lambda} m u, \quad (1)$$

where  $m$  is the mixing ratio of the tracer,  $R$  the earth's radius,  $\phi$  the geographic latitude,  $\lambda$  the longitude,  $p$  the pressure,  $\omega$  the substantial pressure derivative following an individual air parcel, and  $u$  and  $v$  the wind's eastward and northward components respectively.

The local mean of any dependent variable in (1) is defined as its average computed over a volume characteristic of the grid distance to be used in the integration. The value at any point within the region can now be represented by the sum of this mean and a departure from the mean

$$\begin{aligned} m &= \bar{m} + m^* & u &= \bar{u} + u^* \\ v &= \bar{v} + v^* & \omega &= \bar{\omega} + \omega^*, \end{aligned} \quad (2)$$

where the starred variables are the departures and the barred ones are the means. These relations are then substituted into (1) and the entire relation is averaged recognizing that, while the average of a fluctuation alone or of the product of a fluctuation with a mean vanish, the averaged product of two fluctuations does not. (See Haltiner & Martin, 1957).

$$\begin{aligned}
 -\frac{\partial \bar{m}}{\partial t} = & \frac{\partial}{\partial p} (\bar{m} \bar{\omega}) + \frac{1}{R \cos \phi} \left\{ \frac{\partial}{\partial \phi} (\bar{m} \bar{v} \cos \phi) + \frac{1}{R \cos \phi} \frac{\partial}{\partial \lambda} (\bar{m} \bar{u}) \right\} \\
 & + \frac{\partial}{\partial p} (\overline{m^* \omega^*}) + \frac{1}{R \cos \phi} \left\{ \frac{\partial}{\partial \phi} (\overline{m^* v^* \cos \phi}) + \frac{1}{R \cos \phi} \frac{\partial}{\partial \lambda} (\overline{m^* u^*}) \right\}
 \end{aligned} \quad (3)$$

The terms containing products of fluctuations are then approximated by using the Prandtl mixing-length assumption that the correlation between velocity and mixing-ratio is proportional to the gradient of mean mixing ratio as given by

$$\begin{aligned}
 \overline{m^* \omega^*} &= -K_1 \frac{\partial \bar{m}}{\partial p} & \overline{m^* v^*} &= -\frac{K_2}{R} \frac{\partial \bar{m}}{\partial \phi} \\
 \overline{m^* u^*} &= -\frac{K_2}{R \cos \phi} \frac{\partial \bar{m}}{\partial \lambda}
 \end{aligned} \quad (4)$$

The vertical and horizontal eddy diffusivities,  $K_1$  and  $K_2$ , are assumed to be constant in both space and time. This particular choice of constants, with the same eddy diffusivity in both horizontal directions and without any off-diagonal elements in the diffusivity tensor, implies that diffusion is isotropic in the horizontal plane with the axis of least diffusion oriented vertically since  $K_1 \ll K_2$ .

By substituting (4) for the eddy correlation terms in (3) and writing



the flux terms back in advective form through use of the mass continuity equation for the local mean flow, one obtains

$$\begin{aligned}
 -\frac{\partial \bar{m}}{\partial t} = & \bar{\omega} \frac{\partial \bar{m}}{\partial p} + \frac{\bar{v}}{R} \frac{\partial \bar{m}}{\partial \phi} + \frac{\bar{u}}{R \cos \phi} \frac{\partial \bar{m}}{\partial \lambda} - K_1 \frac{\partial^2 \bar{m}}{\partial p^2} \\
 & - \frac{K_2}{R^2 \cos \phi} \frac{\partial}{\partial \phi} \left( \cos \phi \frac{\partial \bar{m}}{\partial \phi} \right) - \frac{K_2}{R^2 \cos^2 \phi} \frac{\partial^2 \bar{m}}{\partial \lambda^2}. \quad (5)
 \end{aligned}$$

At this point (5) is placed in non-dimensionalized form by the following linear transformation of the velocity fields:

$$\bar{u} = u_0 u', \quad \bar{v} = v_0 v', \quad \bar{\omega} = \omega_0 \omega'. \quad (6)$$

Here the sub-zero values are constants with magnitudes ( $u_0 = v_0 = 20$  kt,  $\omega_0 = 5$  mb day<sup>-1</sup>) so chosen that the primed variables, whose variations contain the spatial and temporal changes of the velocities, are of order one. Since the equation is linear in  $\bar{m}$  no such scaling needs to be done for that variable and (5) becomes

$$\begin{aligned}
 -\frac{\partial \bar{m}}{\partial t} = & \omega_0 \omega' \frac{\partial \bar{m}}{\partial p} + \frac{v_0 v'}{R} \frac{\partial \bar{m}}{\partial \phi} + \frac{u_0 u'}{R \cos \phi} \frac{\partial \bar{m}}{\partial \lambda} - K_1 \frac{\partial^2 \bar{m}}{\partial p^2} \\
 & - K_2 \left\{ \frac{1}{R^2 \cos \phi} \frac{\partial}{\partial \phi} \left[ \cos \phi \frac{\partial \bar{m}}{\partial \phi} \right] + \frac{1}{R^2 \cos^2 \phi} \frac{\partial^2 \bar{m}}{\partial \lambda^2} \right\}. \quad (7)
 \end{aligned}$$

For solution on a digital computer, the infinitesimal derivatives in (7) have to be replaced by finite differences, thus, converting the partial differential equation into a system of algebraic equations in the mixing ratio and wind components at discrete points in the region of integration.

This procedure requires that the independent variables of the problem be expressed as multiples of small, but finite increments, so that the coordinates of a point  $(p, \phi, \lambda, t)$  become  $i, j, k$  and  $n$ ; where  $i = p/\delta p$ ,  $j = (\phi - \phi_0)/\delta \phi$ ,  $k = \lambda/\delta \lambda$  and  $n = t/\delta t$  and the values assumed by  $(p, \phi, \lambda, t)$  are required to make  $i, j, k$  and  $n$  integers. In this formalism  $\bar{m}(p, \phi, \lambda, t)$  is  $m_{i,j,k}^n$  and  $v(p, \phi, \lambda, t)$  is  $v_{i,j,k}^n$ .

Once such a coordinate system is set up, it becomes possible to approximate the time derivative by a forward difference

$$\frac{\partial \bar{m}}{\partial t} = \frac{m_{i,j,k}^{n+1} - m_{i,j,k}^n}{\delta t}, \quad (8)$$

the first order space derivatives by centered differences, for example,

$$\frac{\partial \bar{m}}{\partial p} = \frac{m_{i+1,j,k}^n - m_{i-1,j,k}^n}{2\delta p} = \frac{\Delta_i m^n}{2\delta p}, \quad (9)$$

and to use the three point approximation in place of the second order space derivatives

$$\frac{\partial^2 \bar{m}}{\partial p^2} = \frac{m_{i+1,j,k}^n - 2m_{i,j,k}^n + m_{i-1,j,k}^n}{(\delta p)^2} = \frac{\Delta_i^2 m^n}{(\delta p)^2}. \quad (10)$$

The  $\Delta$  operator always applies at the point  $i, j, k$ ; although the space subscripts are usually omitted to simplify the notation. The subscript on the operator denotes the coordinate direction along which the difference is to be taken and the superscript the order of that difference.

With all the derivatives replaced by finite differences and after

multiplication through by  $\delta t$ , (7) becomes

$$\begin{aligned}
 m^{n+1} = m^n & - \left[ \frac{\omega_o \delta t}{2\delta p} \right] \omega^l \Delta_1 m^l - \left[ \frac{v_o \delta t}{2R\delta\phi} \right] v^l \Delta_j m^l \\
 & - \left[ \frac{u_o \delta t}{2R\delta\lambda} \right] \frac{u^l \Delta_k m^l}{\cos(\phi_o + j\delta\phi)} + \left[ \frac{K_1 \delta t}{(\delta p)^2} \right] \Delta_1^2 m^l \\
 & + \left[ \frac{K_2 \delta t}{R^2 (\delta\phi)^2} \right] \frac{\Delta_j (\cos(\phi_o + j\delta\phi) \Delta_j m^l)}{\cos(\phi_o + j\delta\phi)} \\
 & + \left[ \frac{K_2 \delta t}{R^2 (\delta\lambda)^2} \right] \frac{\Delta_k^2 m^l}{\cos^2(\phi + j\delta\phi)} \quad (11)
 \end{aligned}$$

where the  $n$  and  $n + 1$  superscripts denote the base time level and the newly generated time level, respectively, and the  $l$  superscript, which also denotes time, can take on only one or the other of these two values.

Each of the factors in brackets in (14) is the product of  $\delta t$  with a collection of constants which, when combined, has the units of reciprocal time. Thus, each bracket forms the dimensionless ratio of the time-step to a time characteristic of the particular process changing the mixing ratio. For example, in the first term  $2\delta p/\omega_o$  represents the vertical advection time or in the fourth term  $(\delta p)^2/K_1$  is the meridional diffusion time.

Since each of these factors is a constant, (11) is simplified by replacing them with single quantities to reproduce the simpler form

$$\begin{aligned}
m^{n+1} = m^n &- b_1 \omega^\ell \Delta_1 m^\ell - b_2 v^\ell \Delta_j m^\ell - [b_3 / \cos(\phi_0 + j\delta\phi)] u^\ell \Delta_k m^\ell \\
&+ b_4 \Delta_1^2 m^\ell + [b_5 / \cos(\phi_0 + j\delta\phi)] \Delta_j \cos(\phi_0 + j\delta\phi) \Delta_j m^\ell \\
&+ [b_6 / \cos^2(\phi_0 + j\delta\phi)] \Delta_k^2 m^\ell
\end{aligned} \tag{12}$$

The pressure increment is 12.5 mb, that of latitude  $5^\circ$  and that of longitude  $10^\circ$ . With this information the first three advection times are evaluated to give:

$$\begin{aligned}
\tau_1 &= 2\delta p / \omega_0 = 5 \text{ days}, \quad \tau_2 = 2R\delta\phi / v_0 = 1.25 \text{ days}, \\
\tau_3 &= 2R\delta\lambda / u_0 = 2.5 \text{ days}.
\end{aligned} \tag{13}$$

The value of  $\tau_3$  does not represent the actual advection time entering into the calculation, since a factor of  $\cos \phi$  is not included in its evaluation. This factor represents the decrease in advection time, as the distance corresponding to  $\delta\lambda$  shrinks with approach to the pole. Since the cosine of the latitude varies from .819 at 35 N to .087 at 85 N, the actual zonal advection time changes by nearly an order of magnitude over the region of integration.

Since a state of nearly total ignorance exists in regard to the actual magnitudes of the eddy diffusivities in the stratosphere, the diffusion time along a given axis is set to a simple multiple of the advection time along the same axis. In this study, the multiple (called  $1/b_7$ ) is chosen to be eight. This means that the parameterized diffusion

can remove departures from equilibrium  $1/8$  as fast as advection operating by itself. This assumption leads to the following values for the diffusion times:

$$\begin{aligned}\tau_4 &= 40 \text{ days,} & \tau_5 &= 5 \text{ days,} \\ \tau_6 &= 20 \text{ days.}\end{aligned}\tag{14}$$

The difference of a factor of four between  $\tau_5$  and  $\tau_6$  arises because  $\delta\lambda = 2\delta\phi$ . Since the horizontal diffusion is assumed to be isotropic, the transport must occur four times as rapidly over half the distance.

The values of  $K_1$  and  $K_2$ , corresponding to  $\tau_4$  and  $\tau_5$ , are  $1 \times 10^4 \text{ cm}^2 \text{ sec}^{-1}$  and  $4.5 \times 10^8 \text{ cm}^2 \text{ sec}^{-1}$  compared to  $2 \times 10^4$  and  $1 \times 10^{10}$  used in Prabhakara's parameterized study. That author's definition of diffusion and the one used here are essentially different. In the former case the diffusion was used to simulate transfer by the large-scale eddies, while in this study it has only to account for transfer by fluctuations too small to be represented in synoptic-scale data. The similarity between the two vertical diffusivities is unfortunate; one would have preferred to use a vertical diffusivity that differed from that of Prabhakara by a factor of at least ten because, in the parameterized studies, diffusion is called upon to provide much of the transport that advection accomplishes in this model.

The entire treatment of diffusion is rather artificial, but since it

serves as a computational smoother, its effect can not be minimized without sacrificing numerical stability.

## B. TIME INTEGRATION

Integration in time is accomplished using a backward corrected Euler scheme (see Kurihara, 1965). If the advective and diffusive terms in (12) may be replaced by  $f(m^n, \omega^n, v^n, u^n)$ , this scheme may be represented as:

$$m^{\ell} = m^n + f(m^n, \omega^n, v^n, u^n), \quad (15)$$

$$m^{n+1} = m^{\ell} + f(m^{\ell}, \omega^{n+1}, v^{n+1}, u^{n+1}). \quad (16)$$

Given the field of  $m^n$  and the wind at the  $n$  time level,  $m^{\ell}$  is computed from (15). Then,  $m^{\ell}$  and the winds at the  $n+1$  time level are used in (16) to obtain  $m^{n+1}$ . Therefore,  $m^{n+1}$  is first predicted using a forward difference, and then corrected with a backward difference, the entire process repeated at each successive time level until  $m$  is known for the entire period of interest.

According to Kurihara (1965), if this method is applied to the one dimensional advection equation,

$$x' = x^n + b\Delta_1 x^n \quad (17)$$

$$x^{n+1} = x^n + b\Delta_1 x^{\ell}, \quad (18)$$

stability will result for  $b \leq 1$ . By experiment, it was discovered that optimum results are obtained by using a time step  $\delta t = 1/48$  day, producing the following values for the  $b$ 's ( $b_7 = 1/8$ ):

$$b_1 = 4.17 \times 10^{-3}, b_2 = 1.67 \times 10^{-2}, b_3 = 8.33 \times 10^{-3},$$

$$b_4 = 0.52 \times 10^{-3}, b_5 = 4.17 \times 10^{-3}, b_6 = 1.04 \times 10^{-3}. \quad (19)$$

These values are obviously much less than one, but the factor of  $1/\cos \phi$  makes the coefficient of the third term much larger near the pole. At 80 N, the most northerly point at which (15) and (16) are applied,  $\cos \phi = .174$ , so  $b_3/\cos \phi = 0.047$  is still well within the region of stability. Unfortunately, a longer time-step drastically reduces the quality of the results. Although no theoretical investigation is attempted, this may be caused by either mass imbalances in the wind data or by the variability of the space increment resulting from the  $\cos \phi$  effect.

### C. WIND DATA

The wind data, used by Mahlman (1967, 1969), are employed in the advective terms of (11). The data, which cover the 41 day period from 15 November until 25 December 1958, consist of the three wind components and the fields of temperature and geopotential height, tabulated at 50 and 100 mb for the region from 40 to 80 N. Originally, the two horizontal wind components, as well as the temperature and height fields, were extracted directly from the Weather Bureau (1963) stratospheric daily chart series for the IGY, while the  $\omega$ 's were computed from the other fields, using the thermodynamic equation with an assumed diabatic heating rate (Mahlman, 1967).

During the early portion of the period of data coverage, the polar

night vortex is intensifying with the circulation dominated by a cold low over northern Asia. Then, on 21st of November the flow undergoes a pulsation or "minor breakdown", becoming more meridional in character and remaining disturbed until 11 December when the vortex re-stabilizes with an important wave number two component. During this last period one trough lies over Asia and the other over North America with the two intervening ridges over the oceans.

With the exception of the ten-day period from 5 December until 15 December, the mean cell in these data has rising motion over the pole and descent in middle latitudes (Mahlman, 1969). Even during the time in December when the vertical motion reverses at the pole, descent takes place only in the immediate region of the pole with rising motion continuing in the 60 and 70 N band. This means that, except for that brief period in December, the mean cell operates in the exact opposite sense to that required by the Brewer-Dobson theory.

Unfortunately, the data are tabulated every 24 hours on only two pressure surfaces, and for a somewhat coarser horizontal grid. This means that the data has to be extended by extrapolation and interpolation in both space and time. First, using the thermal wind equation, the horizontal winds are extrapolated upward to 12.5 mb and downward to 150 mb, and the  $\omega$ 's at these two levels are assumed to be zero. This is done at every point in the horizontal that carries the initial data fields (every  $40^\circ$  of longitude at 80 N, every  $20^\circ$  at 70 N, and every  $10^\circ$  of longitude at



60, 50 and 40 N). Values for every  $10^{\circ}$  longitude at 70 N and 80 N are generated by linear interpolation between the tabulated values. The same process is applied again to produce winds at odd multiples of five degrees of latitude. Finally, a cubic Lagrange interpolating polynomial is fitted to the data at each horizontal grid intersection for the four levels and evaluated at the intermediate pressure levels to complete the wind field for each day. The wind for each time step is obtained from the daily wind fields by simple linear interpolation in time.

The wind data require still more treatment before they are suitable for use in the integration scheme. Due to inaccuracies in observation and processing, the probable errors in the  $v$  wind component are at least as large as the real mean cell. Furthermore, the omegas generated by the thermodynamic method are not necessarily consistent with the divergences of the horizontal wind. Mass imbalances in the large-scale eddies, while undesirable, tend to cancel each other when integrated over the entire region; but a mean cell with spurious mass sources may seriously distort the results of the computation. It was decided to remedy the situation by removing the natural mean cell and replacing it with an artificial time independent one, which exactly satisfied the zonally-averaged continuity equation. The following transformation accomplishes this end:

$$\begin{aligned} u_{i,j,k}^{n\ell} &= u_{i,j,k}^{\ell} \\ v_{i,j,k}^{n\ell} &= v_{i,j,k}^{\ell} - \tilde{v}_{i,j}^{\ell} + v_{i,j}^{\ell} \\ \omega_{i,j,k}^{n\ell} &= \omega_{i,j,k}^{\ell} - \tilde{\omega}_{i,j}^{\ell} + \Omega_{i,j}^{\ell} \end{aligned} \quad (20)$$

Here, the double primed quantities are the new values, the unprimed, the old, the tilded, the zonal mean, old values, and the capitals, the contrived mean. This new mean is usually run with ascent at the poles, although some experiments were run with the cell reversed for comparison. Typical magnitudes for the new mean were on the order of a knot for  $V$  and  $.5 \text{ mb day}^{-1}$  for  $\Omega$ . The new cell was constant in time and no attempt was made to introduce time variations resembling those of the natural mean cell.

While use of an artificial mean cell seems to introduce the very element of arbitrariness that was avoided through employing observed winds, it should be pointed out that this approach both permits experimentation with mean cells of differing character and allows use of mean circulations that are more or less consistent with heat and momentum considerations.

### III. EXPERIMENTS

#### A. OZONE SIMULATION

##### 1. Boundary and Initial Conditions

The behavior of stratospheric ozone is simulated by the evolution of an inert tracer from a zonally symmetric initial state roughly corresponding to the observed zonal mean ozone distribution (Hering, 1960). Throughout the integration, the observed initial values at 12.5 and 150 mb are retained at the top and bottom boundary points. This condition can be justified, since it is assumed that the value at 12.5 mb is controlled only by photochemistry and is time-independent except for diurnal and seasonal variation which are not reproduced. Similarly the mixing-ratio at 150 mb is assumed to represent a constant equilibrium between downward transport and destruction in the troposphere.

Originally, it was the intention to parameterize advection into the region from the tropics by retaining the observed zonal mean values at the southern boundary points, but the final version of the model is permitted to generate its own southern boundary condition inasmuch as the points at 35 N are all set to the generated zonal mean of those at 40 N.

Near the pole, the cosine of the latitude becomes small, causing an apparent singularity in the prognostic equation. This difficulty can be avoided by applying a cartesian version of the prognostic equation at the pole; however, a simpler solution is suggested by the treatment of the

southern boundary, so the values at 85 N are set to the zonal mean of those at 80 N.

These boundary conditions imply that the system is not closed, since boundary fluxes can occur through all surfaces of the region of integration. A horizontal flux through the southern boundary is physically reasonable, since advection from tropical regions is an important source of mid- and high-latitude ozone. Similarly, the flux over the pole is to be expected, although the boundary scheme used does not properly simulate it; a spurious over-the-pole transfer arises which distorts the final results. The upper boundary condition allows ozone to be transported downward into the region of integration but does not permit it to leave through the top. The values at 12.5 mb are invariably higher than those in the interior of the region. Since the vertical motion is small near the upper boundary, diffusion predominates allowing the tracer to flow inward but never outward. A similar set of conditions arises at the lower boundary; except here, the boundary values are always lower than those in the interior so only outward fluxes can occur. Thus, although no source or sink terms are explicitly included in the model, the boundary conditions crudely approximate the behavior of photochemical sources in the upper stratosphere with a sink at the tropopause.

## 2. Results

Figures 1 through 6 are a series of charts portraying the ozone mixing ratio and geopotential height on the 50 and 100 mb levels at

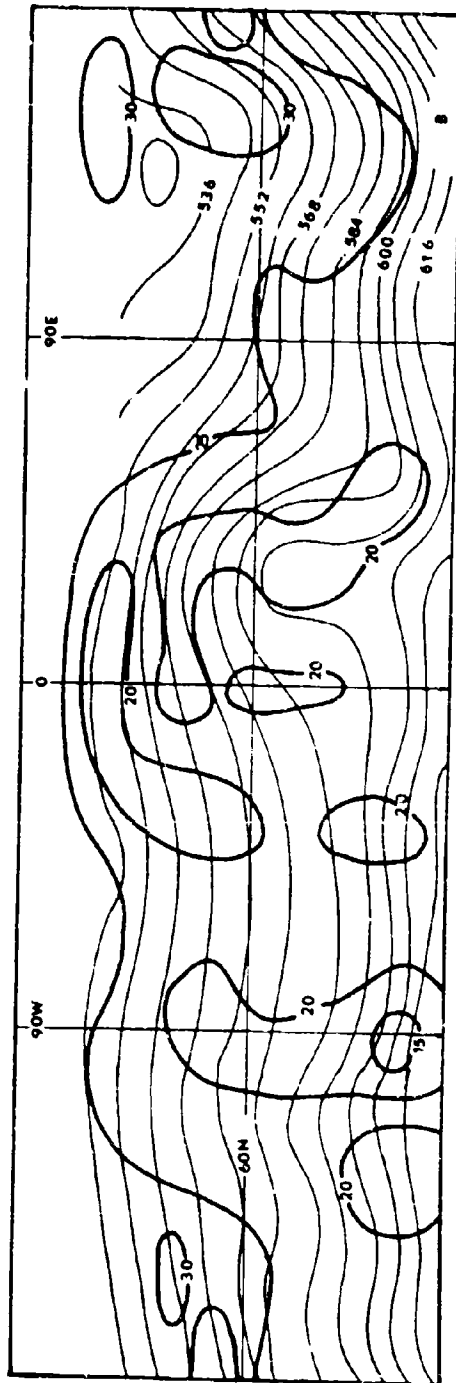
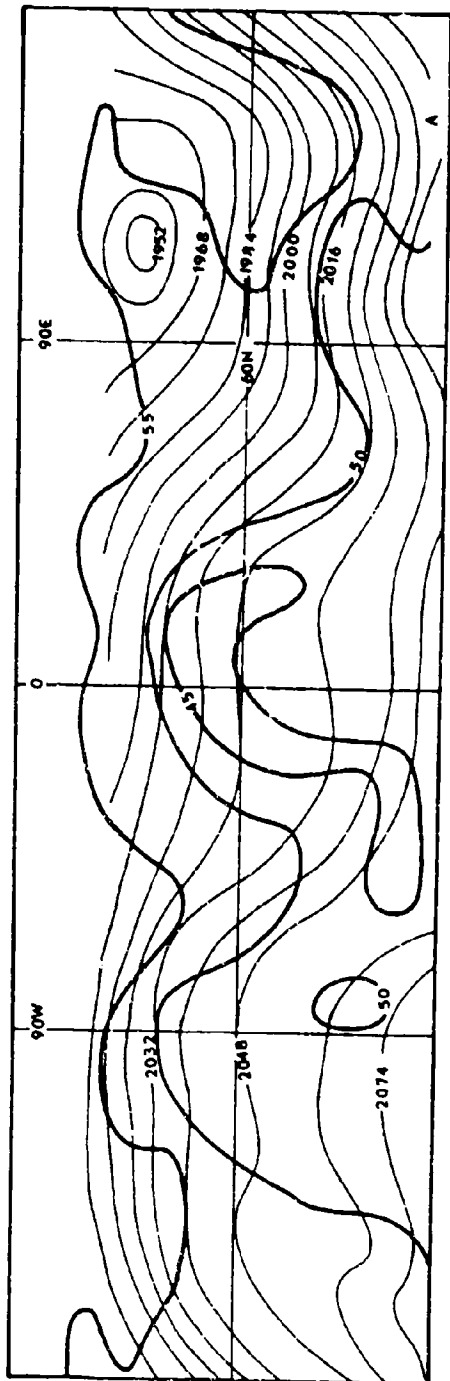
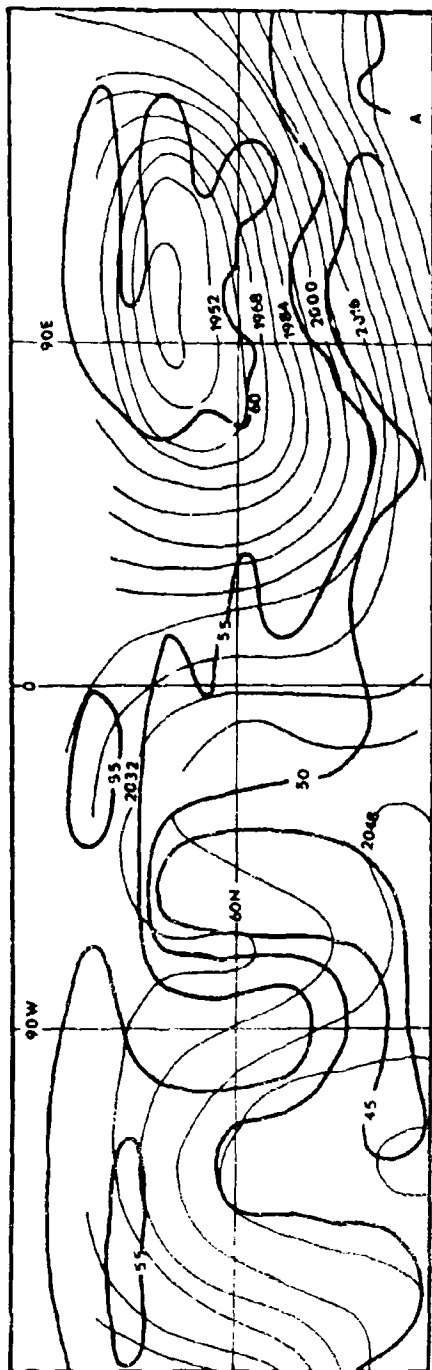


FIG. 1. Simulated ozone mixing ratio in  $10^{-7}$  gm-gm $^{-1}$  on 20 November at pressure altitudes of A: 50 mb; and B: 100 mb. Heavy lines are the mixing ratio contours while the lighter lines are geopotential height contours.



2

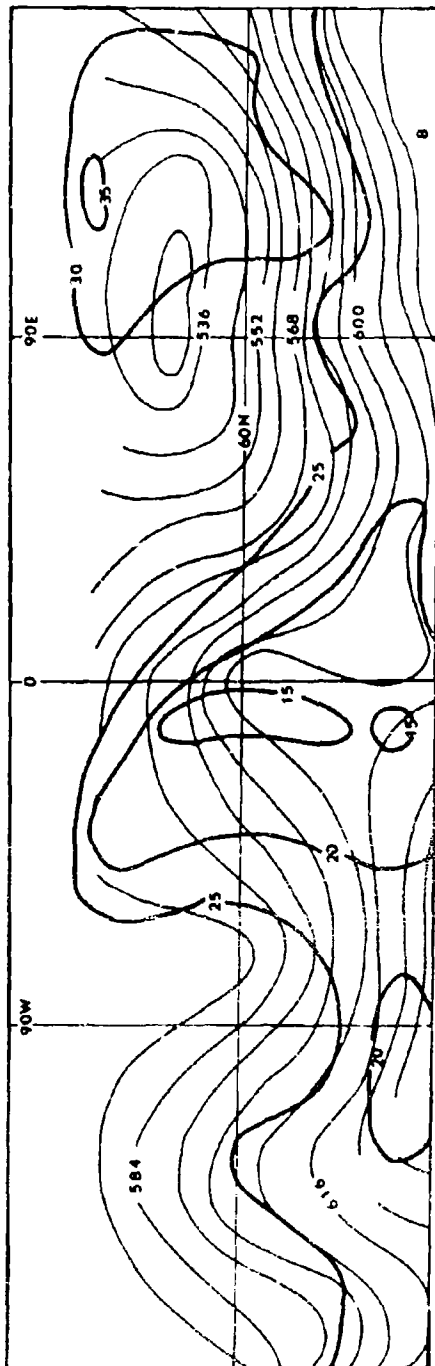
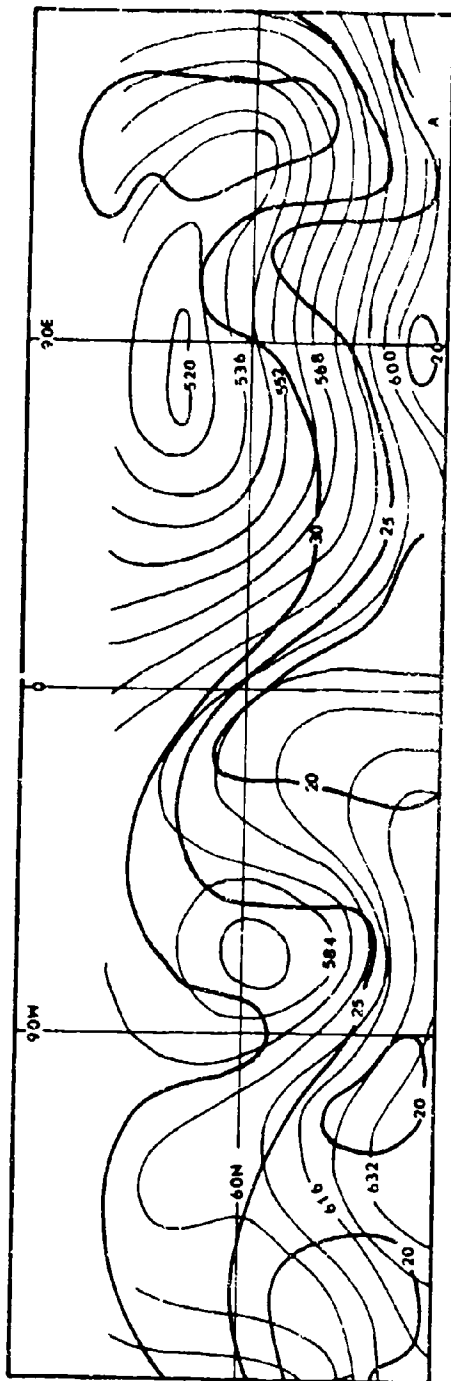


FIG. 2. Simulated ozone mixing ratio on 25 November at A: 50 mb; and B: 100 mb.



3

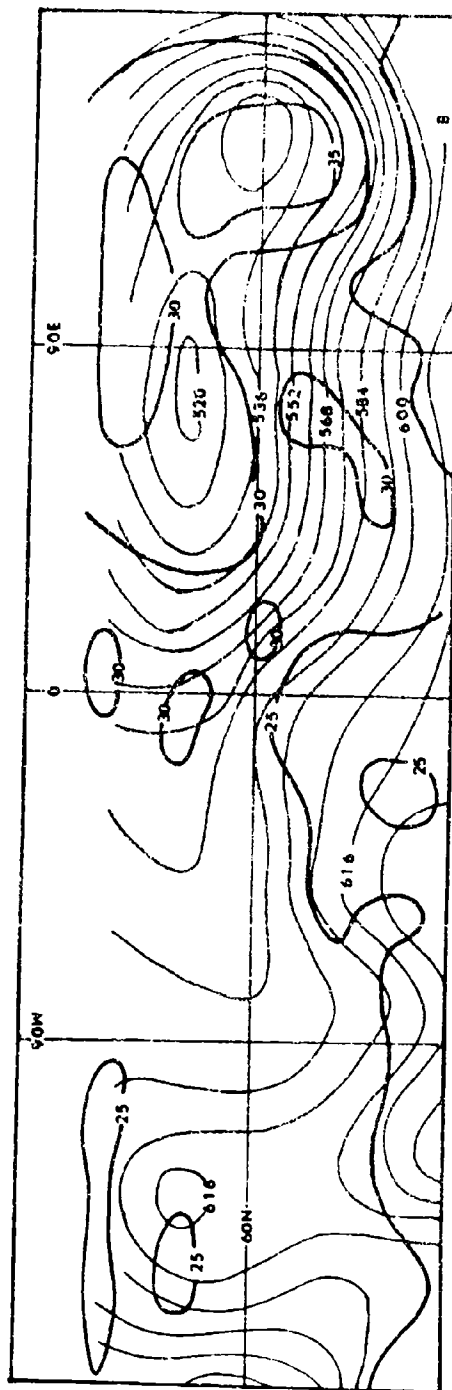


FIG. 3. Simulated ozone mixing ratio at 100 mb on A: 30 November; and B: 5 December.

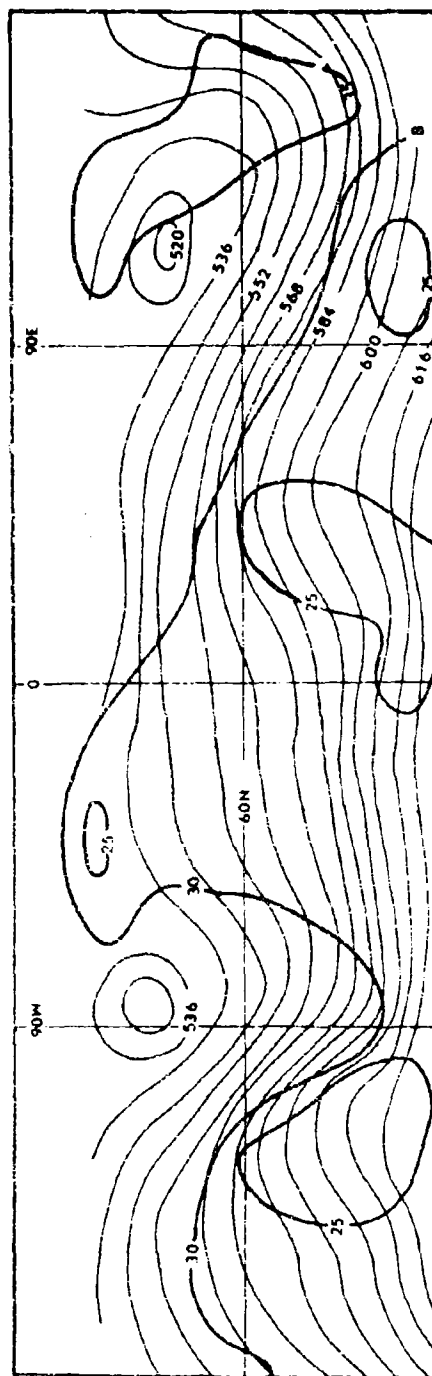
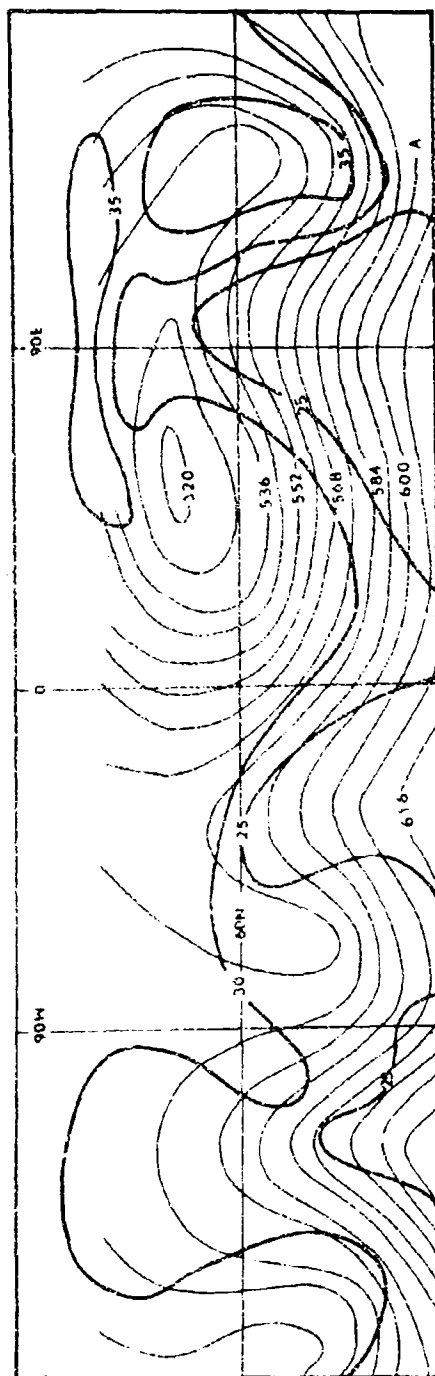
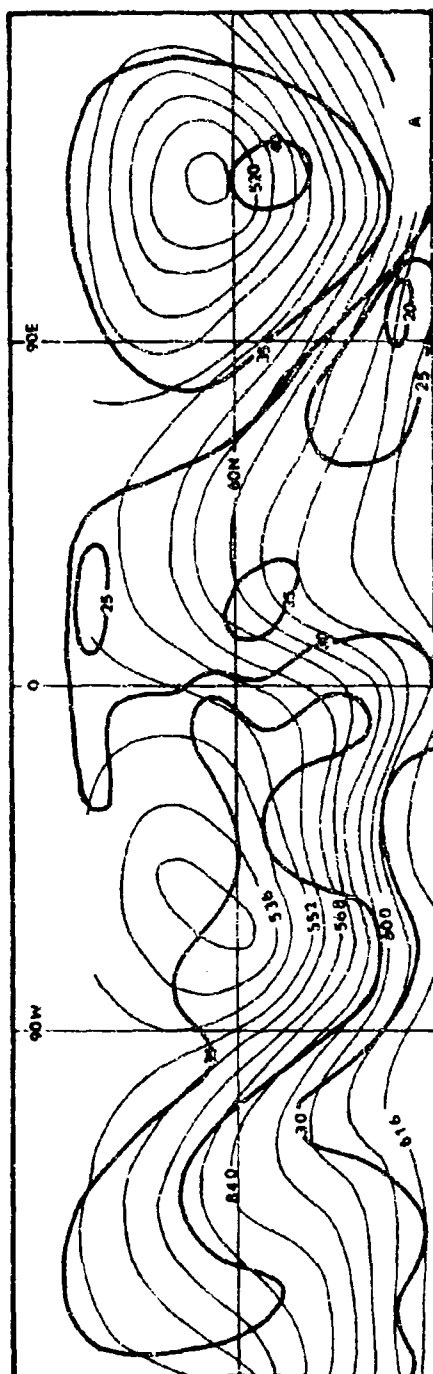


FIG. 4. Simulated ozone mixing ratio at 100 mb on A: 10 December; and B: 15 December.





5

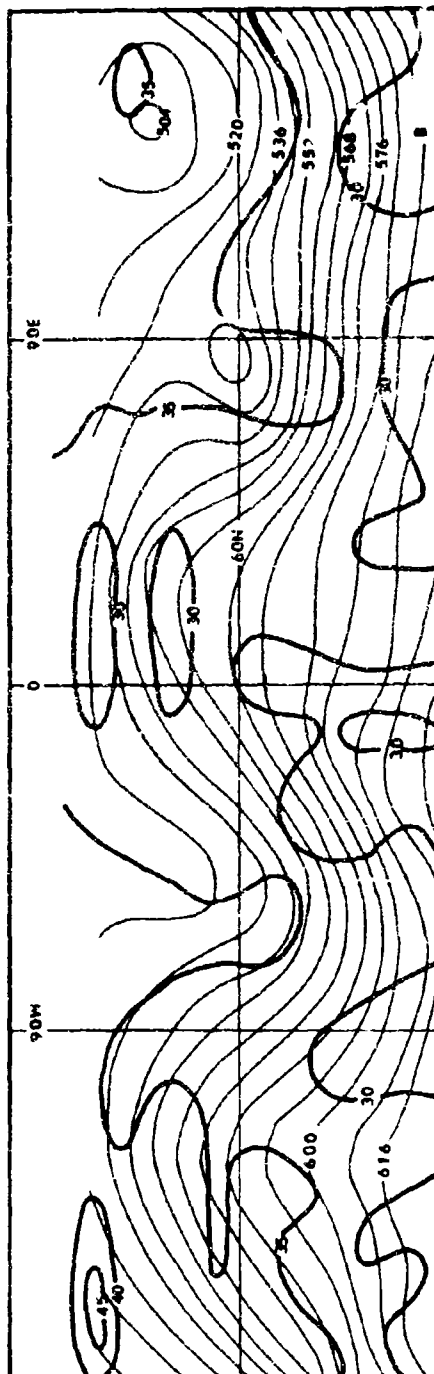


FIG. 5. Simulated ozone mixing ratio at 100 mb on A: 20 December; and B: 25 December.

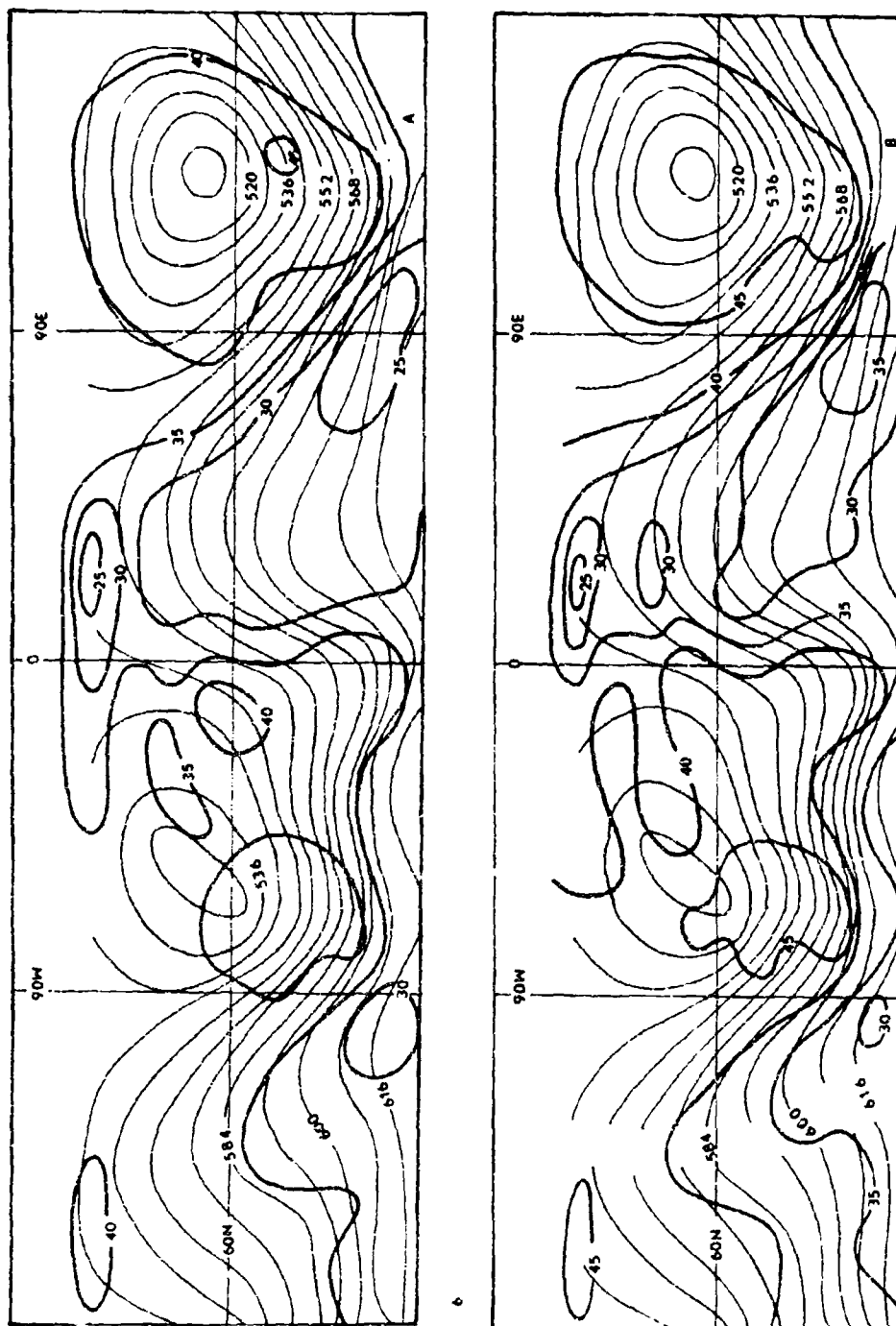


FIG. 6. Simulated ozone mixing ratio on 20 December for A: reverse mean cell;  
and B: zero mean cell.

intervals of 5 days during the period of integration. Comparison between the 50 mb and 100 mb pressure levels indicate that the degree of continuity of the ozone field between these two levels is comparable to that observed in the geopotential height field so that representation of more than one horizontal section of the ozone field is superfluous, and only the 100 mb surfaces are presented after 25 November.

These charts show a number of qualitative features that are reassuringly similar to the characteristics of the real atmospheric ozone field. Dobson's (1924) observations of ozone maxima in the troughs are reproduced. Similarly, Bozkov's (1968) observations of sinusoidal isopleths of concentration with ozone maxima in the standing troughs over continents and minima over the intervening seas appear in these fields.

At 50 mb and 60 N the normalized correlation coefficient between  $\omega$  and  $m$ , computed over the entire period of integration, is 0.22. This means that the high mixing ratios in the lows can be explained in terms of advection from above just as Reed (1950) and Normand (1953) postulated.

On the 50 mb surface the ozone mixing ratio values initially decrease from 5.3  $\mu\text{gm/gm}$  at 35 N to 3.9  $\mu\text{gm/gm}$  at 85 N while at 100 mb the initial values increase from 1.2 to 3.1 in the same interval. As the integration proceeds, the transport processes reverse the 50 mb gradient by 18 November and establish a mid-latitude maximum at 75 N by 25 November. This maximum tends to drift southward appearing most frequently at about 65 N during the latter portion of the experiment. It

is quite persistent in this latitude, but often it disappears for several days, being absent a total of 19 of the 41 simulated days. A similar maximum appears in the 100 mb profile on 2 December but it is less pronounced and not nearly so persistent in time (being present on 10 of 41 days). At both altitudes the maximum zonal mean gradient occurs south of the latitude of maximum mixing ratio, with the field being flatter over the pole. These results are consistent with Bozkov's work. Since they arise during the integration and do not represent mere persistence of the initial state, they enhance confidence in the model.

When time series of the zonal mean mixing ratio and of the various processes modifying it are considered (see FIG. 8), it is found that the horizontal eddies and horizontal diffusion are very highly correlated with the fluctuations of the mixing ratio. The other processes, the vertical eddies, the vertical and horizontal mean cells and the vertical diffusion are all about an order of magnitude smaller than these first two effects and did not produce noticeable, short-term changes in the mixing ratio.

The direction of horizontal eddy transport changes during the integration. At the beginning it is poleward, but during the pulsation of the polar night vortex it changes sign and remains negative for 22 days until the vortex begins to re-intensify. When the normalized mixing-ratio and meridional velocity correlation coefficient is computed for the

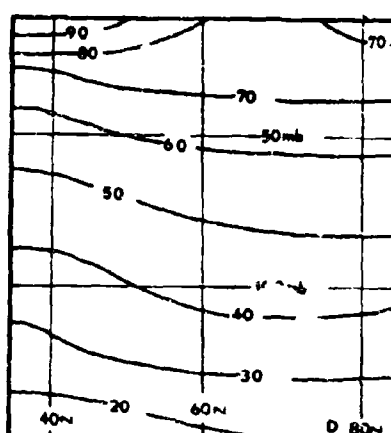
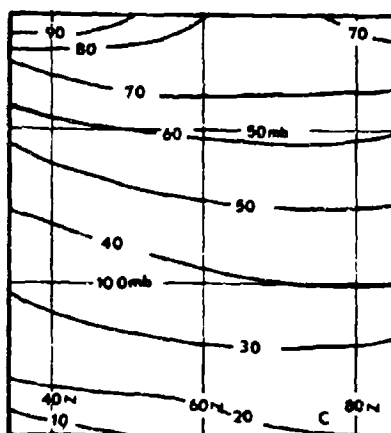
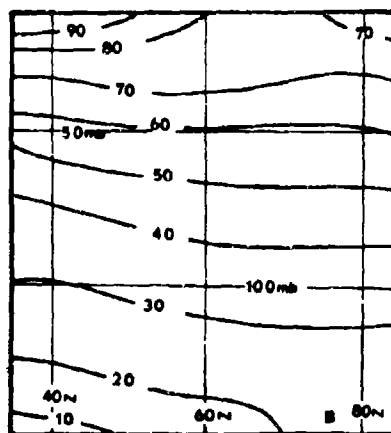
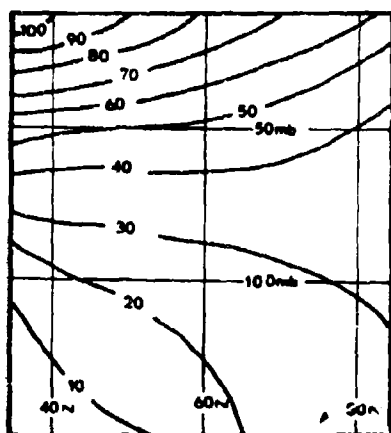


FIG. 7. Simulated zonal-mean ozone cross section in  $10^{-7} \text{ gm-gm}^{-1}$   
 A: Initial cross section; B: cross section for 20 December with mean ascent at the pole; C: for the same date with a zero mean cell; and D: for a mean cell with descent at the pole.

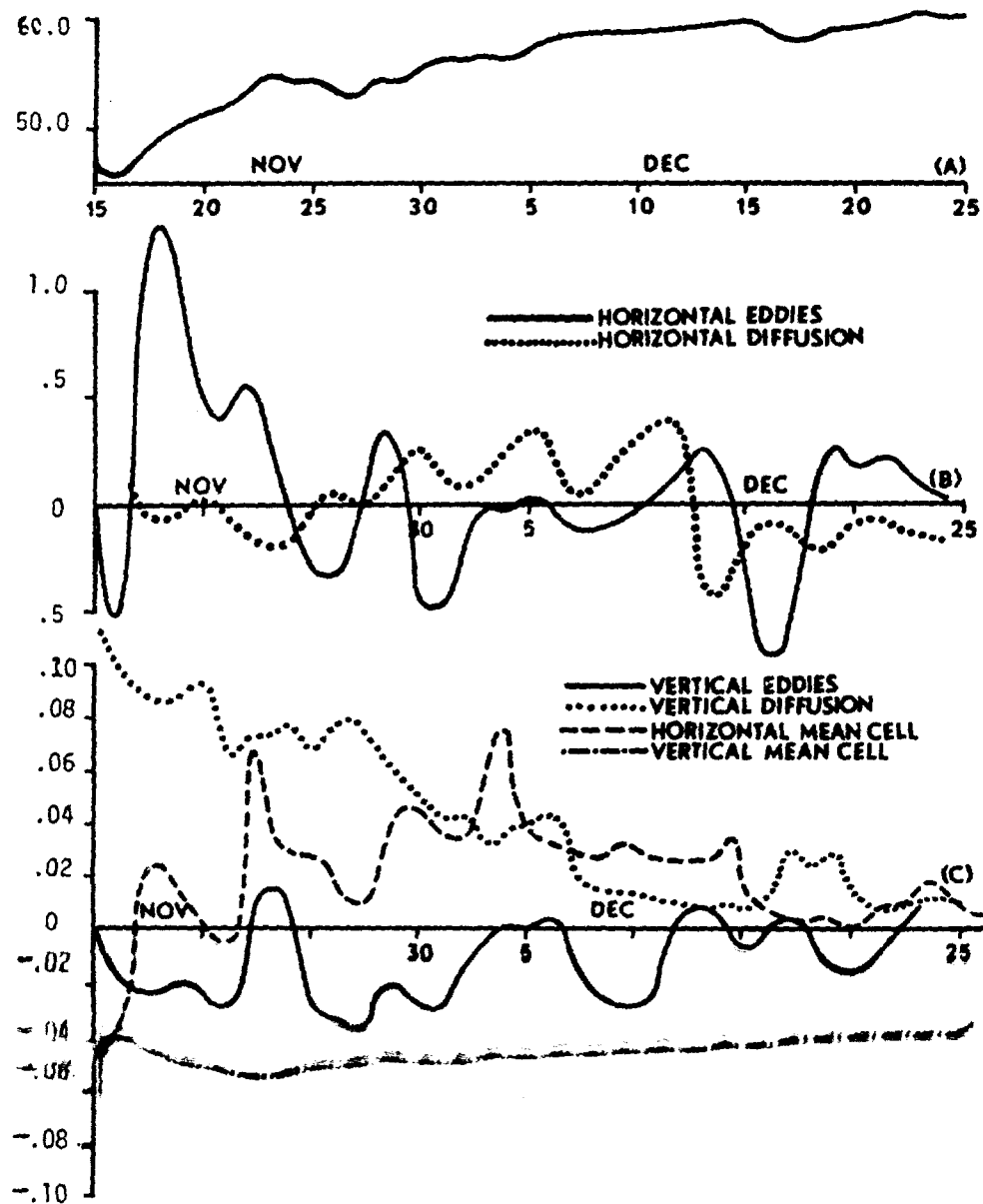


FIG. 8. A: Simulated zonal-mean ozone mixing-ratio at 60 N and 50 mb as a function of time; B: the effect in  $10^{-7} \text{ gm-gm}^{-1} \text{ day}^{-1}$  of the horizontal eddies and diffusion on the zonal-mean mixing-ratio at 60 N and 50 mb as a function of time; and C: the effect of the horizontal mean cell, and the vertical eddies, diffusion and mean cell in the same units.

entire period, its value is  $+0.023$  at 50 mb and 60 N. But when the data are stratified into poleward and equatorward transport periods, the correlation during the former is  $+0.317$  and the latter  $-0.237$ . Since the omega-mixing-ratio correlation is  $+0.22$ , this indicates that the difference in the effectiveness between the vertical and horizontal eddies is primarily caused by the smaller ratio of characteristic velocity to space increment for the former.

Because the mean cell is constant in time and the zonal mean gradient is nearly so, the sign and magnitude of the instantaneous change resulting from the mean cell, is quite persistent. This means that, while the short-term effect is small, the mean cell produces a marked change in the field when integrated over 41 days.

This effect is well illustrated by the differences among the 20 December 100 mb fields (FIG. 5 and FIG. 6). Figure 6 shows the 20 December mixing-ratio field, resulting from a zero mean cell as well as that resulting from a reversed mean cell. Comparison among these three charts indicates that in all cases the features are very similar in shape and location but the values differ as though the fields were translated by addition of a constant. This is very nearly what happened. Figure 7 shows the zonal mean cross sections for each of these three cases on 25 December as well as the initial zonal mean. Each different mean cell changes the inclination of the mixing ratio isopleths, tending to increase their slopes when sinking occurs at the pole and decrease them when rising takes place at the pole. This effect is most important

in the northern portions of the region where it moves the lines in the vertical while toward the south they remain at about the same altitude in all cases. It should be pointed out that, while this effect becomes important only after long integration times, it will eventually attain an equilibrium with the other processes and not accumulate indefinitely.

Apparently, the model seeks to attain just such an equilibrium during this simulation. At 50 mb and 60 N, the mixing ratio rises asymptotically to a value of about  $60 \cdot 10^{-7} \text{ gm/gm}^{-1}$  (see FIG. 8). The horizontal eddies, the vertical diffusion and the horizontal mean all appear to contain decaying transients that largely damp out by 10 December. Apparently about 25 days are required to recover from the disequilibrium introduced when the model is initiated from a zonally symmetric initial state.

The contribution of both components of the sub-grid-scale diffusion is disturbingly large. This phenomenon is dependent upon a completely arbitrary sub-grid-scale parameterization scheme and probably is much stronger than any real atmospheric diffusion. It is unfortunate that the diffusivities cannot be reduced without impairing the model's computational properties. The unnaturally strong diffusion may mask important advective processes and spuriously shorten the equilibrium time as well as displace the equilibrium from its true value.



## B. RADIOACTIVE DEBRIS SIMULATION

### 1. Boundary and Initial Conditions

Clouds of radioactive debris are simulated by permitting the distribution of tracer to evolve from an initial three-dimensional Gaussian distribution, centered at a point within the region of integration. It would be more satisfying to use an initial state in which all the tracer is concentrated at a single grid point, but in such experiments an undesirable computational mode is excited by the steep gradients so that the results are meaningless.

The boundary conditions imposed upon the evolving cloud of debris represent a serious problem. For the previous experiment with zonally symmetric ozone fields as an initial state, the generated zonal mean of points along the next interior latitude circle represents a reasonable boundary value. Because the point source problem is ~~asymmetrical~~, constraining the gradient at the southern boundary to zero seems to constitute a reasonable boundary condition; but computational difficulties arise in this case when the wind normal to the boundary is strong. The final solution to this problem lies in a compromise between the two approaches. Each boundary point at 35 N or 85 N is set to a weighted average of the zonal mean at the next interior parallel and the value at the adjacent point along that parallel. The weighting factors are 0.7 times the mean and 0.3 times the adjacent point at the southern boundary, and equal weights are used at the northern boundary.

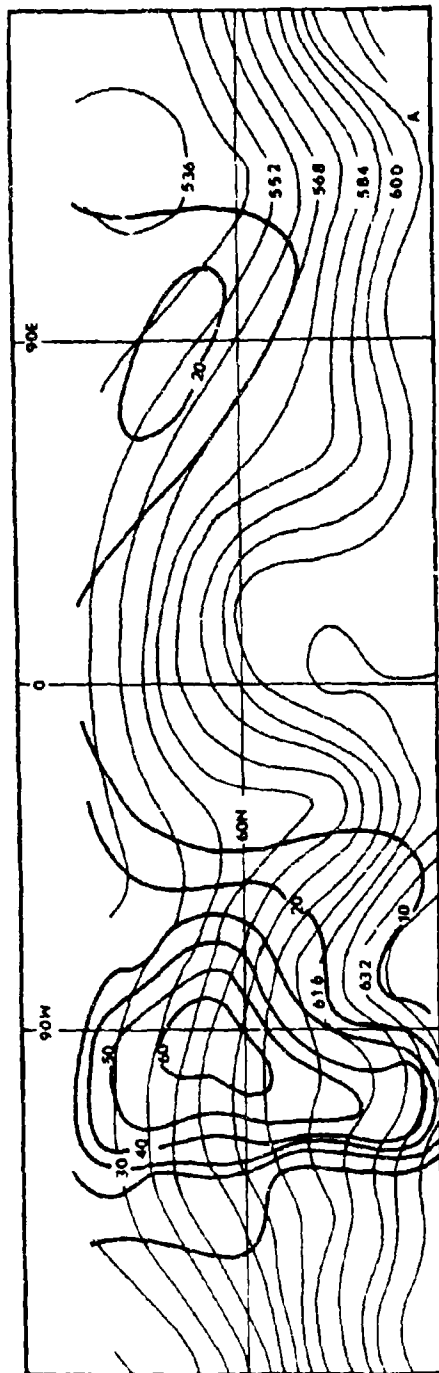
At the top and bottom of the region there is little inflow or outflow because the vertical velocities are small. Furthermore, these regions are fairly remote from the centers of concentration. This means that zero gradient at 12.5 and at 150 mb constitutes a physically reasonable and numerically stable boundary condition there.

## 2. Results

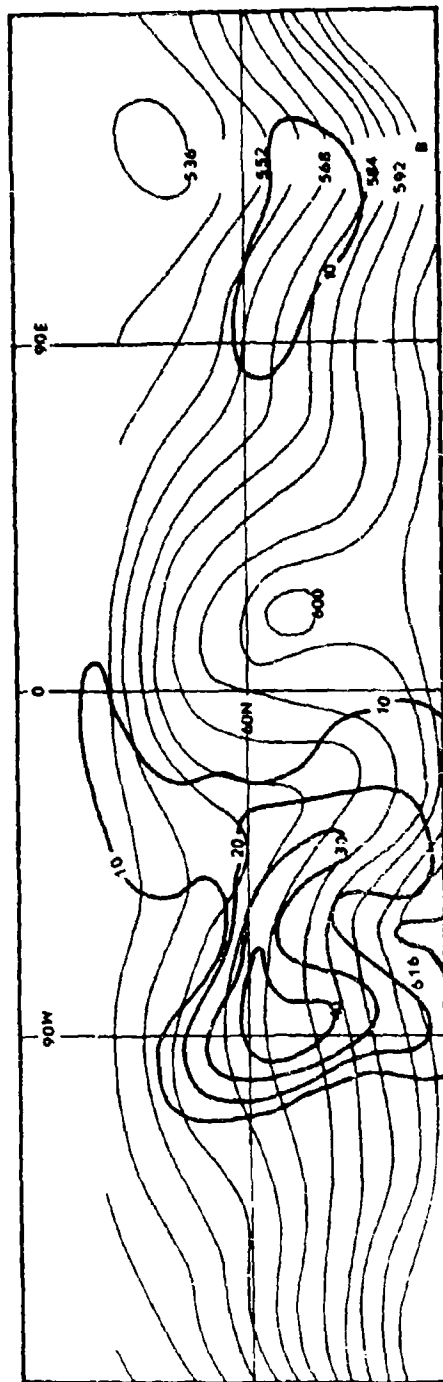
The evolution of a cloud injected at latitude 60 N longitude 140 W with initial standard deviation  $10^\circ$  of latitude,  $20^\circ$  of longitude and 25 mb of pressure was simulated for eleven days (See FIGS. 9, 10). This initial position lies in the almost purely zonal flow in the ridge over the Northern Pacific so that the main mass of debris is carried eastward along the height contours while gradually spreading and dispersing. By 23 November the cloud has migrated about  $90^\circ$  of longitude and lies in the eastern portion of the Atlantic ridge. During this period the mixing ratio at the last closed contour decreases from 80, its initial value, to 20 (arbitrary units).

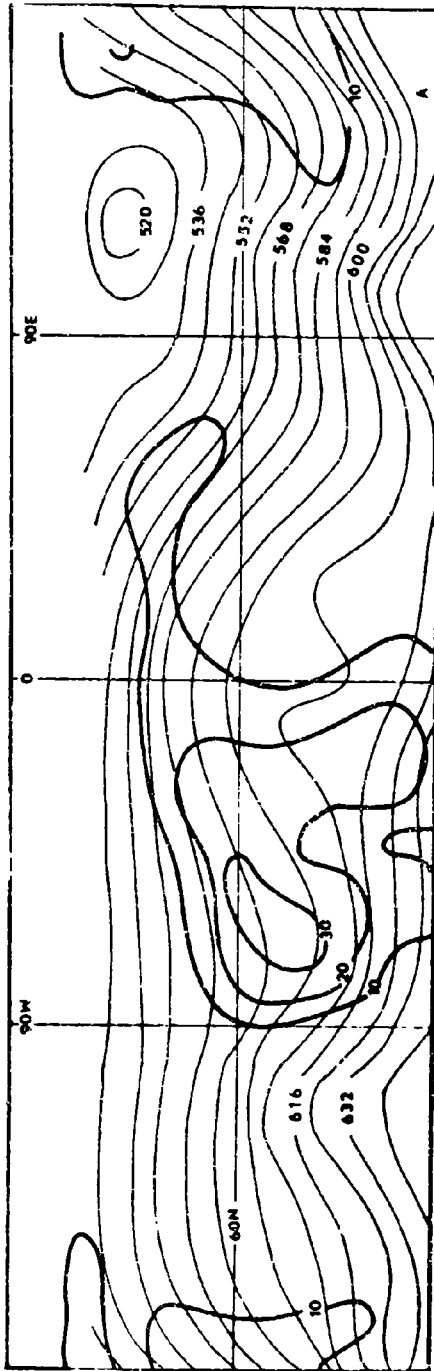
On 17 November part of the cloud is carried over the pole and then southeastward around the Siberian low. Between 19 and 21 November the mass rounds the trough and begins to move northward so that by 23 November, it has circumnavigated the pole at high latitudes and re-merged with the main cloud.

In the zonal mean, the center of the initial distribution lay at 60 N and a pressure altitude of 75 mb (See FIG. 11). As the cloud evolves,



11





12

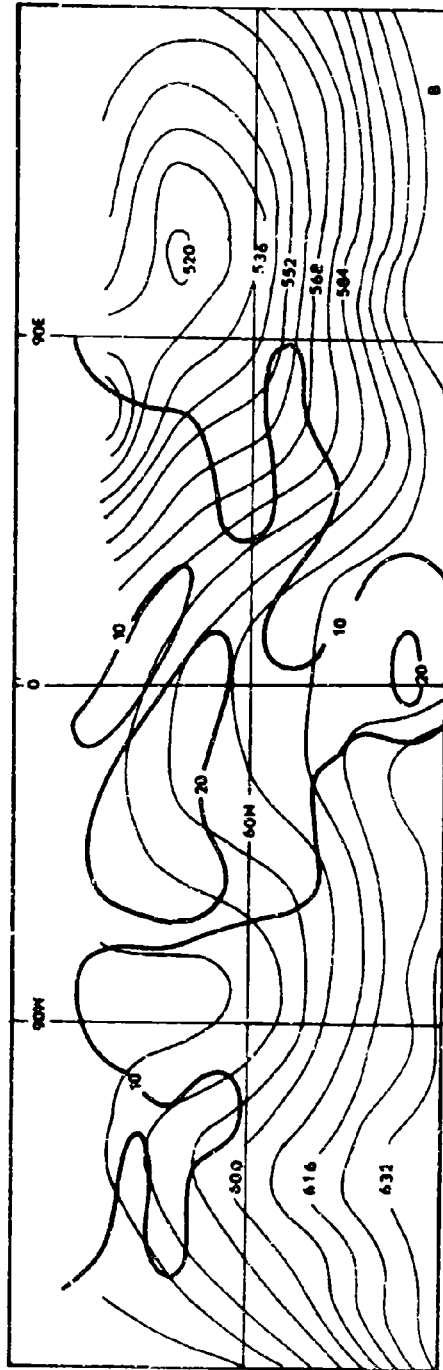


FIG. 10. Simulated radioactive debris at 100 mb on A: 22 November; and B: 24 November.

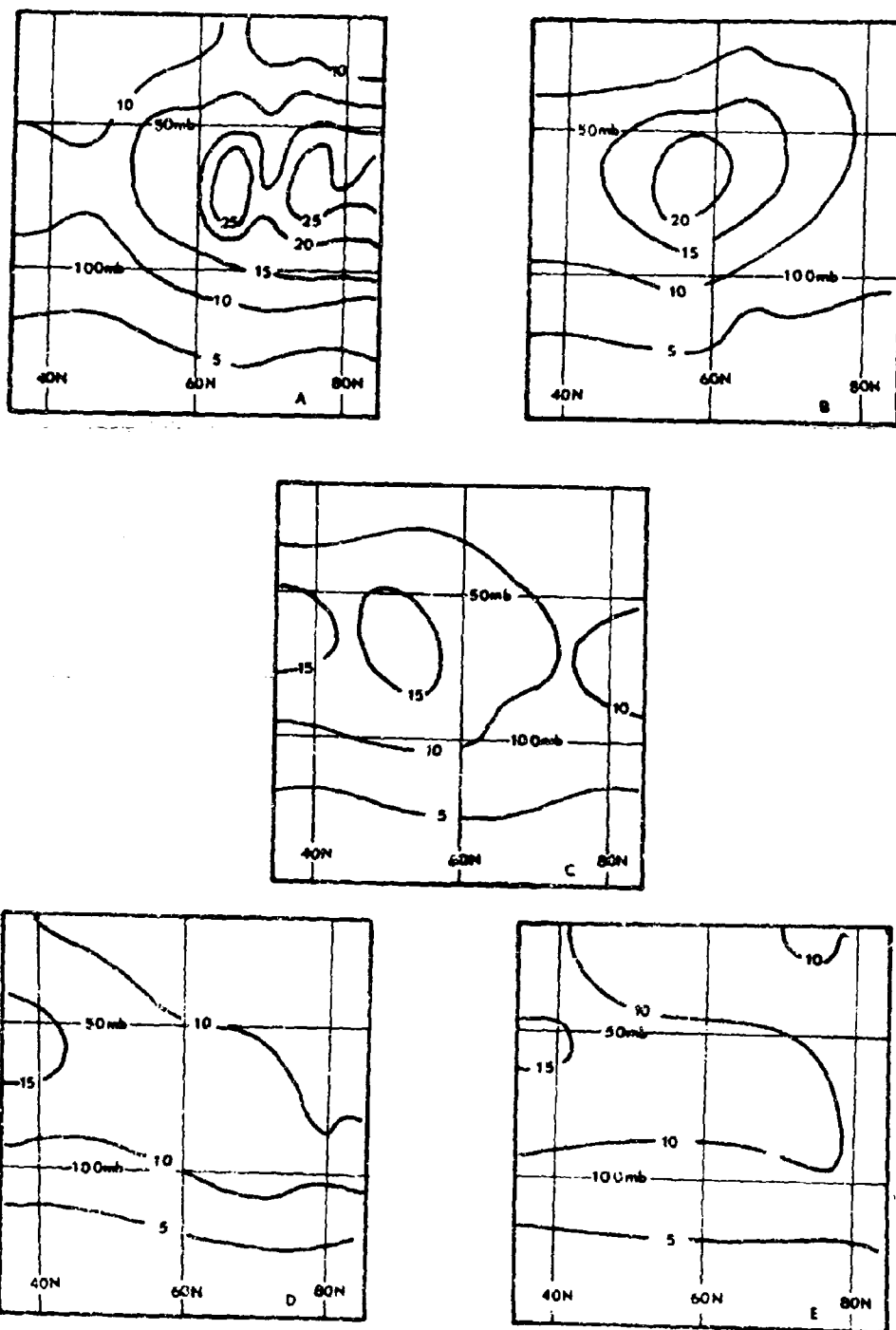


FIG. 11. Zonal-mean simulated radioactive debris in arbitrary units on A: 18 November; B: 20 November; C: 22 November; D: 24 November; and D: 26 November.

the center of maximum mixing ratio gains altitude and moves toward the south, at the same time spreading laterally in such a manner that its axis slopes downward toward the pole. By 23 November, the zonal mean bears a striking resemblance to both the results of parameterized studies and to observations (Gudiksen et al., 1969), showing that this model can, through advection and diffusion alone, quickly shape any reasonable distribution of inert tracer into a fair reproduction of observed mixing ratio fields. In fact, this process took place much more quickly than it would have in the real atmosphere because of the large standard deviation in the initial distribution.

No detailed analysis is made of the principal agencies responsible for the tracer's evolution, but the horizontal eddies and diffusion combined are about an order of magnitude stronger than the sum of the other four agencies. Therefore, as in the ozone experiments, the sign of the tendencies, produced by the mean cell terms, remain consistent in time so that over periods longer than eleven days their effect becomes significant.

#### IV. CONCLUSIONS

This model successfully simulates many observed qualitative features of stratospheric transports of both ozone and radioactive debris. Apart from some numerical difficulties which result from mass imbalance in the wind field and from inadequate treatment of the singularity at the pole, no obstacles exist to prevent the use of this model to predict the evolution of stratospheric tracers.

If the erroneous exaggeration of the parameterized diffusion may be neglected, the instantaneous derivative is primarily determined by the horizontal eddies. Although the effect of the vertical eddies is about an order of magnitude weaker than that of the horizontal eddies, it cannot be neglected in the zonal mean. The two components of the mean cell are still weaker than the vertical eddies. However, over long periods of time, they may assume greater importance because they do not change sign or fluctuate greatly in magnitude.

## BIBLIOGRAPHY

- Bozkov, D., 1968: Planetary distribution of total ozone during IQSY. Khidrologiia i Meteorologiia, 23, 29-39.
- Brewer, A. W., 1949: Evidence for a world circulation provided by measurements of helium and water vapor distributions in the stratosphere, Quarterly Journal of the Royal Meteorological Society, 75, 351-363.
- Craig, R. A., 1965: The Upper Atmosphere, Meteorology and Physics. Academic Press, 509 pp, 200-208.
- Davidson, B., Friend, J. P. and Seltz, H. 1965: Numerical models of diffusion and rainout of stratospheric radioactive materials. Tellus, 18, 301-315.
- Dobson, G. M. B., Harrison, D. N., and Lawrence, J., 1937: Measurements of the amount of ozone in the earth's atmosphere and its relation to other geophysical conditions. Proceedings of the Royal Society of London, Ser A, Part II, 114, 521-541.
- Dobson, C. M. B., 1956: Origin and distribution of the polyatomic molecules in the air. Proceedings of the Royal Society of London, Ser A, 236, 187-193.
- Godson, W. L., 1960: Total ozone and the middle stratosphere over Arctic and Sub-Arctic areas in winter and spring. Quarterly Journal of the Royal Meteorological Society, 86, 301-317.
- Gudiksen, P. H., Fairhall, P. W., and Reed, R. J., 1968: Roles of mean meridional circulation and eddy diffusion in the transport of trace substance in the lower stratosphere. Journal of Geophysical Research, 73, 4461-4473.
- Haltiner, G. J., and Martin, F. L., 1957: Dynamical and Physical Meteorology. McGraw-Hill, 454 pp, 244-247.
- Hering, W. S., 1965: Ozone and atmospheric transport processes. Tellus, 18, 329-336.
- Hunt, B. E., 1969: Experiments with a stratospheric general circulation model III. Monthly Weather Review, 97, 287-306.
- Hunt, B. E., and Manabe, S., 1968: Experiments with a Stratospheric General Circulation Model II. Large-scale diffusion of tracers in the Stratosphere. Monthly Weather Review, 96, 503-539.



- Kurihara, Y., 1965: On the use of implicit and iterative methods for the time integration of the wave equation. Monthly Weather Review, 93, 33-46.
- Mahiman, J. D., 1967: Further studies on atmospheric general circulation and transport of radioactive debris. Atmospheric Science Paper No. 110, Colorado State University, 68.
- Mahiman, J. D. 1969: Energetics of a "minor breakdown" of the stratospheric polar night vortex. Journal of the Atmospheric Sciences, 26, 1306-1317.
- Normand, Sir Charles, 1953: Atmospheric ozone and the upper air conditions. Quarterly Journal of the Royal Meteorological Society, 79, 39-50.
- Newell, R. L., 1961: The transport of trace substances in the atmosphere and their implication for the general circulation of the stratosphere. Geophysica Pura e Applicata, 49, 137-138.
- Prabhakara, C., 1963: Effects of non-photochemical processes on the distribution and total amount of ozone in the atmosphere. Monthly Weather Review, 91, 411-431.
- Reed, R. J., 1950: Role of vertical motions in ozone-weather relationships. Journal of Meteorology, 7, 263-267.
- Reed, R. J. and German, K. E., 1965: A contribution to the problem of stratospheric diffusion by large-scale mixing. Monthly Weather Review, 93, 313-321.

NUMERICAL CALCULATIONS OF  
STRATOSPHERIC OZONE TRANSPORT

by

Richard H. Stender  
Lieutenant, United States Navy

This material is based on a thesis submitted as  
partial fulfillment of the requirements for the  
requirements for the M. S. degree at the Naval  
Postgraduate School.

### Abstract

The vertical distribution of ozone was observed by the Air Force Cambridge Research Laboratories North American ozonesonde network from 29 April 1963 to 10 May 1963 on a daily basis. This observed data, supplemented by twenty-four hour trajectory calculations, was used to prepare distributions of ozone mixing ratio on the 200, 100, 50 and 30 mb surfaces. The ozone distributions were evaluated for the calculation of ozone transport by mean and eddy motions in the lower stratosphere. The results of these calculations show the magnitude of the horizontal and vertical transport of ozone into and out of the 30/50, 50/100, and 100/200 mb volume over North America. The mean vertical transport, supported by the vertical eddy transport, is combined to move the ozone primarily downward through the stratosphere. At the tropopause, the vertical eddies transport the ozone to the troposphere for eventual destruction.

## TABLE OF CONTENTS

I.	INTRODUCTION - - - - -	- III-9
II.	PREPARATION OF DATA AND THE COMPUTATIONAL SCHEME - - -	- III-16
	A. BACKGROUND - - - - -	- III-16
	B. PHYSICAL LIMITATIONS - - - - -	- III-16
	C. BASIC ATMOSPHERIC PARAMETERS - - - - -	- III-17
	D. OZONE DATA AND ANALYSIS - - - - -	- III-23
	1. The AFCRL Ozonesonde Network - - - - -	- III-23
	2. Reliability of Measured Chemiluminescent Ozonesonde Data - - - - -	- III-25
	3. Preparation of Ozone Data for Analysis - - - - -	- III-26
	4. Hand Analysis Techniques - - - - -	- III-28
	5. Ozone Distribution in the Lower Stratosphere - - - - -	- III-29
	E. THE OZONE BALANCE EQUATION FOR A VOLUME BOUNDED BY TWO PRESSURE SURFACES - - - - -	- III-35
III.	EVALUATION OF THE TERMS OF THE OZONE BALANCE EQUATION - - -	- III-39
	A. THE LOCAL CHANGE TERM - - - - -	- III-41
	B. THE MEAN TERMS - - - - -	- III-43
	C. THE EDDY TERMS - - - - -	- III-44
	D. PRODUCTION AND RECOMBINATION TERM - - - - -	- III-45
	E. THE ERROR TERM - - - - -	- III-45
IV.	ADDITIONAL CALCULATIONS - - - - -	- III-49
V.	SUMMARY AND CONCLUSIONS - - - - -	- III-55
	APPENDIX A: STREAMLINE AND OZONE MIXING RATIO ANALYSES - - -	- III-56

# LIST OF TABLES

<u>Table</u>	<u>Page</u>
I    Ozonesonde Network - - - - -	III-24
II   Ten-Day Mean Ozone Balance - - - - -	III-40

# LIST OF FIGURES

<u>Figure</u>		<u>Page</u>
1	Ten-day Zonal Mean Temperature - - - - -	III-19
2	Ten-day Zonal Mean u-component of the Wind - - - - -	III-20
3	Ten-day Zonal Mean v-component of the Wind - - - - -	III-21
4	Ten-day Zonal Mean Vertical Motion - - - - -	III-22
5	Twelve-day Zonal Mean Ozone Mixing Ratio - - - - -	III-30
6	Ten-day Mean Ozone Balance in Advective Format - - - -	III-42
7	Ten-day Mean Correlation Coefficients Between Meridional Wind and Ozone Mixing Ratio - - - - -	III-50
8	Ten-day Mean Correlation Coefficients Between Vertical Motion and Ozone Mixing Ratio - - - - -	III-52
9	Ten-day Mean Correlation Coefficients Between Meridional Wind and Vertical Motion - - - - -	III-54
A-1	The 200 mb Streamline Analysis for 3 May 1963 - - - - -	III-57
A-2	The 200 mb Ozone Mixing Ratio ( $\text{mg g}^{-1}$ ) Analysis for 3 May 1963 - - - - -	III-58
A-3	The 100 mb Streamline Analysis for 3 May 1963 - - - - -	III-59
A-4	The 100 mb Ozone Mixing Ratio ( $\text{mg g}^{-1}$ ) Analysis for 3 May 1963 - - - - -	III-60
A-5	The 50 mb Streamline Analysis for 3 May 1963 - - - - -	III-61
A-6	The 50 mb Ozone Mixing Ratio ( $\text{mg g}^{-1}$ ) Analysis for 3 May 1963 - - - - -	III-62
A-7	The 30 mb Streamline Analysis for 3 May 1963 - - - - -	III-63
A-8	The 30 mb Ozone Mixing Ratio ( $\text{mg g}^{-1}$ ) Analysis for 3 May 1963 - - - - -	III-64

# LIST OF SYMBOLS

$A$	= area enclosed within lateral boundary of computational grid
$c_p$	= specific heat of air at constant pressure
$H$	= heat per unit mass
$i$	= grid index in east-west direction, positive eastward
$j$	= grid index in the north-south direction, positive northward
$K_H$	= $K_x = K_y$
$K_p$	= eddy-diffusion coefficient of $\chi$ in $p$ direction
$K_x$	= eddy-diffusion coefficient of $\chi$ in $x$ direction
$K_y$	= eddy-diffusion coefficient of $\chi$ in $y$ direction
$l$	= distance around the lateral boundary of computational grid
$n$	= coordinate direction perpendicular to lateral boundary of computational grid, defined positive inward
$p$	= air pressure in millibars
$Q$	= a dummy variable used for illustrative purposes
$\bar{Q}$	= average along a horizontal line
$\bar{\bar{Q}}$	= area average $\equiv \frac{1}{A} \iint Q \, dA$
$\tilde{Q}$	= vertical average $\equiv \frac{1}{\Delta p} \int Q \, \delta p$
$T$	= temperature in degrees absolute
$t$	= time
$u$	= zonal component of the wind
$w_2$	= wind velocity
$v$	= meridional component of the wind
$\overline{(v'w')}$	= covariance of the meridional and vertical eddy components of the wind along a latitude circle

- w = vertical motion in height coordinates =  $\frac{dz}{dt}$
- $\alpha$  = specific volume
- $\chi$  = mixing ratio of ozone expressed as micrograms per gram
- $\omega$  = vertical velocity of wind in pressure coordinates =  $\frac{dp}{dt}$



### ACKNOWLEDGEMENT

The author would like to thank all members of the Faculty of the Naval Postgraduate School for the guidance they have provided during his period of study there. In particular, he wishes to acknowledge and thank Professor Jerry D. Mahlman, not only for his assistance in formulating and conducting this study, but also for the stimulation of thought, encouragement, and patient counsel he has given the author throughout the entire meteorological curriculum.

Special thanks go to Professor Russell L. Elsberry for many valuable suggestions in the preparation of the manuscript. Thanks, also go to Mr. Paul Adler and to Mr. Gregorio Ramos for assistance in the preparation of the ozone data, Mr. Michael McDermet and Mr. Kenneth Roberts for drafting of the figures, to the Computer Facility of the Naval Postgraduate School for assistance in the numerical computations, and to Mrs. Joann Madler who typed the manuscript.

## I. INTRODUCTION

Ozone is an important but not well-documented atmospheric gas. Its importance to meteorologists is twofold. First, ozone can be used as a quasi-conservative atmospheric trace substance below 30 kilometers; secondly, as an absorber of ultraviolet light, ozone affects the heat balance through the diabatic heating term of the first law of thermodynamics. Although the exchange of energy by ozone is worthy of investigation, ozone, as an atmospheric tracer, is the subject of this study. Before proceeding, a review of the significant works of earlier investigators is desirable.

The first major investigation of the measurement and distribution of atmospheric ozone was carried out under the direction of G. M. B. Dobson during a five-year period from 1924 to 1929. Dobson and his associates reported the findings of their study in a series of four articles in the Proceedings of the Royal Society of London (1926, 1927, 1929, 1930). Based on the work of previous investigators, Dobson developed a spectroscopic instrument for use on the earth's surface that measures the total amount of atmospheric ozone in a vertical column. The results of daily measurements of total ozone at Oxford during 1924 and 1925 were compared with surface pressure. It was found that surface pressure had a high negative correlation, on the order of  $-.5$ , with total ozone measurements. On an annual basis, a maximum of total ozone was observed in the spring with a corresponding minimum in the fall. Comparisons of total ozone were made with atmospheric pressure at nine, twelve, and fourteen kilometers. A high negative correlation, on the order of  $-.8$ , was observed.

In 1926 instruments were sent to various locations in northwestern Europe. The observations produced similar conclusions as the Oxford findings of 1925. Using the results of 1926-1927, a complete description of the ozone conditions relative to cyclones and anticyclones, was presented. In general, high total ozone was measured in the area of northerly wind flow and low total ozone in the sectors associated with southerly wind flow. Highest total ozone values were found to the southwest of the surface low pressure centers.

During 1928 and 1929 the spectrographs were redistributed, so that observations were taken at Arosa (Switzerland), Table Mountain (California), Helwan (Egypt), Kodaikanal (India), Christchurch (New Zealand), Oxford (England), and Montezuma (Chile). The analysis of the measurements showed that the midlatitude stations had similar observations as discussed for northwestern Europe. The tropical stations observed no significant pressure or total ozone variations.

Several years later, using the observations obtained during the period 1928-1932 in northwestern Europe, Meetham (1937) found a high positive correlation between total ozone and temperature at a height of 12, 15, and 18 kilometers. The magnitude of the correlation coefficients was on the order of  $+0.5$ . He also found a high negative correlation between total ozone and pressure at 9, 12, 15, and 18 kilometers altitude and between total ozone and the height of the tropopause. Although values vary somewhat, the pressure correlation coefficients have a magnitude of  $-0.4$ , while the corresponding tropopause figures are  $-0.5$ .

Godson (1960) has summarized Northern Hemisphere total ozone observations over many years by month and latitude. His results show a strong

middle and north latitude minimum during the month of October. Relatively constant values over the seasons are shown in the tropics with increasing values northward. The maximum value is reported above 70N during the month of March. The steepest latitudinal gradient occurs across middle latitudes during late winter and early spring. The flattest gradient occurs during late summer and early autumn. This elaborates upon and confirms earlier and limited observations. Godson's summary is generally accepted as a reasonable description of the mean distribution of total ozone.

The vertical distribution of ozone has been difficult to obtain. This is attributed to the lack of a reliably accurate, inexpensive, and expendable instrument. A summation of the various methods of measuring the vertical distribution of ozone is presented by Craig (1965), and therefore is not presented here. The most widely used technique has been the Umkehr method devised by F. P. W. Gotz in 1931 (Craig, 1965). Using photometry, this method breaks the atmosphere into five or nine layers. For each layer a single ozone value is computed. Of more recent use are the Regener chemiluminescent ozonesonde and the Brewer-Mast ozonesonde. Both of these instruments are capable of being used on radiosondes and are able to give a much finer vertical ozone structure than the Umkehr method.

Investigators (see, for example, Gotz, 1951; Ramanathan and Kulkarni, 1960; Kulkarni, 1962; Mateer and Godson, 1960; Craig, 1960, 1965; Hering and Borden, 1965; or Bojkov, 1965, 1969) agree on the general shape of the vertical ozone profile. Low, relatively constant, mixing ratios of ozone are found in the troposphere with a very sharp increase at the tropopause. The

maximum value of ozone mixing ratio is most often found in the 15 to 30 kilometer layer with the altitude of the maximum decreasing poleward. Above this maximum the ozone mixing ratio slowly decreases or remains relatively constant with altitude. Maximum hemispheric values are observed near the 30 kilometer altitude of the equatorial latitudes. In the stratosphere isolines of ozone distribution normally slope poleward and downward from the tropical regions. Large daily fluctuations in ozone content are observed in the region between the tropopause and the primary ozone maximum. The fluctuations are weakest in tropical regions and strongest in middle and north latitudes.

It is worthwhile at this point to consider the expected distribution of ozone, assuming photochemical equilibrium. Gotz (1951), Craig (1950, 1965), Prabhakara (1963), and Brewer and Wilson (1968) have discussed the origin and details of photochemical theory with respect to atmospheric ozone. Therefore, photochemical theory will not be reviewed here. From the work of the previously noted authors, two salient points are noted:

1. Photochemical equilibrium theory correctly predicts the observed amount of ozone in the atmosphere above approximately 30 kilometers. Predicted by this theory is the equatorial maximum region and decreasing values poleward and with altitude. Below this region, photochemical theory does not agree with observed distributions.

2. Production and recombination can be considered small below the 30 kilometer maximum observed values. Therefore, in this region ozone must be quasi-conservative and can be used as an atmospheric tracer.

Since the observed distribution and photochemical theory disagree, the discrepancy must be due to transport processes. Transport mechanisms must move the ozone from high equatorial source regions to the lower stratosphere in middle and high latitudes. From the lower stratosphere ozone is passed to the troposphere for eventual destruction with atmospheric constituents or the earth's surface (Craig, 1950, 1965). Craig further mentions that the process would have to be "most effective in middle and high latitudes in winter, when the total amount of ozone increases most rapidly" (Craig, 1950).

Prabhakara (1963) performed a study of a mathematical model of ozone distribution based on photochemical equilibrium below 41 kilometers, and the effect of transport processes upon this distribution. His conclusion, that "photochemical theory by itself cannot explain the latitudinal and seasonal variation of ozone," lends further support to ideas advanced by Craig (1950, 1965).

In the past, sufficient ozone measurements on a hemispheric and vertical scale were unavailable. This prevented direct calculations of the transport of ozone by dynamic processes in the stratosphere. Newell (1961, 1962, 1964) advanced the idea, that since the total ozone measured at the surface was highly correlated with the ozone amount in the 12 to 24 kilometer layer, then a measurement of the flux of total ozone would be indicative of the flux in the lower stratosphere. Using 100 and 50 mb winds and total ozone measurements during the International Geophysical Year, Newell computed the mean and eddy fluxes of ozone in this layer. Newell concluded that the mean meridional

circulation and standing eddies did not serve as effective transport mechanisms. Thus, he argued that most ozone transport was attributed to quasi-horizontal transient eddies.

To explain the observed change in total ozone measured at the surface, a mechanism was proposed by Reed (1950) and Normand (1953). Although proposed separately, this theory is usually called the "Reed-Normand effect." On a synoptic scale the mechanism combines the horizontal advection and vertical motion to explain the variation of total ozone with the synoptic features of the upper troposphere and lower stratosphere. Basically the argument is as follows.

Air blows through the ridge and trough patterns of the height field. The temperature pattern, associated with the height field in the lower stratosphere, is fairly constant with warm areas in the base of troughs and cold areas in the ridges. Therefore, the quasi-stationary temperature patterns must be maintained by adiabatic warming and cooling of air parcels moving through them. The subsidence associated with the warming, brings down ozone-enriched air from above. The lifting, associated with the cooling, transports ozone-poor air from lower altitudes. Since this region is below the level of the observed equatorial maximum, higher ozone values are brought southward to the trough and lower values are brought northward from equatorial regions to the ridge.

The basic qualitative theories of movement and approximate distribution of ozone in the lower stratosphere have been proposed. Quantitative confirmation of these theories has been lacking, due to a minimum of information with

respect to the horizontal and vertical distribution of ozone in the lower stratosphere (and elsewhere). With the challenge thus defined, this study was undertaken to compare earlier theories with a quantitative description of ozone movements.

As a first step, the distribution of ozone mixing ratio on standard pressure surfaces in the lower stratosphere was constructed from the observations taken by the Air Force Cambridge Research Laboratories ozonesonde network during 29 April 1963 to 10 May 1963. It follows that ozone motions can be evaluated, using basic meteorological data.

To accomplish this evaluation, a computational scheme was proposed by Professor J. D. Mahlman of the Department of Meteorology, Naval Postgraduate School. This scheme puts the continuity equation for ozone (Haltiner and Martin, 1957) into a form that enables computation of the mean and eddy flux of ozone mixing ratio into a volume bounded by two pressure surfaces. The intent of the study is to perform quantitative calculations of ozone transport, due to various physical processes based upon this formulation and assess their significance in terms of previous estimates.



## II. PREPARATION OF DATA AND THE COMPUTATIONAL SCHEME

### A. BACKGROUND

In 1963 an attempt was made to gather a more complete representation of the distribution of ozone on a synoptic scale. The Air Force Cambridge Research Laboratories (AFCRL) operated an eleven-station ozonesonde network in North America. Daily observations, obtained by this network between 29 April 1963 and 10 May 1963, provide the basic data for this study (Hering and Borden, 1964). This period is just after the observed spring maximum of total ozone. Wind and temperature fields at standard levels were available from the National Weather Records Center, Asheville, North Carolina and from the Free University of Berlin (1963, 1966).

### B. PHYSICAL LIMITATIONS

Considering the geographical locations of the ozonesonde stations on the North American continent, an upper boundary of 24 kilometers defined by sufficient ozonesonde observations, and a lower boundary defined by the tropopause, the volume in which calculations can be made is limited.

Four pressure levels - 200, 100, 50 and 30 mb - were chosen on the basis of readily available wind and temperature data. The selection of the grid boundaries at 30N-140W, 75N-140W, 75N-60W, and 30N-60W minimizes the Atlantic Ocean, Pacific Ocean, and Northern Canada data-sparse areas.

A latitude-longitude oriented grid was used in order to measure fluxes across boundaries of meridians and parallels. The grid interval on a pressure surface is five degrees, which is sufficient to represent synoptic scale motions in the stratosphere.

For the four isobaric surfaces involved the distance between them is on the order of four kilometers. Considering the vertical distribution of ozone, this interval is larger than desired and forces rough approximations in computing vertical derivatives.

The time interval was chosen as one day corresponding to the frequency of ozonesonde observations. Considering the expected movement of ozone in this region and the synoptic scale of the analysis, this interval is reasonable.

#### C. BASIC ATMOSPHERIC PARAMETERS

Hand analyses of streamline, isotach, and isotherm patterns were prepared at each pressure surface for the time period of the calculations. The daily 200 and 100 mb 1200 GMT Weather Bureau synoptic analysis and the daily 50 and 30 mb 0000 GMT synoptic analysis from the Free University of Berlin were used as a plotted data source.

As shown in Appendix A, the streamline analysis describe typical patterns for this time of year. The lower levels reflect deep tropospheric systems that weaken with altitude. At the 30 mb surface the weakening winter circumpolar vortex is observed with weak anticyclonic centers forming and dissipating at the southern latitudes. The ten-day period of this investigation's major calculation is during the spring reversal of the upper stratospheric circulation from winter westerlies to summer easterlies.

Since the ozonesonde observations were taken at 1200 GMT, an approximation to the parameters of the atmosphere at the 50 and 30 mb surfaces was

made as follows. The zonal and meridional components of the wind field and the temperature field were linearly interpolated for 1200 GMT values from the 0000 GMT fields.

Vertical motions were computed by solving the first law of thermodynamics in the form

$$\omega = \frac{\frac{\partial T}{\partial t} + w_2 \cdot \nabla T - \frac{1}{c_p} \frac{dH}{dt}}{\frac{\alpha}{c_p} - \frac{\partial T}{\partial p}} \quad (1)$$

The diabatic heating term was evaluated, using the net heating rates, as proposed by Kennedy (1964) for the spring period. Unrepresentative changes in vertical motions between grid points and excessive magnitudes at certain grid points are the result of computational inaccuracies attributed to the assumption of a linear change of wind and temperature across a horizontal grid interval. To avoid these unrepresentative and dynamically untenable vertical motions, a smoothing scheme was used as follows:

$$\omega_{i,j} = .15\omega_{i,j+1} + .15\omega_{i,j-1} + .15\omega_{i-1,j} + .15\omega_{i+1,j} + .4\omega_{i,j} \quad (2)$$

To aid in establishing the state of the atmosphere for the area of interest during the period of the calculations, ten day latitudinal averages by pressure surface were prepared for the temperature field and the zonal, meridional, and vertical components of the wind fields. These values are presented in meridional cross section format as figures 1 - 4.

The values in figures 1 - 4 are in general agreement with results presented by other authors (e.g. Craig, 1965). The temperature field (fig. 1) is typical





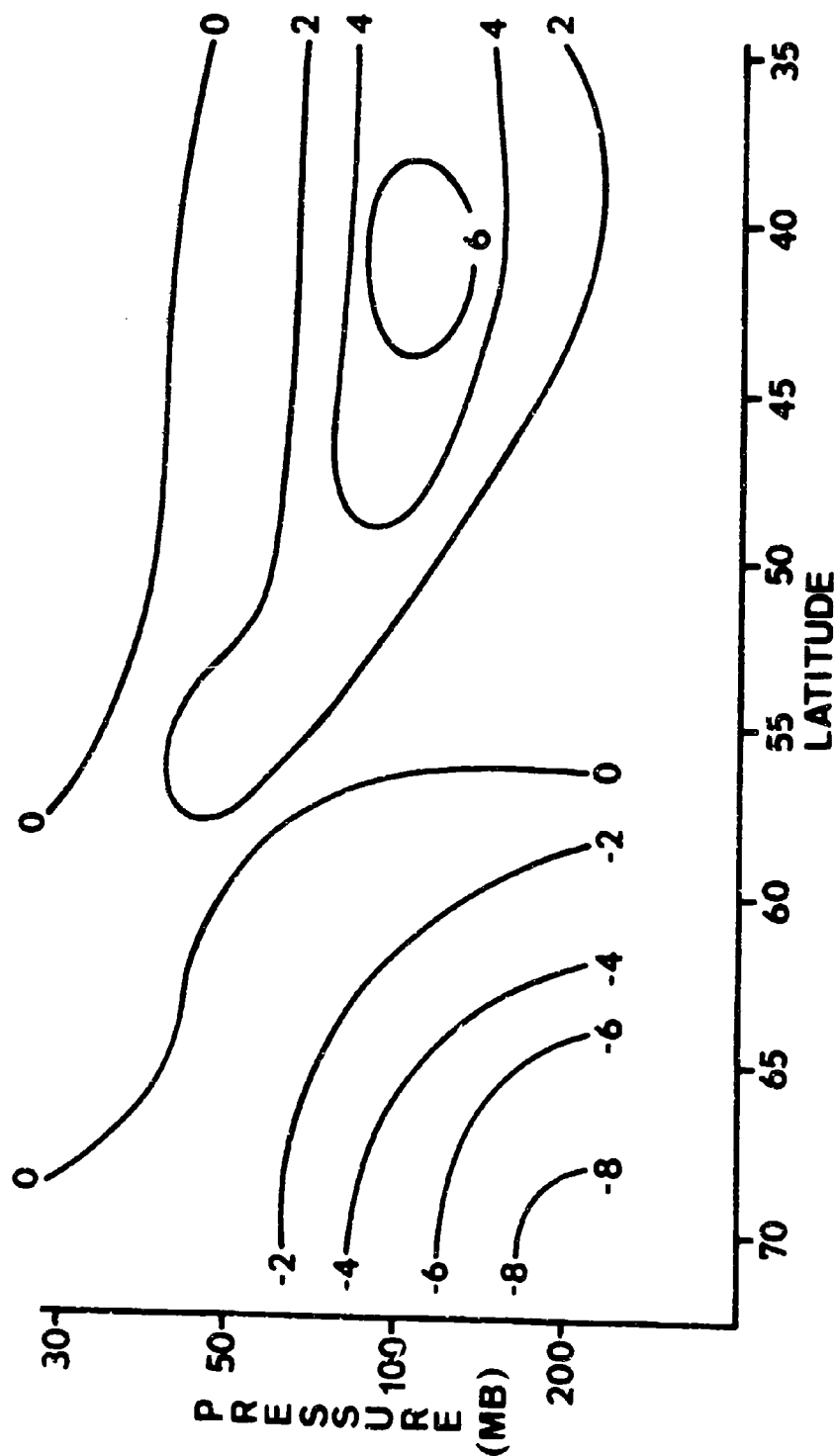


FIG. 3. Ten-day Zonal Mean v-component of Wind (Knots) for the Period 30 April to 9 May 1963. Computed between longitudes 60W and 140W.



for the lower stratosphere at this time of year. Cold temperatures at southern latitudes give way to the warm temperatures associated with the middle and northern latitude troughs. This latitudinal temperature gradient weakens with altitude. The u-component of the wind (fig. 2) supports the earlier observation that the winter circumpolar vortex is weakening and being replaced from above by summer easterlies as can be seen at 30 mb and 35N. The mid-latitude wind maximum, associated with the mean polar front jet position, is seen at 200 mb and 45N. The v-component of the wind (fig. 3) shows little motion at the 30 and 50 mb levels. At 100 mb strong, southerly movement north of 65N and strong, northerly movement south of 50N is observed. At 200 mb strong, southerly motions are seen north of 65N. The vertical motions (fig. 4) show a general subsidence over the volume of calculations except for a weak rising area at 50 mb and strong upward motions between 45N and 50N at 200 mb.

Most investigators presenting similar results use time scales of months or seasons. This study is limited to ten days, and hence the values are not directly comparable. In addition, to properly discuss the various details of these mean atmospheric parameters, a separate and more thorough treatment is required than can be presented here. Therefore, further discussion of figures 1 - 4 is not presented.

#### D. OZONE DATA AND ANALYSIS

##### 1. The AFCRL Ozonesonde Network

For most of its duration the AFCRL ozonesonde network made weekly observations on Wednesday except for selected periods when more frequent



observations were made. During one such period from 29 April 1963 to 10 May 1963, daily observations were taken at 1200 GMT. Participating stations are listed in Table I.

OZONESONDE NETWORK  
(after Hering and Borden, 1964)

STATION	LATITUDE (Deg. N)	LONGITUDE (Deg. W)
Albrook Field, Canal Zone (AWS)	9.0	79.6
Colorado State University, Fort Collins	40.6	105.1
Eielson AFB, Fairbanks, Alaska (AWS)	64.8	147.9
Florida State University, Tallahassee	30.4	84.3
Fort Churchill, Manitoba (Canadian Met. Br.)	58.8	94.1
Goose Bay, Labrador (Canadian Met. Br.)	53.3	60.4
L. G. Hanscom Field, Bedford, Massachusetts	42.5	71.3
Thule AFB, Greenland (AWS)	76.5	68.8
University of New Mexico, Albuquerque	35.0	106.6
University of Washington, Seattle	47.4	122.3
University of Wisconsin, Madison	43.1	89.4

TABLE I

The instrument, used in determining the amount of ozone in the atmosphere, was the dry chemiluminescent ozonesonde, developed by Regener (1960). The ozonesonde was attached to a sounding balloon with a standard radiosonde package. The instrument measures the amount of ozone by drawing ozone-laden air across a disk coated with a chemical that produces

a luminescent reaction with ozone. The intensity of the reaction is measured by a photomultiplier tube and in turn is telemetered back to ground using standard radiosonde equipment (Regener, 1960, 1964). Samples were taken every 15 seconds for a vertical resolution of approximately 250 feet (Hering and Borden, 1964).

## 2. Reliability of Measured Chemiluminescent Ozonesonde Data

In view of the uncertainties inherent with the measurement and calibration of the Regener ozonesonde, it is worthwhile to note the major corrections applied to the soundings and to note the results of several inter-comparison tests with other ozonesondes.

The disk, coated with the chemiluminescent substance, is sensitive to light, moisture, and ozone. Therefore, as a check, calibration shortly before launch is required (Regener, 1964). Hering and Borden (1964) report that achievement of reliable preflight calibration was difficult. This in turn required a correction to the telemetered data. The correction was achieved by adjusting the integrated observed ozone density to a simultaneously observed total ozone measurement, using a spectrophotometer. The ozonograms published by Hering and Borden (1964) have this correction applied.

Hering and Dütsch (1965) compared the results of simultaneous soundings of the Regener chemiluminescent ozonesonde and the bubbler-type electrochemical ozonesonde. Their conclusion is that "ozonesondes of the types tested are capable of providing reliable high-resolution measurements of the vertical ozone distribution."

More recently Komhyr, Grass, and Proulx (1968) made intercomparison tests in various combinations between the Regener chemiluminescent ozonesondes, carbon-iodine ozonesondes, and Brewer-Mast ozonesondes. The result of the comparisons after corrections was, that the chemiluminescent ozonesonde compared with the other ozonesondes in the stratosphere and gave "relatively reliable" results.

Hering and Borden (1964) considered the data, obtained by the ozone-sonde network, as "provisional." Considering the results of the two intercomparison tests and the observation that other investigators (Berggren and Labitzke, 1966, 1968; Breiland, 1964, 1965, 1967, 1968; Craig, Deluisi, and Sticksel, 1967; Hering, 1966; Hering, Touart, and Borden, 1967; and Sticksel, 1966) have published studies using the corrected ozonesonde data, the reliability of the ozonesonde soundings as published by Hering and Borden (1964) is accepted.

### 3. Preparation of Ozone Data for Analysis

Although the ozone soundings were accepted, there are several features of the soundings that had to be modified to be consistent with the scale of the intended calculations. On the ozonagram thin layers with large unrepresentative gradients and layers in which the ozone values fluctuated excessively and with apparent randomness were considered not representative of the synoptic scale distribution. These features of the vertical distribution may either be a failure of the instrument or a smaller-scale ozone distribution which is presently below our ability to identify. To overcome these apparent

inconsistencies, a subjective smoothing of the individual soundings was completed as the first step in analysis. This smoothing is not to be over-emphasized since extreme care was taken not to destroy the characteristics of the soundings. The severest smoothing was on the order of .3 kilometers on the height scale with 95 percent of the ozonagram values being unaffected by the smoothing process.

With the smoothed values obtained, a time series for the twelve-day period was prepared for each station. Linearly interpolated values were calculated for stations missing an observation, but having an observation 24 hours prior to and after the missing observation. Linear interpolations were also made in the case of the Fairbanks station where observations were reported at 0000 GMT.

To supplement the small number of observations for the area under consideration, hand trajectories were calculated for the 24-hour periods prior to and following an observation. This technique used 12-hour streamline and isotach patterns to obtain the position of the parcel 24 hours before and after the observation time. Under conservation of ozone mixing ratio ( $\chi$ ), these new points then possess a value of  $\chi$  corresponding to the value measured at the original point. An estimate of the vertical motion during the trajectory was made, using an approximation derived from the Eulerian expansion of the total derivative of pressure with respect to time, the hydrostatic equation, and the first law of thermodynamics. With this estimate of the vertical motion applied to the initial ozonagram sounding, a corrected trajectory value was obtained. The trajectory calculations are justifiable, assuming the conservative property

of ozone mixing ratio. As linearly interpolated values were not used for trajectory computations, this calculation increased the number of data points between two and three times the original number of ozone data points available for analysis on a pressure surface.

#### 4. Hand Analysis Techniques

The manner in which the data was to be analyzed presented somewhat of a problem. Synoptic models of ozone distribution on a pressure surface have not been published to the author's knowledge--with the exception of the six analyses presented by Berggren and Labitzke (1968). Other investigators have published information about the synoptic distribution of ozone but none have presented distributions on a pressure surface. Pittock (1969) has investigated the synoptic climatology of ozone, using statistical methods. His "preliminary results," using 546 Brewer-Mast ozonesonde soundings, are primarily in tabular format, classed into general synoptic conditions by season. Breiland (1964, 1965, 1967, 1968) studied the distribution of ozone on a sub-synoptic scale, primarily using vertical cross sections, time sections, and individual AFCRL network soundings. Sticksel (1966) analyzed the vertical distribution of ozone with data collected at the Tallahassee station of the AFCRL network. Briggs and Roach (1963) and Danielsen (1968) have investigated the ozone distribution, along with other parameters, near the jet stream and the tropopause, using aircraft observations.

The first attempt to analyze the plotted data points was inconclusive. Merely constructing isolines of ozone mixing ratio from plotted data points left too much to the imagination. This resulted in inconsistent analyses when

compared to the work of the previously mentioned authors. These analyses were also in consistent in time.

To overcome this problem the appropriate streamline analysis was put under the plotted ozone data. With the streamlines to guide the analyst in sparse data areas, the desired consistency was achieved. To elaborate further, the criteria for placement of isolines of ozone mixing ratio are listed below in order of priority:

- a) observed data at map time;
- b) data from trajectory calculations as corrected for vertical motion;
- c) streamline pattern;
- d) vertical motion patterns.

Justification for this priority is obvious in the case of the first two criteria. The choice of the streamline pattern, as the third criteria followed by the vertical motion patterns, is based on Reed's (1950) conclusion that the horizontal advection contributed  $2/3$  of the day-to-day change whereas the vertical motions contribute  $1/3$  of the daily change.

##### 5. Ozone Distribution in the Lower Stratosphere

Before discussing the individual ozone analyses it is worthwhile to compare the twelve-day mean ozone mixing-ratio distribution obtained here with distributions prepared by other investigators.

The twelve-day mean ozone mixing ratio computed for the period 29 April to 10 May 1967 is presented in figure 5. It is seen that maximum values at southern latitudes and high altitudes give way to lower values at northern

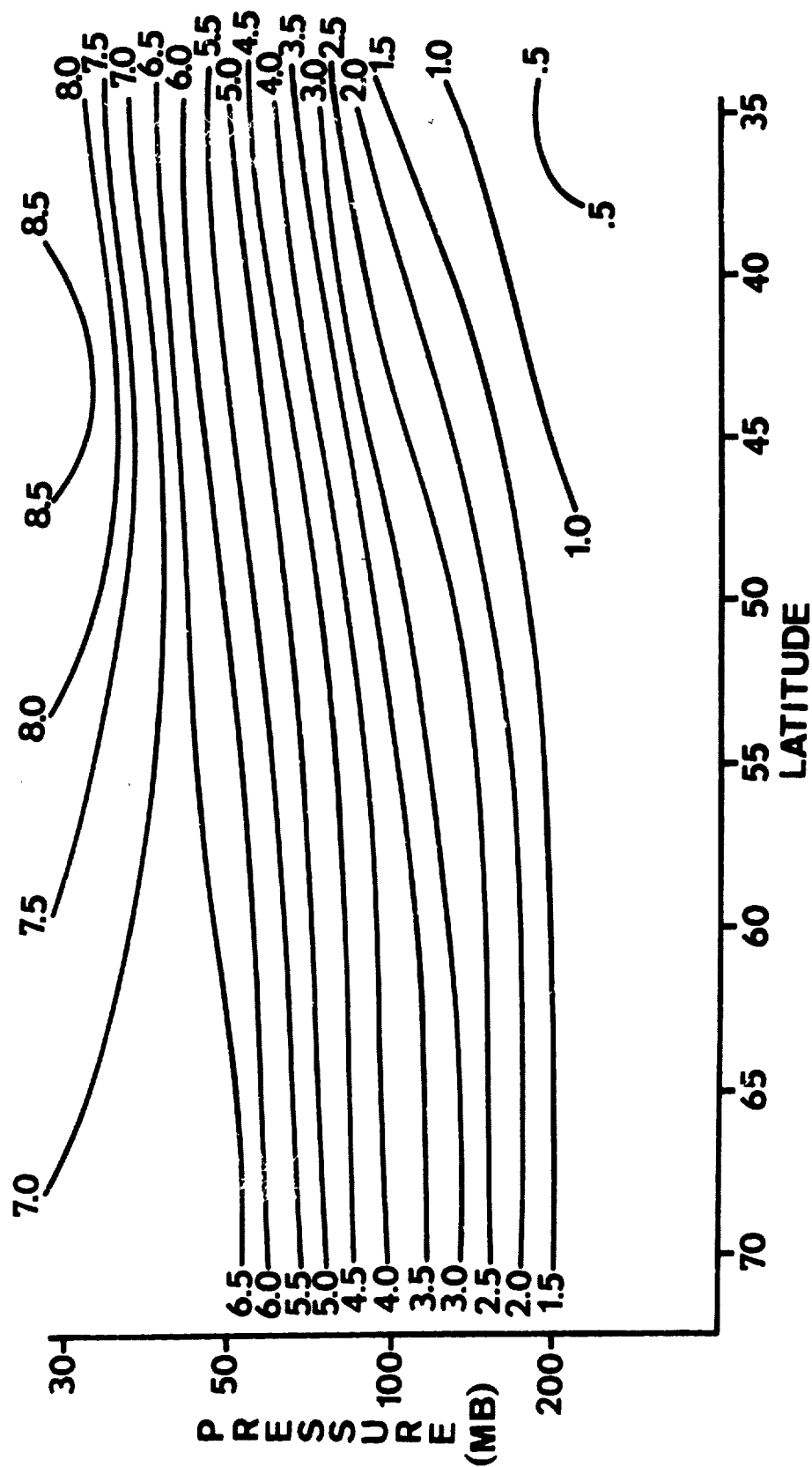


FIG. 5. Twelve-day Zonal Mean Ozone Mixing Ratio ( $\text{mg g}^{-1}$ ) for the period 29 April to 10 May 1963. Computed between longitudes 60W and 140W.

latitudes. The latitudinal gradient reverses between the 30 and 50 mb surfaces with the lower altitudes, having higher values at northern latitudes. The latitudinal gradient reverses between the 30 and 50 mb surfaces with the lower altitudes, having higher values poleward. The slope of the isolines between 50 and 200 mb is markedly downward. In comparison the isolines between 50 and 30 mb are quasi-horizontal between 35N and 50N and rise northward between 50N and 70N.

A direct comparison of ozone mixing ratio values may be made with the values presented by Hering (1966) for the spring of 1963-1964. The two figures are similar with the exception that slightly higher values are given hereby using the 29 April 1963 to 10 May 1963 data. Although Hering uses the same data source as this study, these are the only available, directly comparable, mean ozone mixing ratio values computed from vertical soundings.

Bojkov (1969) presents an annual vertical ozone distribution as determined by the Umkehr method. The units of this distribution are micromillibars and not easily comparable in a quantitative sense. Qualitatively, the same conclusions revealed by the twelve-day mean values are observed in Bojkov's distribution.

Taking into account the information presented by Bojkov and Hering, it is concluded that the twelve-day mean cross section is in agreement with their results, and therefore, lends credibility to the individual analyses from which the mean distribution was prepared. A representative sample of the distribution of ozone mixing ratio on the 200, 100, 50 and 30 mb pressure surfaces is presented in Appendix A.



The patterns made by the 30 mb ozone mixing ratio isolines are dominated by the effects of the horizontal component of the wind. Ozone-rich air is associated with the northward flow of the subtropical anticyclones forming on the southern edge of a weakening winter circumpolar vortex. Ozone-poor air is associated with the southward flow on the western side of the large scale troughs superimposed on the circumpolar vortex. The two contrasting air masses meet in the middle latitudes and mix. The air, continuing to move eastward, then diverges with relatively ozone-poor air associated with the southward flow on the eastern side of the subtropical anticyclones. Correspondingly, relatively ozone-rich air is associated with the northward flow on the eastern side of the large scale troughs.

If long meridional trajectories form in connection with these cyclonic and anticyclonic wind systems, unusually large values of ozone can be observed at northern latitude stations while lower values are observed several hundred miles east or west of that station. The converse holds true for southern latitude stations. The movement of these wind systems will affect the daily observations at a station in that large day-to-day fluctuations of ozone can be caused by the associated wind shift.

By comparing the vertical motion fields on a pressure surface (not reproduced here) with the ozone mixing ratio distribution, some very interesting observations can be made. The western side of the anticyclones are associated with rising vertical motion, northerly trajectories, and high ozone values while the western side of troughs are associated with sinking motions, southerly trajectories, and low ozone values. Therefore, it is qualitatively

observed that the Reed- Normand effect is operating in the opposite sense than at lower altitudes. The result of this mechanism is in evidence in the mean ozone mixing ratio distribution of figure 5 where the isolines between 30 and 50 mb slope upward at northern latitudes.

Masses of air with similar ozone characteristics can be identified and tracked for periods of several days. Such identifiable air masses seem to be prevalent in the wind fields of the southern anticyclones.

Ozone mixing ratio patterns at 50 mb are similar to the patterns at 30 mb with several exceptions. Streamline patterns at this level reflect the upper, weakening portions of tropospheric systems. Weaker southern anticyclones are also present. The ozone mixing ratio pattern shows ozone-rich air associated with the southward flow that at 30 mb is associated with ozone-poor air. Similarly, ozone-poor air is associated with the northward flow that at 30 mb is associated with ozone-rich air.

A qualitative comparison of the vertical motion patterns with the ozone mixing ratio patterns show the Reed-Normand effect to be operating in the manner originally proposed by Reed (1950) and Normand (1953). The sinking, southward moving air into troughs are areas of high ozone values while rising northward moving air is associated with low ozone values.

Masses of ozone-rich and ozone-poor air can be identified as at 30 mb. However, at both pressure levels it noted that these identifiable ozone masses may be an unnatural consequence of the trajectory supplementation of the data and a weak latitudinal gradient of ozone.

The ozone mixing ratio patterns at 100 and 200 mb are similar to the 50 mb patterns. The effect of the streamline pattern is more pronounced.

The vertical motion pattern on a broad scale reflects the Reed-Normand effect; however, vertical motion maxima with horizontal dimensions on the order 2 or 3 grid intervals are not clearly associated with the Reed-Normand predicted high and low ozone values. This is caused by the density of the ozone data, being insufficient to isolate these smaller scale features or by bad  $w$  calculations. Support for this point of view is gained from a calculation of the local change, horizontal advection and vertical advection terms of the Eulerian expansion of the total derivative of ozone mixing ratio with respect to time. This calculation was made on a point by point basis for the entire grid. The results were inconclusive since the error term, computed by assuming ozone is conserved and summing the three remaining terms, was too large in most cases. This indicated a smaller scale ozone distribution that was not able to be identified with the data available.

The ozone analyses prepared for this study compare in a general manner with the distributions used by Breiland (1964, 1965, 1967, 1968), Stickse (1965), Pittcock (1969), Briggs and Roach (1963), Danielsen (1968), and Berggren and Labitzke (1965, 1968) in their respective studies. Only the 200 mb analyses for 3 and 4 May 1963 presented by Berggren and Labitzke (1968) are directly comparable with the analyses compiled here. The analyses are similar in that the major features are the same; yet minor differences occur with the smaller features. It is significant to note that although the AFCRL data was the initial input in both cases, Berggren and Labitzke used isentropic trajectories to supplement their data points while this study used 24-hour isobaric trajectories corrected for vertical motion.

With the data apparently consistent with the earlier theories, previous investigators, and consistent with respect to other atmospheric parameters, it was decided that these analyses would provide an acceptable data base for a quantitative calculation of ozone transport mechanisms.

#### E. THE OZONE BALANCE EQUATION FOR A VOLUME BOUNDED BY TWO PRESSURE SURFACES

As a first step in evaluating earlier theories of ozone distribution and movement, the calculation of the mean and eddy fluxes of ozone on a synoptic scale is desirable. Considering the minimum amount of ozonesonde observations at a given time, the uncertainty in the synoptic distribution of ozone on a pressure surface, and the uncertainty in the performance of the ozonesonde, an averaging scheme over many data points is preferred as compared to a point by point evaluation. To achieve this, the continuity equation for ozone is written in pressure coordinates as

$$\frac{\partial \chi}{\partial t} = -w_2 \cdot \nabla \chi - \omega \frac{\partial \chi}{\partial p} + (P - R) + \frac{\partial}{\partial p} \left( K_p \frac{\partial \chi}{\partial p} \right) + \nabla \cdot K_H \nabla \chi \quad (3)$$

By putting the advection terms in equation (3) into flux form and taking the area average, equation (3) becomes

$$\frac{\partial \bar{\chi}}{\partial t} = - \overline{\nabla \cdot \chi w_2} - \overline{\frac{\partial \omega \chi}{\partial p}} + (P - R) + \frac{\partial}{\partial p} \left( \overline{K_p \frac{\partial \chi}{\partial p}} \right) + \overline{\nabla \cdot K_H \nabla \chi} \quad (4)$$

Now by applying the divergence theorem, equation (4) may be rewritten as

$$\frac{\partial \bar{\chi}}{\partial t} = \frac{1}{A} \oint \chi c_n dl - \overline{\frac{\partial \omega \chi}{\partial p}} + (P - R) + \frac{\partial}{\partial p} \left( \overline{K_p \frac{\partial \chi}{\partial p}} \right) - \frac{1}{A} \oint K_H \frac{\partial \chi}{\partial n} dl, \quad (5)$$

where  $c_n$ , the component of the wind normal to the boundary, is defined as

positive toward the center of the volume.

Along a line let  $\chi = \bar{\chi}'$ , where  $\bar{\chi}$  is the line average and  $\chi'$  is the point deviation from the line average. Similarly, for averaging operations, equation (5) becomes

$$\begin{aligned} \frac{\partial \tilde{\chi}}{\partial t} = & \frac{\bar{\chi} \bar{c}_n}{A} \Delta l + \frac{1}{A} \overline{\chi' c_n'} \Delta l - \frac{\partial \tilde{\omega} \tilde{\chi}}{\partial p} - \frac{\partial \omega^* \chi^*}{\partial p} \\ & + (P - R) + \frac{\partial}{\partial p} \left( K_p \frac{\partial \chi}{\partial p} \right) - \frac{K_H}{A} \frac{\partial \bar{\chi}}{\partial n} \Delta l, \end{aligned} \quad (6)$$

where it is assumed that  $K_H$  is constant on a pressure surface and noted that  $\oint dl = \Delta l$ .

Now average equation (6) between two pressure surfaces,  $p_u$  and  $p_L$ , to obtain the ozone balance equation

$$\begin{aligned} \frac{\partial \tilde{\chi}}{\partial t} = & \overset{(LC)}{\frac{\Delta l}{A} \bar{\chi} \bar{c}_n} + \overset{(MFLA)}{\frac{\Delta l}{A} \overline{\chi' c_n'}} - \overset{(EFLA)}{\frac{\tilde{\omega} \tilde{\chi}}{\Delta p} \Big|_{p_L}} + \overset{(MFLO)}{\frac{\tilde{\omega} \tilde{\chi}}{\Delta p} \Big|_{p_u}} + \overset{(MFT)}{\frac{\omega^* \chi^*}{\Delta p} \Big|_{p_L}} \\ & + \overset{(EFLO)}{\frac{\omega^* \chi^*}{\Delta p} \Big|_{p_u}} + \overset{(EFT)}{\frac{\omega^* \chi^*}{\Delta p} \Big|_{p_u}} + \overset{(PR)}{(P - R)} + \overset{(SUBLO)}{\frac{K_p}{\Delta p} \frac{\partial \tilde{\chi}}{\partial p} \Big|_{p_L}} \\ & + \overset{(SUBT)}{\frac{K_p}{\Delta p} \frac{\partial \tilde{\chi}}{\partial p} \Big|_{p_u}} - \overset{(SUBLA)}{\frac{\Delta l}{A} \left( K_H \frac{\partial \chi}{\partial n} \right)}, \end{aligned} \quad (7)$$

where the vertical average has been applied to evaluate the terms in a form for numerical computations.

The terms of the equation are:

- (LC) the time rate of change of average ozone mixing ratio over the volume;

- (MFLA) the mean flux of ozone into the region through the lateral boundaries (the vertical side of the volume);
- (EFLA) The eddy flux of ozone through the lateral boundaries;
- (MFLO) the mean flux of ozone into the region across the bottom boundary;
- (MFT) the mean flux of ozone into the region across the top boundary;
- (EFLO) the eddy flux of ozone into the region across the bottom boundary;
- (EFT) the eddy flux of ozone into the region across the top boundary;
- (PR) the average difference between production and recombination of ozone for the whole volume;
- (SUBLO) the flux of ozone into the region across the upper boundary, due to sub-grid-scale diffusion;
- (SUBLA) the flux of ozone into the region through the sides due to sub-grid-scale diffusion.

All the terms have units of micrograms per gram per day. This unit is convenient in view of the time scale of the observations. In addition, the value of the ozone mixing ratio at a given height appears as a variable on the ozonogram.

Computer programs were written to evaluate all terms on a daily basis for the 30/50, 50/100, and 100/200 mb volumes with the exception of the production and recombination term and the sub-grid scale diffusion terms.

Brewer and Wilson (1968) have evaluated the meridional net ozone production rate for the winter and summer season from the equator to sixty degrees latitude and between 200 and 30 mb. Since the evaluation of the PR term would require a complete and separate treatment, Brewer and Wilson's results are accepted for use in this calculation. To compute an estimated value and the net ozone production rate, a rough interpolation between seasons

and pressure surfaces, followed by an estimated latitudinal average, was necessary. The appropriate unit conversions were made. These values will be presented with the results of the ozone balance equation in a later section.

The sub-grid-scale diffusion terms are expected to be small when compared to the magnitude of the other terms. Lacking a reliable estimate of the eddy-diffusion coefficients of ozone mixing ratio, these terms were not calculated.

The initial attempt to evaluate the ozone balance equation by using the observed wind to directly evaluate each term resulted in unusually large errors that could be traced to the fluctuations of the mean terms. To improve upon these results, the mass continuity equation was solved for the mean normal component of the wind at the side boundaries and in terms of the computed  $\tilde{\omega}$  fields. The evaluation of the mean normal component of the wind can be obtained by applying the divergence theorem to the area-averaged continuity equation and solving the following form,

$$\overline{\tilde{\omega}}_n = \frac{A (\tilde{\omega}_{p_L} - \tilde{\omega}_{p_u})}{\Delta l (p_L - p_u)} \quad (8)$$

Although this scheme assured the conservation of mass, it increases the dependence of the calculations on the computed vertical motions as compared to directly observed winds.

### III. EVALUATION OF THE TERMS OF THE OZONE BALANCE EQUATION

Without further modification the terms of the ozone balance equation were computed. The daily calculations tended to fluctuate rapidly and may be unrealistic. Considering the magnitude of the error term in comparison with the magnitude of the other terms, it was decided to present the ten-day mean values of the terms. These values are given in tabular format in Table II. In the computed format, the individual mean and eddy terms cannot be compared directly. To effect a comparison the mean terms must be summed, thereby giving the net effect of the mean terms on the volume.

To obtain a form in which the mean horizontal and vertical flux may be directly compared to the eddy flux terms, the sum of the mean terms, as presented in Table II, may be computed in another manner. The area-averaged continuity equation can be written as a representation of the net effect of the mean terms at the middle pressure between two pressure surfaces. By applying a vector identity and the divergence theorem, the first and third terms on the right hand side of equation (6) can be written as

$$\text{SUM} = \overline{\frac{1}{c_n}} \bar{\chi} \frac{\Delta 1}{A} - \tilde{\omega} \frac{\partial \tilde{\chi}}{\partial p} - \frac{\tilde{\chi}}{A} \oint c_n \delta 1. \quad (9)$$

By combining like terms and putting into computational format, equation (9) becomes

$$\begin{array}{cc} \text{(MLAD)} & \text{(MVAD)} \\ \text{SUM} = (\bar{\chi} - \tilde{\chi}) \frac{\Delta 1}{A} \overline{\frac{1}{c_n}} - \tilde{\omega} \frac{\partial \tilde{\chi}}{\partial p}. & \end{array} \quad (10)$$



Key: See Section II-E

$$\text{SUM} = \text{MFLA} + \text{MFLO} + \text{MFT}$$

AS COMPUTED:

Volume	(LC)	(MFLA)	(EFLA)	(MFLO)	(MFT)	(EFLO)	(EFT)	(PR)	(ERROR)
30/50 mb	-173	= + 184	+ 54	-688	+696	- 67	-50	-125	+177
50/100 mb	-517	= -1102	- 46	-921	+275	-103	+27	- 44	+806
100/200 mb	-273	= - 229	-321	- 47	+461	-155	+51	- 16	+ 17

COMPARISON FORMAT:

Volume	(LC)	(SUM)	(EFLA)	(EFLO)	(EFT)	(PR)	(ERROR)
30/50 mb	-173	= +192	+ 54	- 67	-50	-125	+177
50/100 mb	-517	= +456	- 46	-103	+27	- 44	+806
100/200 mb	-273	= +185	-321	-155	+51	- 16	+ 17

TABLE II. The Ten-day Mean Ozone Balance for Indicated Volumes. Symbols for each term given in Section II-E. Units are micrograms per gram per day  $\times 10^4$ .

The two terms are defined as:

- |        |  |
|--------|--|
| (MLAD) | the mean advection through the later boundary;                 |
| (MVAD) | the advection into the volume due to the mean vertical motion. |

The two terms of equation (10) were evaluated, using the same input values as for the evaluation of equation (7). The results of the evaluation of equation (10) are presented in pictorial form in figure 6 with the local change and eddy terms as evaluated by equation (7). The net production term is the same in both cases. The error terms in each evaluation are different only to a small degree. It is therefore concluded that the computational scheme, used to arrive at the value of the mean terms, is a reasonable evaluation of the input parameters.

With the mean and eddy ozone flux terms in a format for comparison and some degree of confidence in the method of evaluation of the mean terms, it is appropriate to discuss the individual terms of the ozone balance as presented in figure 6.

#### A. THE LOCAL CHANGE TERM

Computation of this term was made directly from the distribution of ozone on a pressure surface, and therefore, is not affected by other computed parameters. A rough check on the value of this term was made by comparing the computed result, multiplied by 100, with a 100-day difference between area averages estimated from Godson's (1960) mean distribution of total ozone. This period falls after the March maximum of total ozone shown by Godson and the sign of the mean local change term is negative. With these observations

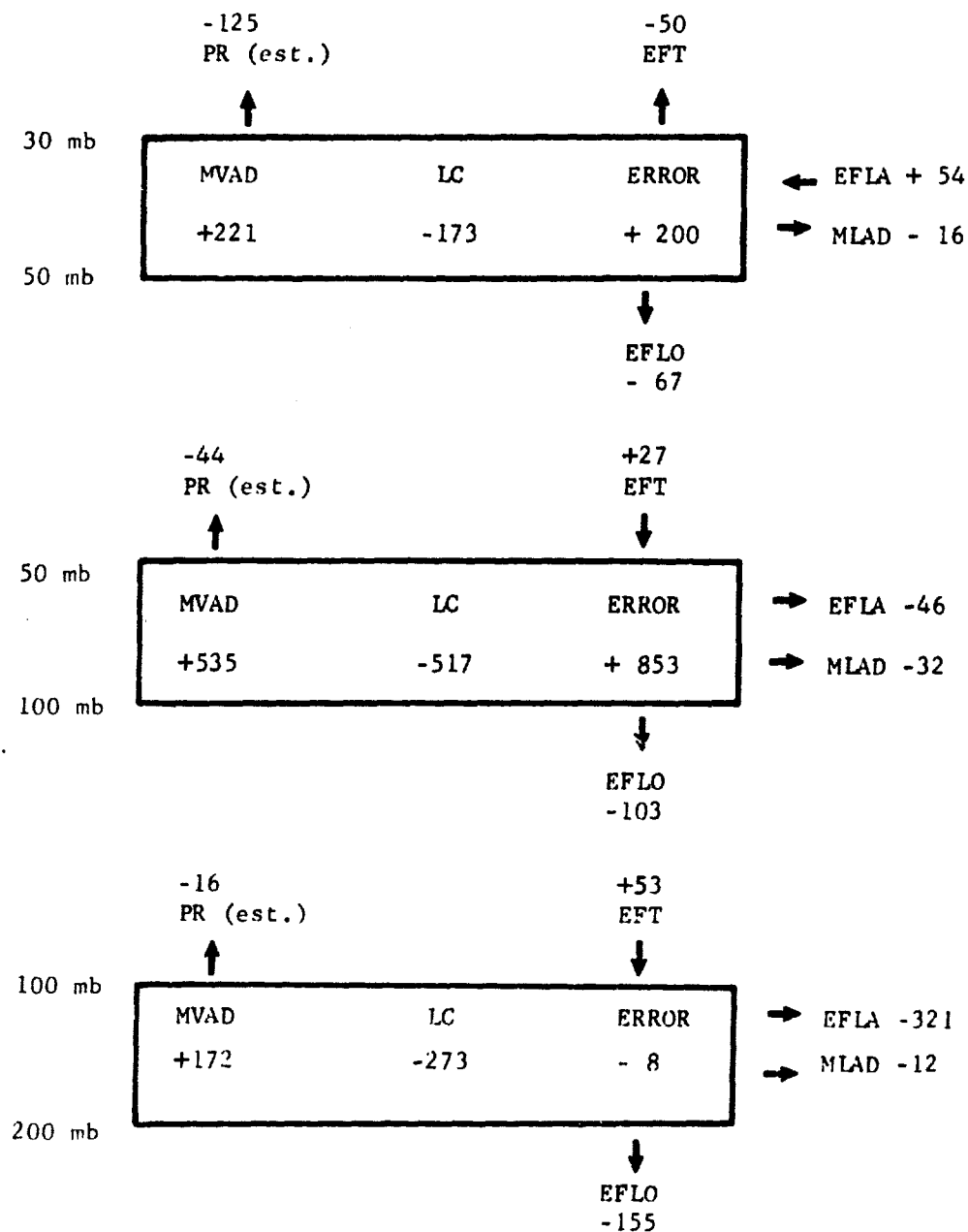


FIG. 6. Ten-day mean ozone balance in advective format. Symbols for each term given in Section II-E and Section III. Units are micrograms per gram per day  $\times 10^4$ .

in mind, the 100-day period between May and August was chosen for comparison.

After making the appropriate unit conversions, the mean local change term accounted for 85 percent of the change in Godson's distribution. Thus, the rate of decrease of ozone within the volume for this period appears representative of the seasonal trend.

It is significant to note that the maximum of total ozone in the atmosphere is observed in March and a net hemispheric decrease is observed after that month (Godson, 1960). The dynamic mechanisms or conditions that created the maximum conditions, particularly at the northern latitudes, must have ceased operating. One may speculate that the mechanism to accomplish this winter-spring northern maximum is the long meridional trajectories set up by the breakdown of the polar night vortex associated with the mid-winter "sudden warmings." Further, the dynamic mechanisms or conditions now operating must be serving to deplete the atmosphere of ozone.

#### B. THE MEAN TERMS

The mean advection through the lateral boundaries can only be evaluated as to direction into or out of the volume. In view of this limitation, the only point to be made is a mention that the term in each volume is contributing a small net loss to the volume and the mean terms (MLAD) are smaller than their respective eddy terms (EFLA) (see fig. 6).

On the other hand, the mean advection in the vertical shows a consistent downward motion through the three volumes of interest. In the two upper volumes, the mean vertical advection is the dominant term.

### C. THE EDDY TERMS

In the 30/50 mb volume the lateral eddy flux term (EFLA) is an input to the volume and agrees with the earlier qualitative observation that the anticyclones on the southern edge of the circumpolar vortex appeared to be transferring ozone northward. The magnitude of the lateral eddy flux term (EFLA) is small relative to the observed change within the volume.

The lateral eddy flux terms at 50/100 and 100/200 mb serve to deplete the volumes of ozone. The value of the term at 50/100 mb is small relative to the mean vertical advection and the vertical eddy flux across the 100 mb surface. In the 100/200 mb volume the lateral eddy flux term is the largest term in the ozone balance. An interesting and unexplained question is the ultimate destination of the ozone advected out of the volume of computations by the lateral eddy flux.

The vertical eddy flux terms show a consistent downward transport from 50 to 200 mb and are a measure of the vertical motion portion of the Reed-Normand effect. At these levels the direction is consistent with that proposed by Reed and Normand. At the 30 mb surface the direction of the vertical eddy flux is upwards. This can be traced to the northward, rising ozone-rich air, associated with the western side of the anticyclones at this level. This is consistent with the earlier section in which the Reed-Normand effect was observed to be operating in the opposite sense as observed in lower altitudes.

By comparing the vertical eddy flux at the upper and lower surfaces at each volume, it can be seen that these eddies contribute a net loss of

ozone to each volume. Another interesting, unanswered question is posed by this observation. If a given amount of ozone is going downward into a trough, what physical process or dynamic mechanisms are operating to prevent an equal amount of ozone from proceeding back upwards to the ridge? The answer probably lies with a smaller scale turbulence phenomenon not yet identified much as the energy cascade in the lowest level of the atmosphere.

The vertical eddy flux terms are the most significant of all the terms computed in the ozone balance. This conclusion is attributed to the fact that the vertical eddy flux computed for this particular area's pressure surfaces may be representative of the whole global pressure surface in question. This cannot be said of the lateral eddy flux terms. As is to be described in a later section, the magnitude of the mean terms is subject to question.

#### D. THE PRODUCTION AND RECOMBINATION TERM

In comparison with the magnitudes of the other terms, the production and recombination term, as estimated from Brewer and Wilson's (1968) values, does not have a significant effect except in the 30/50 mb volume. Here, the magnitude is about  $2/3$  of the local rate of change. In future investigations this must be taken into consideration.

#### E. THE ERROR TERM

The error term in Table II and figure 6 is the value that must be added to the local change in order to equal the sum of the mean, eddy and net production terms. In numerical computations of this sort, errors are expected because of data uncertainties, since many approximations are made to facilitate the evaluations of the individual terms and their components.

The mean errors in each volume are of the order of magnitude of the largest term. The mean errors at 30/50 and 50/100 mb are representative of the daily errors at these levels from which the mean error was derived. This is not true at the 100/200 mb volume where the daily errors average one order of magnitude larger than the ten-day mean error. Thus, it is noted that the ten-day mean error is unrepresentative of the error in the 100/200 mb volume and, further, that the calculations here suffer from the same problems as the upper two volumes.

Considering that the error in all three volumes indicates too much ozone on the right hand side of the balance, the failure to compute the sub-grid scale diffusion terms has to be considered. It is expected that these terms will evacuate ozone from the volume with a magnitude considerably smaller than the magnitude of the error. Therefore it is improbable that the failure to calculate these terms contributes much to the error.

The first serious possible source of error is that the ozone mixing ratio distributions on the pressure surfaces are not accurate enough for the calculations. Only by having a more dense data network will this ever be known for sure. The probability, that this is the major source of error, is diminished, considering the consistency in daily analyses and the consistency of the distributions with the theories and distributions advanced by earlier investigators.

The second and most probable source of error is in the evaluation of the vertical motions. As was noted earlier, the evaluation of the ozone balance equation is heavily dependent upon vertical motions. While a consistent

error in the vertical motions will not affect the eddy terms greatly, it will have considerable effect on the mean terms. Since the continuity equation was used to evaluate the mean flux through the lateral boundaries, this term is affected also. This line of reasoning is consistent with the fact that the mean terms in most cases are large compared to the rest of the terms as can be seen in Table 11 and figure 6. It can be reasoned that a consistent error in the vertical motion at a particular pressure level could affect each of the mean terms enough to produce a significant error.

The size of the error in the vertical motion modes does not have to be very large to seriously affect the calculations. To see this, consider the vertical motion scheme used in the computations and presented as equation (1). The diabatic heating term is the term most subject to question as its values determined by any method are highly uncertain. This is attributed to the lack of an accurate method to check the results of the determination of the diabatic heating. If the area average of equation (1) is taken, and it is assumed that the correction to the vertical motion ( $\tilde{\omega}_{\text{corr}}$ ) is a function only of the correction to the diabatic heating term (corr), then it can be written that approximately,

$$\tilde{\omega}_{\text{corr}} = \frac{-\text{corr}}{\alpha/c_p} \quad (11)$$

A representative value of area averaged diabatic heating at 75 mb as estimated from Kennedy's (1965) results can be considered  $-.35$  degrees per day. If this were incorrect by an arbitrarily selected  $\pm .2$  degrees per day, then the evaluation of equation (11), using representative values for evaluation of the specific volume would produce



$\tilde{\omega}_{\text{corr}} = \pm .24$  mb per day, or about a 25 percent error in the mean vertical motions.

The mean vertical advection of ozone across a pressure surface is represented by  $\tilde{\omega} \frac{\partial \tilde{\chi}}{\partial p}$  in equation (10). Evaluating the effect of  $\tilde{\omega}_{\text{corr}}$  on this term using representative values of  $\tilde{\chi}$  produces uncertainty in this term of approximately  $210 \times 10^{-4}$  micrograms per gram per day. It is easily seen from equations (7) and (8) how this would affect the mean flux through the lateral boundaries as presented in Table II. The value of the mean advection through the lateral boundary is small (Fig. 6). Therefore, it is reasoned that in this form the mean lateral advection is not a major source of error. Similar arguments can be made for the 30/50 and 100/200 mb mean terms.

It can be concluded that the uncertainty in the evaluation of mean stratospheric vertical motions is large enough to result in the observed magnitude of the error to the ozone balance equation through evaluation of the mean terms. Implied from the excess of ozone represented by the error term is that the net input to the particular volume by the mean terms, particularly the mean vertical flux (or advection) terms, is too large although the sense of the individual mean terms is probably correct.

#### IV. ADDITIONAL CALCULATIONS

An attempt was made to support the results of the qualitative evaluation of the distributions of ozone on a pressure surface and the terms of the ozone balance by calculating the correlation coefficients of the meridional wind and ozone mixing ratio and the correlation coefficients of the vertical motion and the ozone mixing ratio. The calculations are presented as figures 7 and 8. For the number of data points involved, a correlation coefficient greater than .2 is statistically significant at the 95 percent level of confidence.

The correlation coefficient for two variables is defined as the covariance divided by the variance. It follows then that the sign of the correlation coefficient is also the sign of the covariance. This relationship allows comparison with the eddy terms of the ozone balance.

Looking at figure 7, it can be seen that there are non-significant values of the lateral transport computed by the ozone balance. The ozone distributions observed on the pressure surfaces are evaluated as having been spread out by the weak wind fields at these levels and accomplishing little transport. The positive area at 30 mb and 70N latitude is not conclusive, since this area was determined by one data point. It is consistent, however, with the assumption that ozone-poor air is advected southward by the horizontal eddy flow at this altitude.

At the 100 mb level the negative values to the north are associated with high ozone values being moved southward by the horizontal eddy flow. The positive values to the south are an indication of a counter-gradient transport (see fig. 5) of high ozone values northward and low ozone values southward

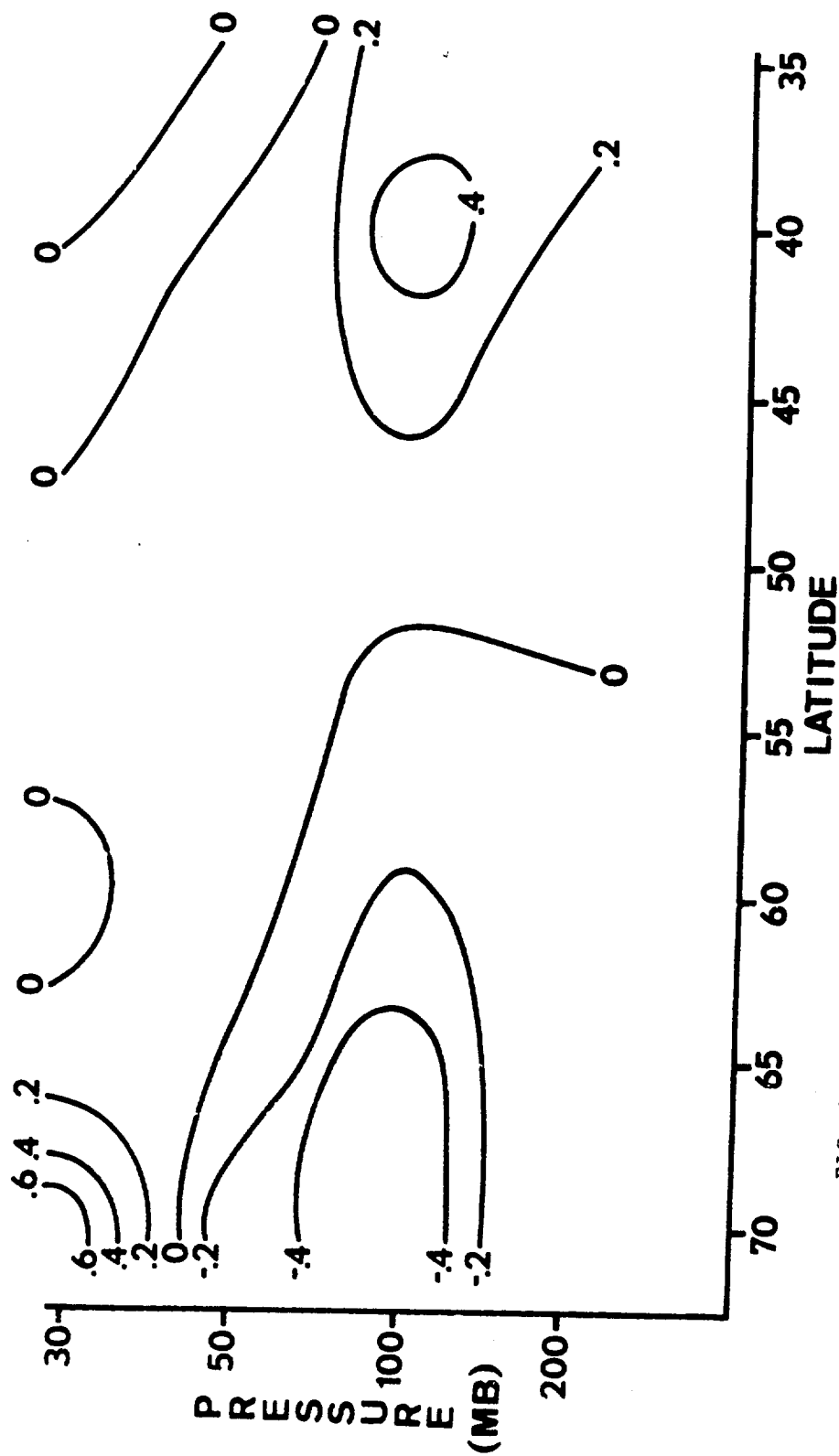


FIG. 7. Ten-day Mean Correlation Coefficients Between Meridional Wind and Ozone Mixing Ratio for the Period 30 April to 9 May 1963. Computed between longitude 60W and 140W.

by the horizontal eddy flow. To evaluate the cause of the counter-gradient transport, the vertical motion patterns (not presented here) were compared with the streamline patterns. It was observed that in many cases the maximum sinking areas connected with ozone-rich air were slightly (45 degrees in phase angle) to the east of the base of the trough. This offset of the vertical motion pattern from the trough line has been discussed by Ohring and Muench (1960). The sinking consequently offset the entire ozone mixing ratio pattern to the east and set the conditions for counter-gradient flow by the horizontal eddies.

The results at 200 mb were expected to be more conclusive than shown in figure 7. The values reflect the stronger relationships at 100 mb, however, they are not at the 95 percent level of significance. Without further calculations, a definite conclusion cannot be advanced.

The results of figure 8 strongly support earlier contentions. The weak positive values are associated with upward eddy transport of high ozone values by the anticyclonic activity at 30 and 50 mbs. The high negative values at the southern latitudes indicate the expected downward transport of high ozone values. These latitudes coincide with the base of the troughs on the circumpolar vortex and hence general areas of maximum sinking motions. At 100 mb the secondary maximum of significant negative values at the northern latitudes are evaluated as downward transport of high ozone values by the weaker semi-permanent trough of the circumpolar vortex. Based on the values at 200 mb, it is further reasoned that the vertical eddy flux of ozone across the tropopause

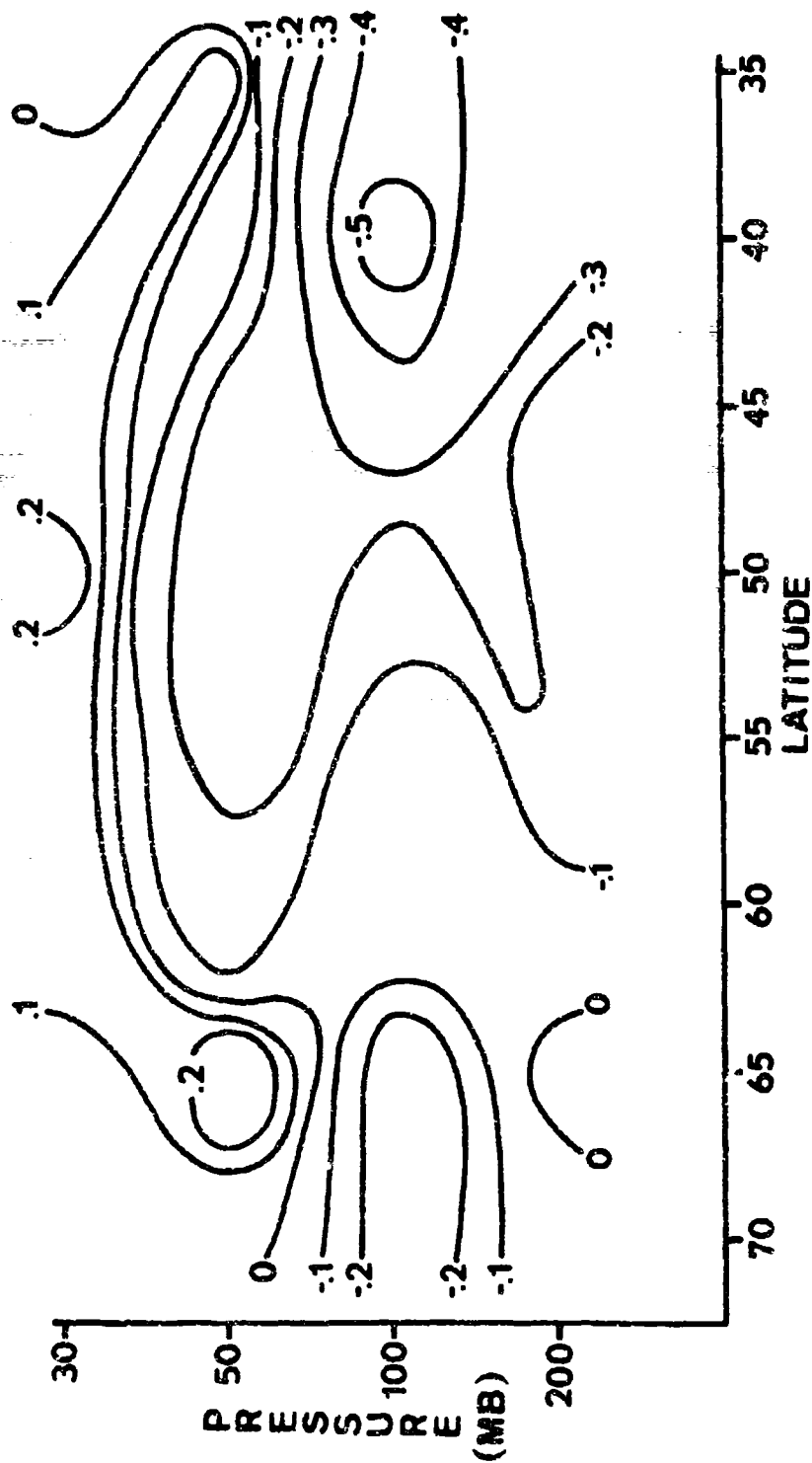


FIG. 8. Ten-day Mean Correlation Coefficients Between Vertical Motion and Ozone Mixing Ratio for the Period 30 April to 9 May 1963. Computed between longitude 60W and 140W.

is taking place in connection with the maximum sinking areas near the base of the transient troughs on the circumpolar vortex.

In the recent past several investigators (Newell 1961, 1962, 1963, 1964; Mahlman, 1966, 1967; and Molla and Loisel, 1962) have used the latitudinal covariance of the meridional and vertical wind components  $\overline{(v'w')}$  as an indication of stratospheric eddy transport processes. As a further check on the validity of the terms of the ozone balance equation, it was decided to compare  $\overline{(v'w')}$ , by using correlation coefficients, with the information prepared for this study. This distribution is presented in figure 9.

The negative values of the correlation coefficients are associated with a northward and downward transport while the positive areas indicate a southward and downward transport. The information from fig. 9 is in agreement with the sense of the vertical eddy flux terms of the ozone balance, and the ozone distribution on a pressure surface except at the 30 mb surface. At this level the mean ozone mixing ratio, streamline and vertical motion patterns show a northward and upward flow of high ozone values. This was confirmed by a vertical eddy flux out of the 30/50 mb volume across the 30 mb surface and figure 8. The vertical eddy flux is a direct calculation of transport, as compared to the correlation coefficients which are only an indication of transport. This implies that the correlation coefficient must be on the order of magnitude of .5 or greater to give confidence in the conclusion that this term is in fact an indicator of transport.

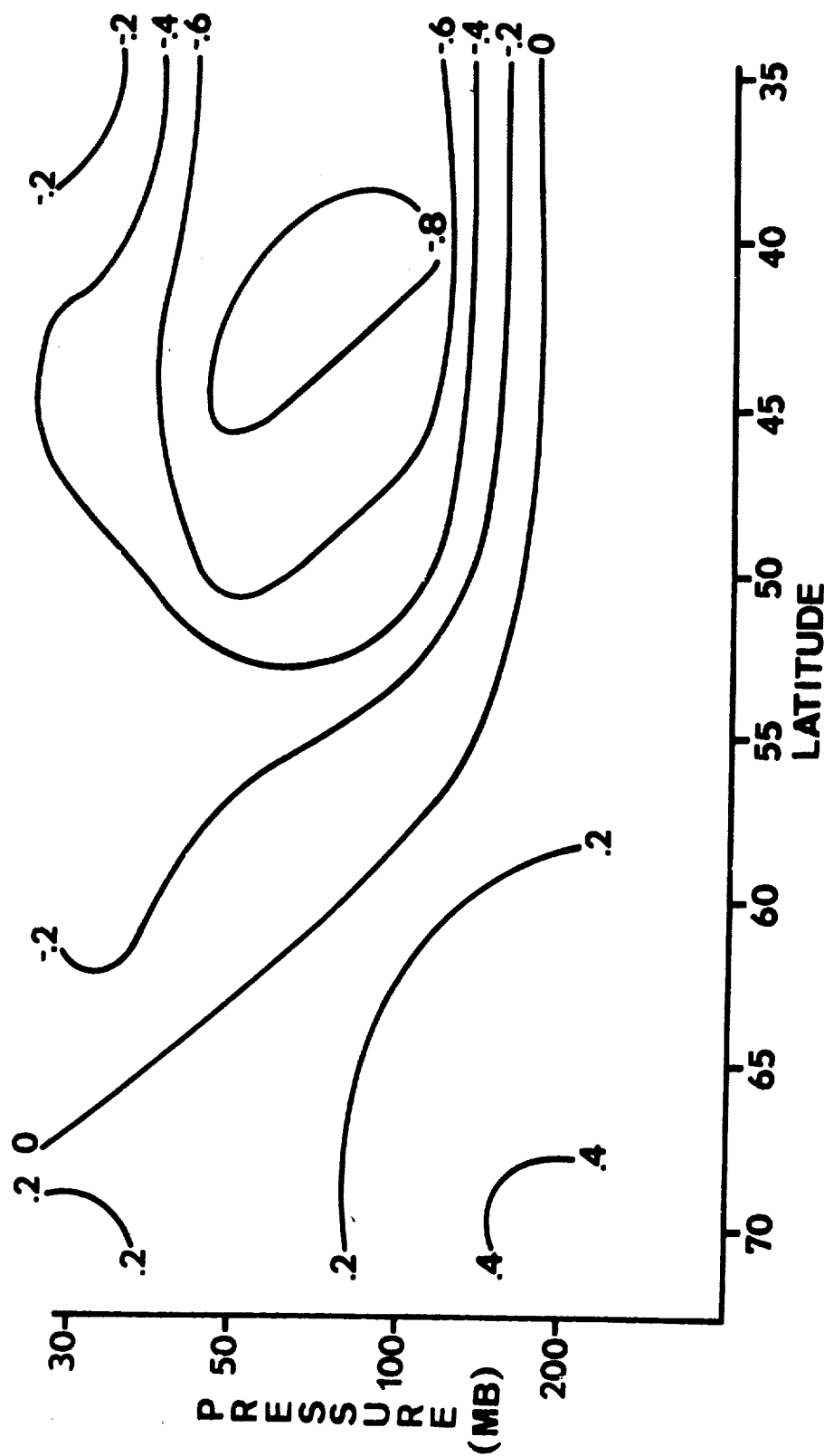


FIG. 9. Ten-day Mean Correlation Coefficients Between Meridional Wind and Vertical Motion for the Period 30 April to 9 May 1963. Computed between longitude 60W and 140W.

## V. SUMMARY AND CONCLUSIONS

Even though the magnitude of the mean terms is subject to question, the distribution of ozone on a pressure surface, the ozone balance, and the supporting calculations allow several general conclusions to be drawn.

1. It is possible to construct the distribution of ozone on a pressure surface from the Regener ozonesonde data, and then perform numerical calculations that provide reasonable results.

2. During this time period, the atmosphere is past its yearly maximum content of ozone at northern latitudes. There is no evidence to support a large northward movement of ozone at this time.

3. During the ten-day period in question, ozone content of the volume is decreasing. To accomplish this, the mean vertical motions, supported by the vertical eddy transport at 50, 100, and 200 mb, are moving ozone downward to the tropopause level where the vertical eddy transport, associated with the transient eddies on the circumpolar vortex, then move the ozone into the troposphere for eventual destruction.

4. The vertical eddy transport is a measure of the vertical part of the Reed-Normand effect. This mechanism is operating the sense as proposed between 50 and 200 mb. At 30 mb the Reed-Normand effect is operating in the opposite sense with ozone-rich air being advected upward.



## APPENDIX A

### STREAMLINE AND OZONE MIXING RATIO ANALYSIS FOR 3 MAY 1967

This appendix presents a representative sample of the distributions of ozone mixing ratio on a pressure surface in the lower stratosphere. To understand the effect of the wind field upon the ozone distribution, the appropriate streamline pattern is presented.

The choice of data was made to facilitate comparison with the patterns published by Berggren and Labitzke (1968).

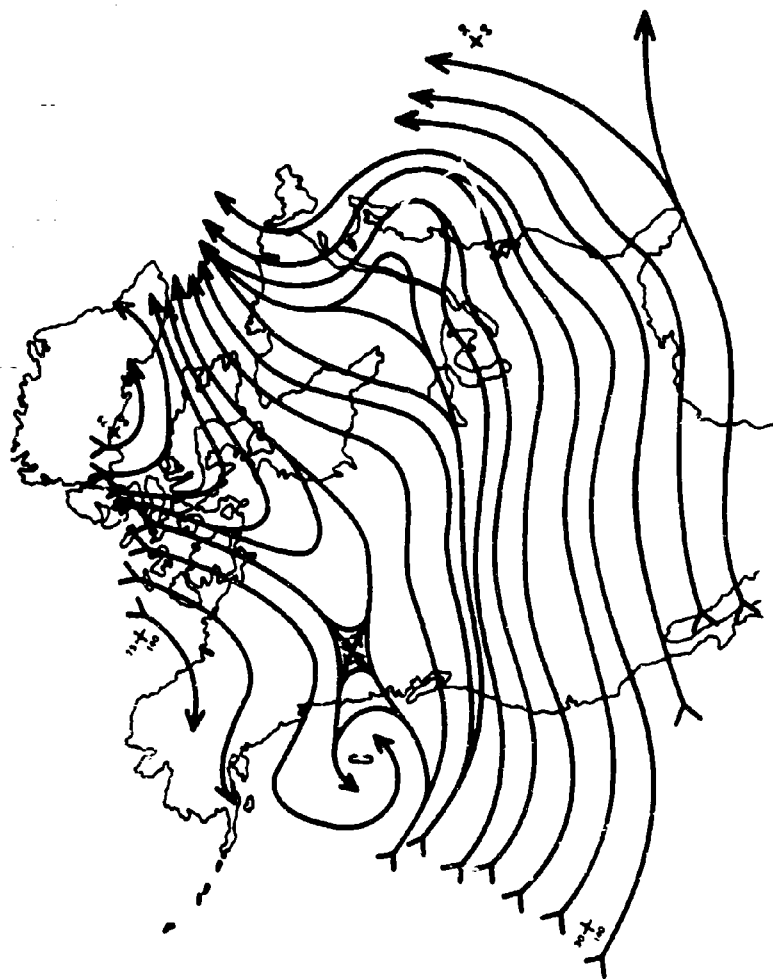


FIG. A-1. The 200 mb Streamline Analysis for 3 May 1963.

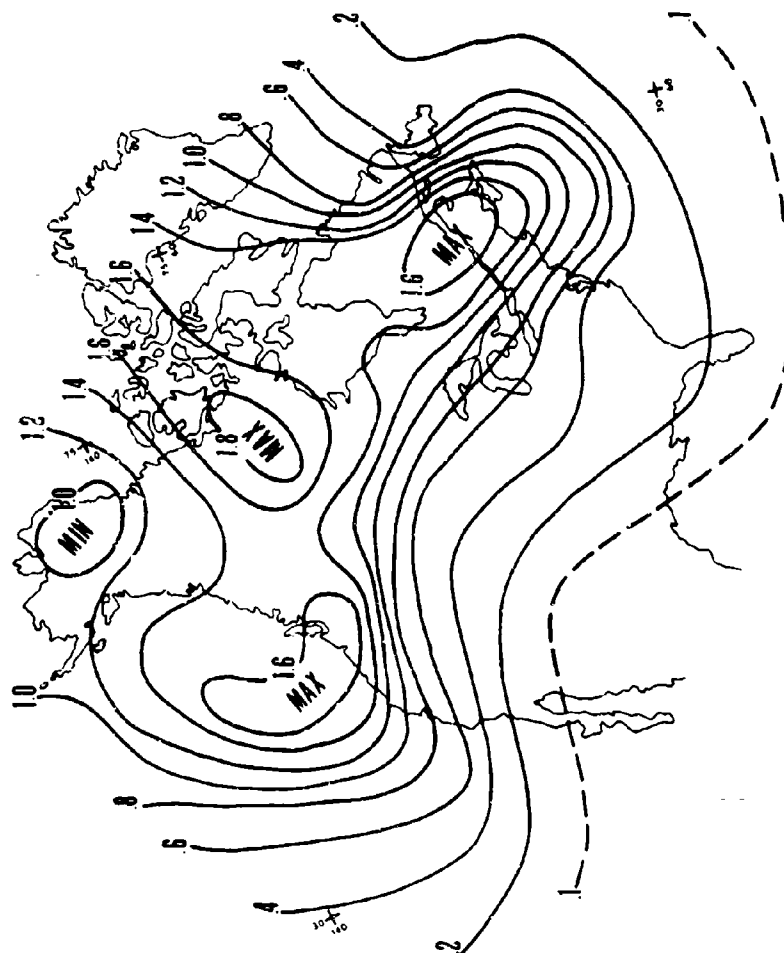


FIG. A-2. The 200 mb Ozone Mixing Ratio ( $\text{mg g}^{-1}$ ) Analysis for 3 May 1963.

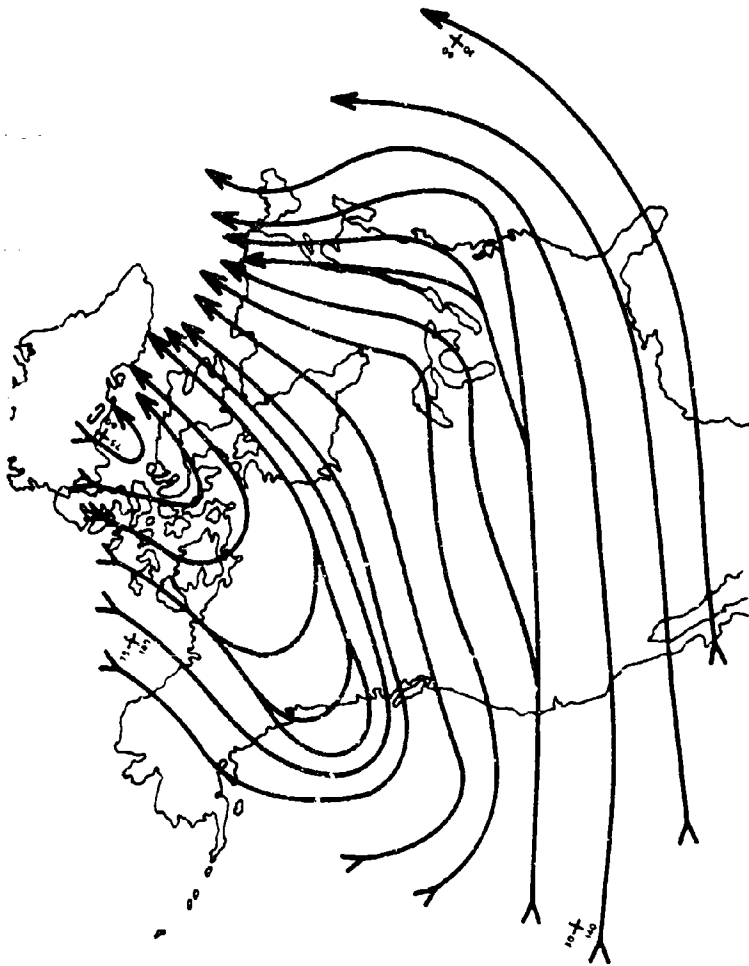


FIG. A-3. The 100 mb Streamline Analysis for 3 May 1963.

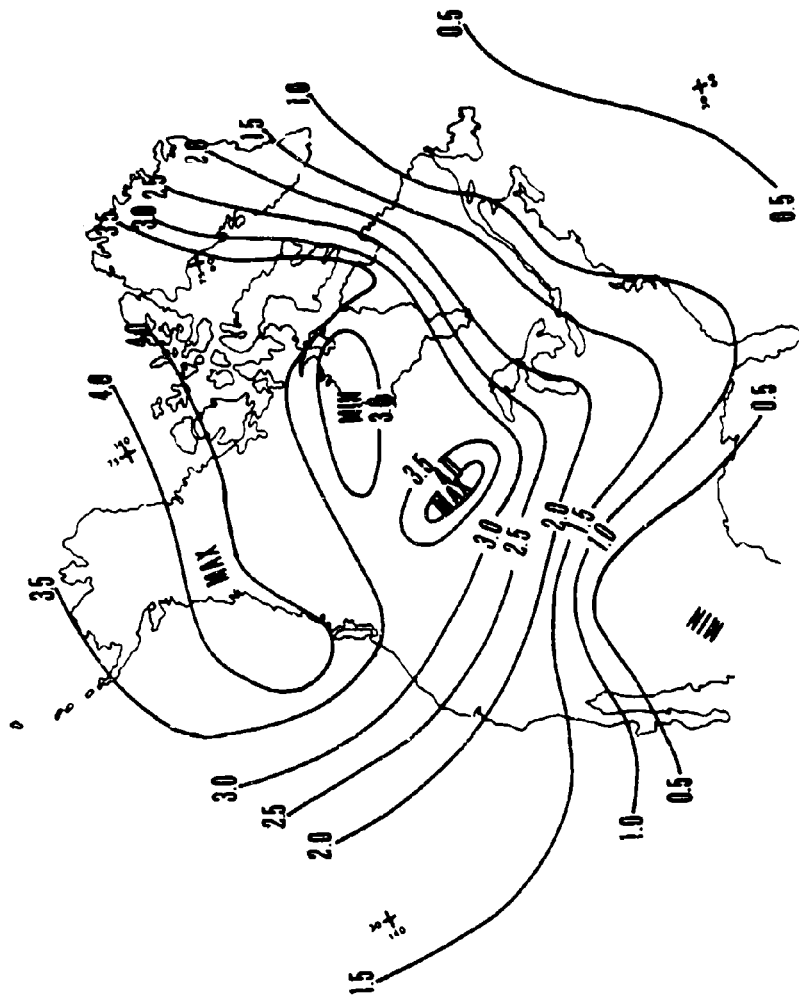


FIG. A-4. The 100 mb Ozone Mixing Ratio Analysis ( $\text{mg g}^{-1}$ ) for 3 May 1963.

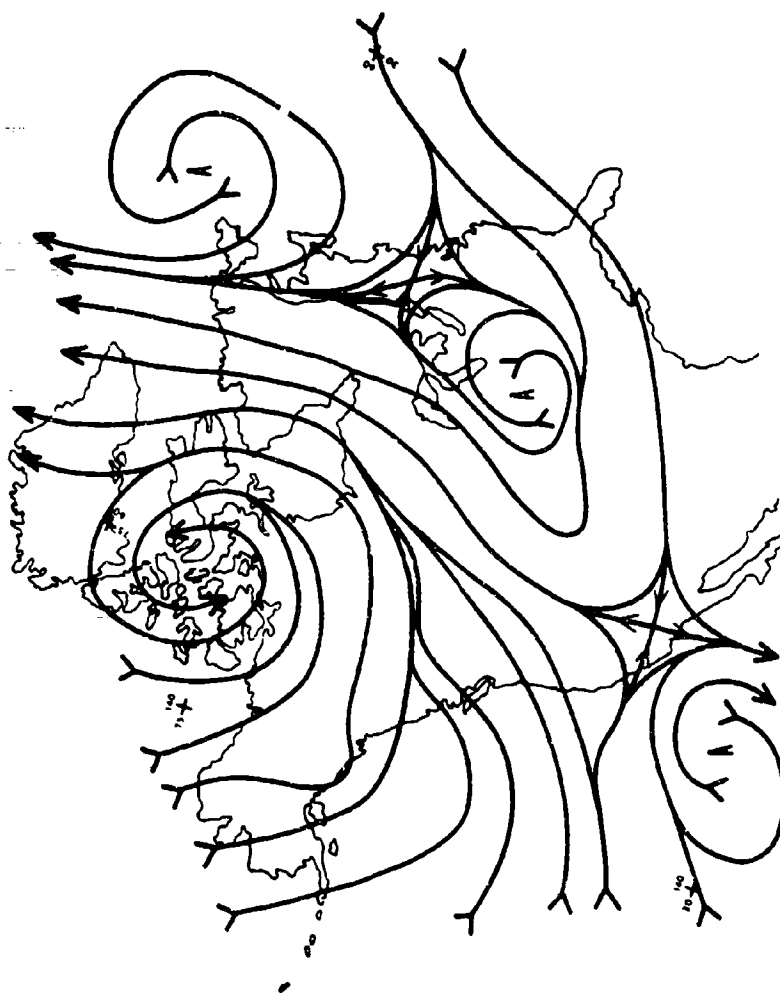


FIG. A-5. The 50 mb Streamline Analysis for 3 May 1963.

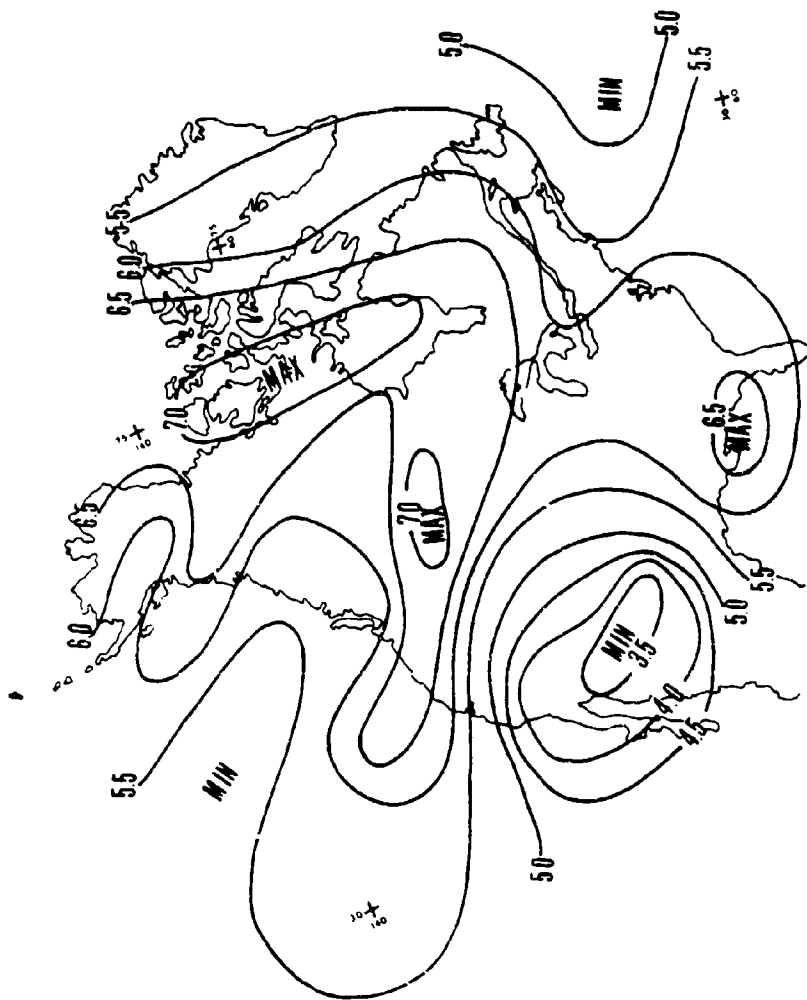


FIG. A-6. The 50 mb Ozone Mixing Ratio ( $\text{mg g}^{-1}$ ) Analysis for 3 May 1963.

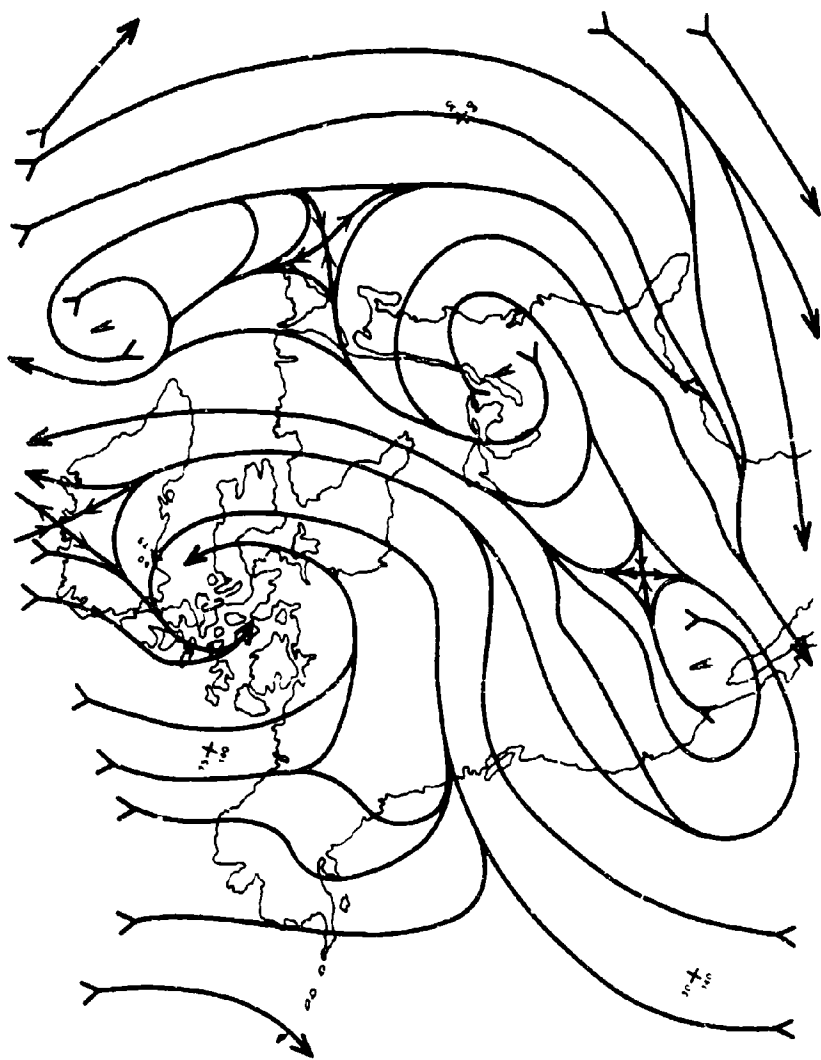


FIG. A-7. The 30 mb Streamline Analysis for 3 May 1963.



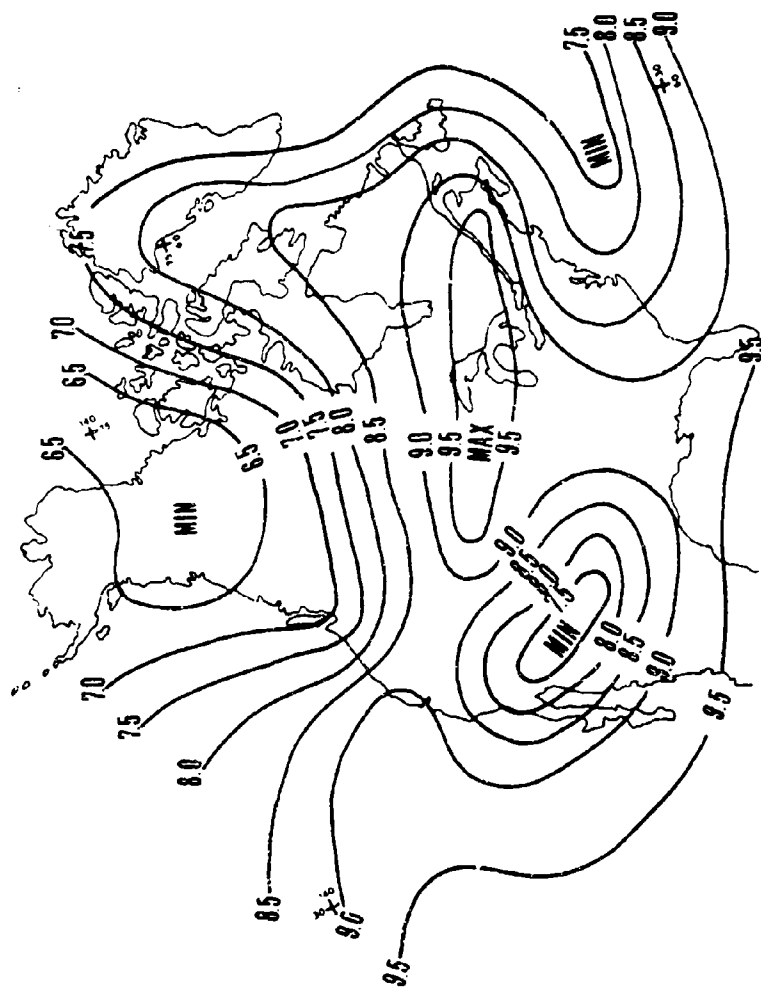


FIG. A-8. The 30 mb Ozone Mixing Ratio ( $\text{mg g}^{-1}$ ) Analysis for 3 May 1963.

## LIST OF REFERENCES

- Berggren, R. and K. Labitzke, "A detailed study of the horizontal and vertical distribution of ozone," Tellus, v. 18, p.761-722, 1966.
- \_\_\_\_\_, "The distribution of ozone on pressure surfaces," Tellus, v. 20, p. 88-97, 1968.
- Bojkov, R. D., "Vertical distribution of ozone in the earth's atmosphere," Meteorologija i Geologija, v. 10, p. 3-11, 1955. (Translated by AFCRL, G.T.R. 66-22, Oct 1966)
- \_\_\_\_\_, "Computing the vertical ozone distribution from its relationship with total ozone amount," Journal of Applied Meteorology, v. 8, p. 284-292, April 1969.
- Breiland, J. C., "Vertical distribution of atmospheric ozone and its relation to synoptic meteorological conditions," Journal of Geophysical Research, v. 69, p. 3801-3808, 15 September 1964.
- \_\_\_\_\_, "A case study of the vertical distribution of atmospheric ozone," Journal of Applied Meteorology, v. 4, p. 357-364, June 1965.
- \_\_\_\_\_, "Comparison of the vertical distribution of thermal stability in the lower stratosphere with the vertical distribution of atmospheric ozone," Journal of the Atmospheric Sciences, v. 24, p. 569-576, September 1967.
- \_\_\_\_\_, "Some large scale features of the vertical distribution of atmospheric ozone associated with the thermal structure of the atmosphere," Journal of Geophysical Research, v. 73, p. 5021-5028, 15 August 1968.
- Brewer, A. W. and A. W. Wilson, "The regions of formation of atmospheric ozone," Quarterly Journal of the Royal Meteorological Society, v. 94, p. 249-265, July 1968.
- Briggs, J. and W. T. Roach, "Aircraft observations near jet streams," Quarterly Journal of the Royal Meteorological Society, v. 89, p. 225-247, April 1963.
- Craig, R. A., The Observations and Photochemistry of Atmospheric Ozone and Their Meteorological Significance, American Meteorological Society, September 1950.
- \_\_\_\_\_, The Upper Atmosphere: Meteorology and Physics, Academic Press, 1965.

- \_\_\_\_\_, J. D. DeLuisti, and P. R. Stickse, "Ozone distribution over Tallahassee, Florida," Journal of Geophysical Research, v. 72, p. 1661-1665, 15 March 1967.
- Danielsen, E. F., "Stratospheric-tropospheric exchange based on radioactivity, ozone and potential vorticity," Journal of the Atmospheric Sciences, v. 35, p. 502-518, May 1968.
- Dobson, G. M. B. and D. Harrison, "Measurements of the amount of ozone in the earth's atmosphere and its relation to other geophysical conditions," Proceedings of the Royal Society of London, v. 110A, p. 660-693, April 1926.
- \_\_\_\_\_, D. Harrison, and J. Lawrence, "Measurements of the amount of ozone in the earth's atmosphere and its relation to other geophysical conditions - Part II," Proceedings of the Royal Society of London, v. 114A, p. 521-541, 1927.
- \_\_\_\_\_, D. Harrison, and J. Lawrence, "Measurements of the amount of ozone in the earth's atmosphere and its relation to other geophysical conditions - Part III," Proceedings of the Royal Society of London, v. 122A, p. 456-486, February 1929.
- \_\_\_\_\_, "Observations of the amount of ozone in the earth's atmosphere and its relation to other geophysical conditions - Part IV," Proceedings of the Royal Society of London, v. 129A, p. 411-433, November 1930.
- Free University of Berlin, Tägliche Hohenkarten der 50-mb-Fläche sowie monatliche Mittelkarten für das Jahr 1963, by Ute Hengelhaupt, Ingrid Reuter, Richard Scherhag, Günter Warnecke and others, v. 38, p. IV/29-V/10, 1966.
- \_\_\_\_\_, Daily and Monthly Northern Hemisphere 30-Millibar Synoptic Weather Maps of the Year 1963, by Barbara Kriester, Karin Labitzke, Drazen Poje, Richard Scherhag, and Renate Stuhmann, v. 39, p. IV/29-V/10, 1963.
- Godson, W. L., Total ozone and the middle stratosphere over arctic and sub-arctic areas in winter and spring," Quarterly Journal of the Royal Meteorological Society, v. 86, p. 301-317, July 1960.
- Gotz, F. W. P., "Ozone in the atmosphere," Compendium of Meteorology, p. 275-291, Waverly Press, 1951.
- Haltiner, G. J. and F. L. Martin, Dynamical and Physical Meteorology, McGraw-Hill Book Company, 1957.

- Hering, W. S., "Ozone and atmospheric transport processes," Tellus, v. 18, p. 329-336, 1966.
- \_\_\_\_\_, and T. R. Borden Jr., Ozonesonde Observations Over North America, Volume 2, Environmental Research Papers, No. 38, Air Force Cambridge Research Laboratories, July 1964.
- \_\_\_\_\_, and T. R. Borden Jr., Mean Distributions of Ozone Density Over North America, 1963-1964, Environmental Research Papers, No. 162, Air Force Cambridge Research Laboratories, December 1965.
- \_\_\_\_\_, and H. Dutsch, "Comparison of chemiluminescent and electrochemical ozonesonde observations," Journal of Geophysical Research, v. 70, p. 5483-5490, 15 November 1965.
- \_\_\_\_\_, C. N. Touart, and T. R. Borden, Jr., "Ozone heating and radiative equilibrium in the lower stratosphere," Journal of the Atmospheric Sciences, v. 24, p. 402-413, July 1967.
- Kennedy, J. S., Energy Generation Through Radiative Processes in the Lower Stratosphere, Planetary Circulations Project, Report No. 11, Massachusetts Institute of Technology, 1964.
- Komhyr, W. D., R. D. Grass, and R. A. Proulx, Ozonesonde Intercomparison Tests, ESSA Technical Report ERL 85-APCL4, September 1968.
- Kulkarni, R. N., "Comparison of ozone variations and of its distribution with height over middle latitudes of the two hemispheres," Quarterly Journal of the Royal Meteorological Society, v. 88, p. 522-534, October 1962.
- Mahlman, J. D., The Atmospheric General Circulation and Transport of Radioactive Debris, Atmospheric Science Paper No. 103, Colorado State University, 1966.
- \_\_\_\_\_, Further Studies on Atmospheric General Circulation and Transport of Radioactive Debris, Atmospheric Science Paper No. 110, Colorado State University, 1967.
- Mateer, C. L. and W. L. Godson, "The vertical distribution of atmospheric ozone over Canadian stations from unkehr observations," Quarterly Journal of the Royal Meteorological Society, v. 86, p. 512-518, October 1960.
- Maetham, A. R., "The correlation of the amount of ozone with other characteristics of the atmosphere," Quarterly Journal of the Royal Meteorological Society, v. 63, p. 289-307, 1937.

Molla, A. C. and C. J. Loisel, "On the hemispheric correlations of vertical and meridional wind components," Geofisica Pura E Applicata, v. 51, p. 166-170, 1962.

Newell, R. E., "The transport of trace substances in the atmosphere and the implications for the general circulation of the stratosphere," Geofisica Pura E Applicata, v. 49, p. 137-158, 1961.

\_\_\_\_\_, "Transfer through the Tropopause and Within the Stratosphere," Planetary Circulations Project, Report No. 7, Massachusetts Institute of Technology, 25 October 1962.

\_\_\_\_\_, "Transfer through the Tropopause and Within the Stratosphere," Planetary Circulations Project, Report No. 7, Massachusetts Institute of Technology, 25 October 1962.

\_\_\_\_\_, "The general circulation of the atmosphere and its effect on the movement of trace substances," Journal of Geophysical Research, v. 68, p. 3949-3962, 1963.

\_\_\_\_\_, "Further ozone transport calculations and the spring maximum in ozone amount," Geophysics, Pure and Applied, v. 59, p. 191-206, 1964.

Normand, Sir Charles, "Atmospheric ozone and the upper-air conditions," Quarterly Journal of the Royal Meteorological Society, v. 79, p. 39-50, January 1953.

Ohring, G. and H. S. Muench, "Relationships between ozone and meteorological parameters in the lower stratosphere," Journal of Meteorology, v. 17, p. 195-206, April 1960.

Pittock, A. B., "A statistical approach to the synoptic climatology of vertical ozone distributions," Journal of Applied Meteorology, v. 8, p. 30-311, April 1969.

Prabhakara, C., "Effects of non-photochemical processes on the meridional distribution and total amount of ozone in the atmosphere," Monthly Weather Review, v. 91, p. 411-431, September 1963.

Ramanathan, K. R. and R. N. Kulkarni, "Mean meridional distributions of ozone in different seasons calculated from umkehr observations and probable vertical transport mechanism," Quarterly Journal of the Royal Meteorological Society, v. 86, p. 144-155, April 1960.

Reed, R. J., "Role of vertical motions in ozone-weather relationships," Journal of Meteorology, v. 7, p. 263-267, August 1950.

Regener, V. H., "On a sensitive method for the recording of atmospheric ozone," Journal of Geophysical Research, v. 65, p. 3975-3977, December 1960.

\_\_\_\_\_, "Measurements of atmospheric ozone with the chemiluminescent method," Journal of Geophysical Research, v. 69, p. 3795-3800, 15 September 1964.

Sticksel, P. R., The Vertical Distribution of Ozone Over Tallahassee, Florida, Ph. D. Thesis, Florida State University, 1966.

**An Overview of Research Techniques  
Employed for Investigation of Trace-Substance Transport  
in the Atmosphere**

**by**

**J. D. Mahlman**

**Preceding Page Blank**

## I. Introduction

The investigation of the mechanisms in the atmosphere, which lead to systematic large-scale transport of trace substances, is still a relatively new research endeavor. Ideally, the most successful experimental setup for such investigations would involve the joint use of meteorological and trace substance data. Normally, both types of data should possess similar spatial and temporal resolutions. Up to the present time, this has been nearly impossible because of the tremendous expense and difficulty involved in obtaining numerous simultaneous measurements of any trace substance in the free atmosphere at the desirable elevations. As a result of these difficulties, previous investigators have employed a variety of approaches for investigating problems of trace substance transport.

One of the goals of the research conducted under this contract for the past two years has been to explore possible new techniques for investigating transport phenomena in the atmosphere. Resulting from this, a number of different approaches have been attempted. Some of these are "traditional" in the sense that other investigators have employed them in the past. Others are "new" in that they had not yet been applied to the investigation of large-scale trace transport.

Because a number of techniques have been attempted here, it seems appropriate to the author that the final project summary be directed toward an overview of the utility and applicability of these various approaches. Consequently, the usual project "review" of pertinent results will not be attempted here, since those results are already published under individual



titles, here and elsewhere.

The approach in this paper will be to list each study performed during the contract period, and then comment on the method employed and results obtained on an individual basis. The publications under this contract listed in order of subsequent referral in the text, are as follows:

- A. Mahlman, J. D., 1969: Heat Balance and mean meridional circulations in the polar stratosphere during the sudden warming of January 1958. Monthly Weather Review, 97, 534-540.
- B. Mahlman, J. D., 1969: Energetics of a "minor" breakdown of the stratospheric polar night vortex. Journal of the Atmospheric Sciences, 26, 1306-1317.
- C. Mahlman, J. D., 1970: Eddy transfer processes in the stratosphere during major and "minor" breakdowns of the polar night vortex, Journal of Geophysical Research, 75, 1701-1705.
- D. Mahlman, J. D., 1970: On the maintenance of the polar front jet stream. (Enclosed as part of this report.)
- E. Mahlman, J. D., 1969: Diagnostic analysis of the transport mechanisms leading to surface fallout increases during November 1966. Naval Postgraduate School, First Progress Report to the Atomic Energy Commission (NPS-51MZ9081B), 5-6.
- F. Mahlman, J. D., 1969: Long-term dependence of surface fallout fluctuations of tropopause-level cyclogenesis. Archiv für Meteorologie, Geophysik und Bioklimatologie, A18, 299-311.
- G. Stender, R. H., 1970: Numerical calculations of stratospheric ozone transport (enclosed as part of this report).
- H. Willoughby, H. E., 1970: A numerical simulation of the advective and diffusive transfer of trace substances in the stratosphere (enclosed as part of this report).

## II. Discussion

Articles A, B, C, and D in the preceding list fall under the category of what shall be termed "dynamical process" studies. These studies are only

indirectly related to the large-scale trace-substance transport problem in that they specifically attempt to understand the structure and dynamics of various circulation phenomena. However, once such circulation characteristics have been properly delineated, it becomes possible to construct inferences on their transport properties as well. This approach has been employed previously by a number of investigators and has provided valuable insights into a great variety of atmospheric processes. Indirectly, these studies have laid a framework for viewing the trace-substance transport problem by helping to isolate the relative importance of the various features of the atmospheric general circulation. Conceptually, it has been found useful to separate these features into distinct categories such as: the mean meridional circulation, "eddies" or waves of various scales, and sub-meteorological-grid-scale "eddies" or "diffusion." Such a separation is, of course, not unique nor are the motions on various scales independent of one another. An example of an alternative framework for viewing atmospheric processes is given in Article D of this discussion.

Articles A, B, and C are oriented toward attempting to understand specific circulation phenomena in the wintertime lower stratosphere. These studies have concentrated on shorter time scales, and have been intentionally designed to complement the studies performed in the Planetary Circulations Project at the Massachusetts Institute of Technology, which have been concerned with circulations on the climatic scale.

In both Articles A and B, one of the major goals was to deduce the mean meridional circulation in order that both the dynamics and transport properties, associated with specific circulation phenomena, could be more fully understood. This was accomplished by employing a heat balance approach. Such

a method proves to give excellent results as long as the temperature changes induced by the mean meridional circulation are significantly larger than the present uncertainty in the specification of diabatic heating rates.

A major breakdown of the stratospheric polar night vortex was the object of study in Article A, while Article B was concerned with a so-called "minor breakdown" event. In the "minor breakdown" work, considerable effort was employed to explain the kinetic energy variations occurring in association with the breakdown. Even though quite consistent mean meridional circulations were obtained, it still was apparent that the kinetic energy balance is sensitive to small errors in the mean cell.

Article C was a combination of the research, lending to Articles A and B to obtain a comparison of the relative efficiency of the eddy transport processes occurring in major and "minor" breakdowns of the polar night vortex. Here, a basic assumption is that the ability of a given circulation event to produce an effective (say northward) transport of trace substance can be indirectly inferred without any detailed knowledge of the distribution of the substance itself. This, of course, is a questionable assumption, but has been a necessary one in the absence of any knowledge about the details of the trace substance distribution.

Article D is the result of a diagnostic study which attempts to determine the mean transverse circulation about the polar front jet stream. Previous studies have shown that significant amounts of stratospheric air can enter the troposphere through the polar front jet stream "front" in association with specific storm systems. Such studies, however, do not answer the question

of whether there is a weak (but systematic) exchange of air between the stratosphere and troposphere, resulting from a mean transverse circulation about this jet stream system.

In this study such a calculation was performed, using vertical motions from a "complete" (Rossby number  $< 1$ ) diagnostic balance  $\omega$ -equation model. These derived vertical motions were averaged with respect to the polar front jet stream core. The results indicated that a direct mean transverse circulation exists about the jet core and may indicate a slow import of stratospheric air into the troposphere. This transverse circulation also was shown to give consistent results in the mean kinetic energy balance. Thus, such a diagnostic balance,  $\omega$ -equation model appears to be a very useful tool for conducting the so-called "dynamical process" studies.

Articles E and F are also "traditional" studies in that they attempt to infer transport processes without detailed knowledge of the distribution of the trace substance (in these cases, radioactivity) in the atmosphere. However, here, as in a number of previous studies by other authors, information is available on the distribution of radioactivity at the earth's surface. This is very valuable because the "history" of a given trace substance can often be traced from source to sink when supplemented by detailed meteorological analysis. Article E falls into this category.

The usefulness of accompanying surface radioactivity is shown in Article F. From previous individual case studies, import of stratospheric air into the troposphere in the polar front jet stream region has been related to strong cyclogenesis is a circulation feature which should serve as an indication of

stratospheric-tropospheric mass exchange. Article F is an effort to relate an index which is an indicator of cyclogenesis to the radioactivity fluctuations at the ground. The results show that there exists a significant correlation between the two--thus, establishing the mechanism on a firm basis. Without the surface radioactivity measurements, however, such an inference would have been difficult, if not impossible.

Articles G and H both employ "new" techniques to investigate trace substance transport problems. They both avoid or reduce the problem of inadequate trace substance data resolution by employing specific techniques. Article G is an attempt to provide direct quantitative calculations of stratospheric ozone transport, using data from the Air Force Cambridge Research Laboratories North American Ozonesonde network. In the past this network has been very difficult to utilize for large-scale transport studies even though the individual observations have proven to be quite reliable. The basic problem with the data has simply been one of inadequate resolution. Observations are normally taken only once weekly in a network of just eleven stations over the North American continent. Such a network is too sparse to be able to routinely establish synoptic analyses of ozone mixing ratio which possess spatial and temporal continuity.

In this study the time resolution problem was minimized by considering only a specific period in early May 1963 in which the ozonesonde observations were taken daily. Also, the effective horizontal data resolution was increased by computing 24-hour forward and backward isentropic trajectories from each of the ozonesonde observation points and assuming conservation of ozone mixing ratio. Ideally, such a technique increases the effective number of

data points by a factor of three. In practice, because the trajectories leave the network region and all stations did not report every day, the number is somewhat less. Use of this technique does allow ozone-mixing ratio analyses to be prepared which are consistent in time and space.

With such analyses, it then becomes possible to compute ozone transport quantities directly. In this study, the calculations were performed by integrating the ozone continuity equation over an arbitrary volume and separating the flux convergence terms into "mean" and "eddy" effects, relative to the computational volume. This calculation was quite successful in that it showed the existence of a systematic downward flux of ozone due to synoptic-scale vertical motions. The vertical flux by the area-mean vertical motions was found to be quite sensitive to small errors in the specification of the diabatic heating. In future studies of this kind, considerable care may have to be exercised in order to reduce this difficulty.

In Article H, an attempt is made to simulate numerically the transfer of trace substances in the stratosphere. In this type of approach, the problem of lacking trace substance data is circumvented because the distribution of the trace substance is evolved numerically from an arbitrary initial state.

Previously, such numerical approaches have been separated into two distinct categories. The first and simplest method is to treat all the possible transport mechanisms as a diffusion process. The second approach is to introduce a tracer into a numerical model of the general circulation and study the subsequent evolution of the tracers. This is potentially a very powerful method which will see considerable application in the future. The first method is limited because of the very arbitrary specification of the diffusion process.

The second method is only limited in that a given general circulation model may or may not properly simulate the real atmosphere with sufficient fidelity to reproduce the observed transport characteristics. At present this may be particularly true in the region of the stratosphere, especially in regard to seasonal variations in the circulation.

Because of these difficulties, an intermediate approach is attempted here. The observed winds in the stratosphere on a daily basis are used to advect the arbitrarily chosen tracers. From these winds and the temperature fields, vertical motions are obtained on the same scale as the horizontal wind data. These horizontal and vertical winds are then adjusted slightly so that they yield a consistent mean meridional circulation when zonally averaged. Therefore, these winds give a quite reliable specification of the atmospheric structure for motions on the scale of the meteorological network or greater. The motions below the resolution of the grid are treated as a sub-grid-scale diffusion process.

The Eulerian form of the continuity equation for a given trace substance is then integrated numerically in time on a three-dimensional grid, using the derived horizontal and vertical motions to provide the necessary advections. This technique gives very encouraging results in that the evolved tracer fields very shortly begin to possess characteristics quite similar to the limited knowledge, available about the observed fields.

This result suggests that such a technique might be applied to a number of specific transport problems for different types and scales of circulations in both the troposphere and the stratosphere.

Security Classification		DOCUMENT CONTROL DATA - R & D	
(Security classification of title, body of abstract and indexing annotation must be entered when the overall report is classified)			
1. ORIGINATING ACTIVITY (Corporate author)		20. REPORT SECURITY CLASSIFICATION	
Naval Postgraduate School Monterey, California 93940		Unclassified	
		21. GROUP	
2. REPORT TITLE			
Dynamical Mechanisms Producing Large-Scale Transport of Trace Substances			
4. DESCRIPTIVE NOTES (Type of report and, inclusive dates)			
Final Report, October 1969--September 1970			
9. AUTHOR(S) (First name, middle initial, last name)			
J. D. Mahlman			
8. REPORT DATE		7a. TOTAL NO. OF PAGES	7b. NO. OF REFS
October 1970		170	185
6a. CONTRACT OR GRANT NO.		5a. ORIGINATOR'S REPORT NUMBER(S)	
b. PROJECT NO. AT(49-7)-3206		NPS-51MZ70101A	
c.		5b. OTHER REPORT NO(S) (Any other numbers that may be assigned this report)	
d.			
10. DISTRIBUTION STATEMENT			
This document has been approved for public release and sale; its distribution is unlimited.			
11. SUPPLEMENTARY NOTES		12. SPONSORING MILITARY ACTIVITY	
This research was sponsored by the U.S. Atomic Energy Commission, Division of Biology & Medicine, Fallout Studies Branch, Washington, D. C.		Naval Postgraduate School Monterey, California	
13. ABSTRACT			
<p>This is a compilation of research results performed under AEC Research Contract AT(49-7)-3206. All of the various efforts have been directed toward gaining a better understanding of the atmospheric processes which lead to systematic large-scale trace substance transport. A variety of approaches have been employed in this and in earlier work on this contract. The last article in this report provides an overview and critique of the applicability of these various methods.</p>			



14

#### KEY WORDS

LINK A

LINK B

LINK C

2515

22

ALL

4

015	
-----	--

## Jet stream

## Energetics

## Diffusion

## Advection

## Numerical simulation

DD FORM 1473 (BACK)  
1 NOV 68  
S/N 0101-807-8821

IV-21

**Security Classification**

A-31409